

# Quantum irreversible decoherence behaviour in open quantum systems with few degrees of freedom. Application to $^1\text{H}$ NMR reversion experiments in nematic liquid crystals.

H. H. Segnorile and R. C. Zamar

*Instituto de Física Enrique Gaviola - CONICET, Facultad de Matemática,  
Astronomía y Física, Universidad Nacional de Córdoba*

*M.Allende y H. de la Torre - Ciudad Universitaria, X5016LAE - Córdoba, Argentina*

(Dated: May 7, 2013)

An experimental study of NMR spin decoherence in nematic liquid crystals is presented. The outcome of the experiments are analyzed in the framework of a theory that considers the spins as an open quantum system coupled to a quantum molecular environment, presented by the authors recently. Decoherence dynamics can be put in evidence by means of refocusing experiments of the dipolar interactions. The experimental technique used in this work is based on the MREV8 pulse sequence. Non-idealities of the experimental setting, like external field inhomogeneity, pulse misadjustments and the presence of non-reverted spin interaction terms are analysed in detail and their effects on the observed signal decay are estimated. It is found that, though all these non-idealities could in principle affect the evolution of the spin dynamics, their influence can be mitigated and they do not present the characteristic behaviour of the irreversible spin decoherence. As unique characteristic of decoherence, the experimental results clearly show the occurrence of eigen-selectivity in a time scale intermediate between those controlled by quantum interference of the closed spin system and thermalization, in complete agreement with the theoretical predictions. We conclude that the eigen-selection effect is the fingerprint of decoherence associated with a quantum open spin system in liquid crystals. Besides, these features of the results account for the quasi-equilibrium states of the spin system, which were observed previously in these mesophases, and lead to conclude that the quasi-equilibrium is a definite stage of the spin dynamics during its evolution towards equilibrium.

## I. INTRODUCTION

Derivation of a thermodynamic-like stationary state, of equilibrium or quasi-equilibrium, from a microscopic quantum mechanical starting point, is a major problem faced today by the physics of irreversible processes in nonequilibrium systems, with impact in a variety of fields, from fundamental research to applications in areas of high current interest like quantum computing and quantum information theory<sup>1-10</sup>.

Particularly, the occurrence of quasi-equilibrium spin states in nematic liquid crystals (LC's) poses the problem of the irreversible evolution of a finite open quantum system of interacting particles, coupled with a large quantum environment, towards a quasi-stationary state<sup>11</sup>. In LC's, due to the rapid molecular motions that average the intermolecular spin interactions to zero, the effective spin system comprises a small number of magnetic degrees of freedom, namely the intramolecular dipolar interactions, which remain because of the typical orientational order of these mesophases<sup>12</sup>. However, the proton Nuclear Magnetic Resonance (NMR) response in LC's is consistent with a true quasi-equilibrium in spite of the small number of the degrees of freedom of the observed system<sup>13</sup>. This topic has attracted the interest of many researchers in the NMR field<sup>14-18</sup> as well as other areas of physics<sup>19</sup>.

In our recent publication on NMR quantum decoherence in LC's, which we shall refer to as QD-I<sup>11</sup>, a theory was presented which describes the irreversible quantum decoherence processes undergone by an observed and

controlled system of quantum interacting particles because of its coupling with an unobserved lattice or environment. It provided a comprehensive explanation, compatible with previous experimental evidence<sup>13,20</sup>, on the mechanisms which turn the proton spin system density matrix of nematic LC's into a quasi-equilibrium form after an arbitrary initial coherent state.

Accordingly, the decoherence process transforms the initial state into a block diagonal matrix in the eigenbasis of the spin-environment interaction Hamiltonian. This evolution occurs over a time scale intermediate between that of the Liouvillian evolution of an isolated observed system and the long time scale where evolution is governed by relaxation and thermalization processes driven by thermal fluctuations.

The fingerprint of quantum decoherence theory is the eigen-selection process, which causes a selective decay of the off-diagonal components of the density matrix, preserving the block diagonal part of the initial state. Such explanation relies on general requirements on the eigenvalue distribution functions of the relevant quantum operators that represent the interaction of the system with the environment. Hence, experimental observation of eigen-selectivity would provide a direct evidence of the correlated dynamics between the spin system and the quantum environment that precludes the reach to quasi-equilibrium.

The aim of this work is the experimental study of decoherence spin dynamics, within the theoretical framework of QD-I. Particularly, we focus on the most relevant as-

pects of this phenomenon, namely eigen-selectivity and the occurrence of the intermediate time scale. Irreversible decoherence is studied by means of refocusing experiments, designed to counteract the effect of the spin dynamics generated by the dipolar spin interactions. Besides of the quantum interference corresponding to a closed system, the intrinsic decoherence coexists with other sources of the signal decay, like the line broadening due to a distribution of the order parameter<sup>21</sup>, non-idealities of the experimental setting like inhomogeneity of the static and rf magnetic fields or pulse imperfections, and the effects of non-secular terms of the dipolar Hamiltonian that cannot be experimentally reversed<sup>22</sup>. Accordingly, to isolate the distinctive features of decoherence associated only with the microscopic dynamics, we explore the intermediate time scale by combining dipolar refocusing with a meticulous theoretical and numerical analysis of the experiments based on hypotheses of general character. This strategy enables us to visualize the physical processes involved and to quantify the influence of the non-idealities.

Confirmation of the irreversibility of the spin dynamics within the intermediate time scale has relevant practical and basic consequences. It implies that the state attained by the spin system over the intermediate scale has a representation in the form of a block diagonal density operator, containing the information of the initial preparation which does not undergo subsequent evolution, except for the slow dynamics imposed by the spin-relaxation process, no matter the details of the coherences present in the initial condition. The traditional introduction of the spin-temperature hypothesis amounts to assuming that the off-diagonal density matrix elements can be forgotten after quantum interference cancels their contribution to the observable expectation value<sup>23</sup>. In this work we provide a quantum explanation for the damping of the off-diagonal elements and for the time scale where it occurs. Clarifying this aspect enables to replace the phenomenological assumption by a specific condition satisfied by the spin system state. Also, understanding the nature of the decoherence mechanism can contribute to the set up of a quantum spin-lattice relaxation theory beyond the Markovian limit, providing insight into the interplay of the quantum correlations developed in the microscopic irreversible dynamics and the dissipative macroscopic evolution. Finally, the analysis carried out in this work may contribute to the current discussion about the role of system-environment entanglement as basic mechanism of quantum decoherence of interacting particle systems<sup>1,24–26</sup>.

The article is organized as follows. In Section II, by means of experiments of refocusing of the dipolar interactions, we show how the eigen-selection process is evidenced during the partial reversion of the spin dynamics, which occurs in an intermediate time scale, between the time scales of the Liouvillian free evolution or adiabatic by one hand, and the thermalization and relaxation processes by the other hand. The initial part of

Section II is devoted to a detailed summary of the concepts developed and results obtained in QD-I, which are exhaustively used in this work. In Section II A a theoretical description of the decoherence dynamics driven by reversion experiments is presented, while a series of experimental measurement are shown in Section II B and the results compared with the theoretical prediction. Section II C is concerned with the analysis of possible sources of eigen-selectivity like effects coming from a closed-spin-system dynamics under experimental misadjustments or non-idealities in the theoretical approach used for its description. A supplementary material<sup>27</sup> is attached to this work, where the details about the origin of the theoretical expression for the reversion evolution operator and the signals obtained in Section II B are brought together the results of numerical calculations for such signals under different experimental settings. Besides, an experimental analysis of the effects of the inhomogeneity of the static magnetic field is presented there.

Finally, Section III is devoted to discuss and conclude about the concepts developed and results obtained along this work.

## II. EIGEN-SELECTIVITY EFFECTS ON COHERENCE EVOLUTION

This section is devoted to the experimental detection of the eigen-selection process which characterizes the irreversible time evolution of the spin coherence in LC's, due to the coupling of the spin system to a quantum lattice or environment. This will be done within the framework of the theoretical proposal presented in QD-I.

For the convenience of the reader, hereinafter we include a brief summary of the steps followed in QD-I to work out the nonequilibrium irreversible dynamics of an observed and controlled system coupled to an external unobserved environment. This problem was approached using the following Hamiltonian:

$$\mathcal{H} = \mathcal{H}_S + \mathcal{H}_{SL} + \mathcal{H}_L, \quad (1)$$

where  $\mathcal{H}_S = \mathcal{H}_S^{(s)} \otimes \mathbf{1}^{(f)}$  and  $\mathcal{H}_L = \mathbf{1}^{(s)} \otimes \mathcal{H}_L^{(f)}$  are the Hamiltonians of the observed system and the lattice or unobserved environment respectively. Symbols of the form  $\mathbf{O}^{(s)}$  and  $\mathbf{O}^{(f)}$  indicate operators acting exclusively on the Hilbert space of the system and the lattice respectively. The interaction Hamiltonian acts on both Hilbert spaces, and is represented by  $\mathcal{H}_{SL} = \sum_q \mathbf{F}_q \mathbf{A}_q$ , with  $\mathbf{F}_q = \mathbf{1}^{(s)} \otimes \mathbf{F}_q^{(f)}$ , and  $\mathbf{A}_q = \mathbf{A}_q^{(s)} \otimes \mathbf{1}^{(f)}$ . Index  $q$  can label different characteristics, like a spin pair or a tensor component of the interaction Hamiltonian.

The existence of distinct time scales associated with different physical processes, which become important as the spin dynamics evolves, was postulated. The occurrence of such time scales is subjected to certain general conditions that the relevant Hamiltonians must fulfill. Such requirements are associated with commutation relations between  $\mathcal{H}_S$ ,  $\mathcal{H}_L$  and  $\mathcal{H}_{SL}$  (it is worth to note

that  $[\mathcal{H}_S, \mathcal{H}_L] = 0$ ). In this way, the dynamics of the observed system in the earlier time scale is obtained by assuming that  $[\mathcal{H}_S, \mathcal{H}_{SL}] = 0$  and  $[\mathcal{H}_L, \mathcal{H}_{SL}] = 0$ , which implies a system model called *essentially isolated system*, where the observed system evolves reversibly and the expectation values of the observables decay due to quantum interference. A later time scale is obtained by assuming  $[\mathcal{H}_S, \mathcal{H}_{SL}] = 0$  and  $[\mathcal{H}_L, \mathcal{H}_{SL}] \neq 0$ , where the system model was referred as *essentially adiabatic system*, and the corresponding dynamics of the observed degrees of freedom is irreversible. Finally, the latest time scale is obtained by assuming  $[\mathcal{H}_S, \mathcal{H}_{SL}] \neq 0$  and  $[\mathcal{H}_L, \mathcal{H}_{SL}] \neq 0$ , and the system model was named *system in thermal contact*.

The focus in QD-I was laid on the study of pure decoherence processes of the observables due to the coupling of the system to a quantum environment, without thermalization and relaxation effects. Therefore, the dynamics of the observed system was studied assuming  $[\mathcal{H}_S, \mathcal{H}_{SL}] = 0$ , namely, the system dynamics was described under *essentially isolated* or *essentially adiabatic* models, where the observed system conserves its energy. Within this framework, NMR experiments on a wide variety of nematic LC's can be described using the following Hamiltonian definitions:

$$\mathcal{H}_S = \sum_i \mathcal{H}_{Si}, \quad \mathcal{H}_{SL} = \sum_i \mathcal{H}_{SLi}, \quad (2)$$

where

$$\mathcal{H}_{Si} = -\omega_0 \mathbf{I}_{\mathbf{zi}} + \langle \mathcal{H}_{di} \rangle_f, \quad (3)$$

$$\mathcal{H}_{SLi} = \mathbf{H}_{\mathbf{di}}^{(s)} \otimes \left( \mathbf{S}_{\mathbf{zzi}}^{(f)} - S_{zz} \mathbf{1}^{(f)} \right). \quad (4)$$

Index  $i$  labels the  $i$ -th molecule (the sum runs over the molecules of the whole sample),  $\omega_0 = \gamma B_0$  is the Larmor frequency,  $\gamma$  the proton gyromagnetic ratio and  $B_0$  the strength of the static magnetic field, which is applied along the laboratory  $\hat{\mathbf{z}}$  axis, and  $\mathbf{I}_{\mathbf{zi}}$  is the  $\hat{\mathbf{z}}$  projection of the spin angular momentum for all the protons in the  $i$ -th molecule.

Following, we will describe the nature of the Hamiltonians in Eq. (2). The operator  $\mathbf{H}_{\mathbf{di}}^{(s)}$  in Eq. (4) is the spin part of the contribution  $\mathcal{H}_{SLi}$  to the interaction Hamiltonian  $\mathcal{H}_{SL}$  between the observed system (the protons) and the environment, and is defined as

$$\begin{aligned} \mathbf{H}_{\mathbf{di}}^{(s)} = & -\frac{3}{2} \gamma^2 \hbar \sum_{j \neq k} \frac{1}{r_{jk}^3} \left( \frac{3}{2} \cos^2 \beta_{jk} - \frac{1}{2} \right) \\ & \times \left( \mathbf{I}_{\mathbf{zi}} \mathbf{I}_{\mathbf{zk}} - \frac{1}{3} \vec{\mathbf{I}}_j \cdot \vec{\mathbf{I}}_k \right)_i^{(s)}. \end{aligned} \quad (5)$$

The indices  $j, k$  run over all the proton sites within the  $i$ -th molecule,  $r_{jk}$  is the internuclear distance between spins  $j$  and  $k$ ,  $\beta_{jk}$  stand for the polar angle of the vector  $\vec{r}_{jk}$  with respect to the system fixed to the molecule.

The spin angular momentum is  $\vec{\mathbf{I}}_j = \mathbf{I}_{\mathbf{xj}} \hat{\mathbf{x}} + \mathbf{I}_{\mathbf{yj}} \hat{\mathbf{y}} + \mathbf{I}_{\mathbf{zj}} \hat{\mathbf{z}}$ . The introduction of the quantum character of the environment variables through the operators  $\mathbf{S}_{\mathbf{zzi}}^{(f)}$  in Eq. (4) is a novel contribution of QD-I, which allows a general description of the dipolar Hamiltonian in liquid crystal NMR with the important consequence that the quantum correlation between the observed system and the environment can be included in the dynamic. Precisely, as shown in QD-I, the irreversibility of the spin dynamics naturally emerges in the decoherence time scale when the full-quantum character of the spin-environment interaction energy is assumed. The meaning of  $\mathbf{S}_{\mathbf{zzi}}^{(f)}$  is that of an operator whose eigenvalues  $S_{zzi}$  are the possible values of the  $\mathbf{zz}$  component of the order parameter,  $S_{zzi} = \left( \frac{3}{2} \cos^2 \theta_i - \frac{1}{2} \right)$ , where  $\theta_i$  is the angle between the long molecular axis of the  $i$ -th molecule and the external static magnetic field  $\vec{B}_0$ . Then, the full-quantum dipolar Hamiltonian of nematic LC's is written as

$$\mathcal{H}_d = \sum_i \mathcal{H}_{di}, \quad (6)$$

where

$$\mathcal{H}_{di} = \mathbf{H}_{\mathbf{di}}^{(s)} \otimes \mathbf{S}_{\mathbf{zzi}}^{(f)}, \quad (7)$$

with

$$\mathbf{H}_{\mathbf{di}}^{(s)} = \mathbf{1}^{(s_1)} \otimes \dots \otimes \mathbf{H}_{\mathbf{d}}^{(s_i)} \otimes \dots \otimes \mathbf{1}^{(s_N)},$$

where the superscript  $(s_i)$  indicates an operator acting on the spin Hilbert space of the  $i$ -th molecule. In the definition of Eq. (6), a motionally averaged dipolar Hamiltonian is used, in which the intermolecular spin interactions are averaged out due to the fast molecular diffusion. This means, in a quantum language, that the eigenvalues of the intermolecular lattice operators of the dipolar Hamiltonian are negligible in comparison with the intramolecular ones and the time scale of the dynamics originated from them is much longer than that of the intramolecular spin interaction. Accordingly, such slow dynamics can be neglected. The average dipolar energy is obtained through the lattice density operator as

$$\langle \mathcal{H}_{di} \rangle_f = \text{tr}_f \{ \mathcal{H}_{di} \rho_{L(eq)} \}, \quad (8)$$

where the trace is taken over the lattice variables,  $\langle \cdot \rangle_f \equiv \text{tr}_f \{ \cdot \rho_{L(eq)} \}$  is the expectation value, and  $\rho_{L(eq)}$  is the lattice density operator at thermal equilibrium,

$$\rho_{L(eq)} = \mathbf{1}^{(s)} \otimes e^{-\beta_T \mathcal{H}_L^{(f)}} / \mathcal{N}_f, \quad (9)$$

where  $\beta_T \equiv \frac{1}{k_B T}$ ,  $k_B$  the Boltzmann constant,  $T$  the absolute temperature, and  $\mathcal{N}_f \equiv \text{tr}_f \{ e^{-\beta_T \mathcal{H}_L^{(f)}} \}$ . The dipolar Hamiltonian corresponding to the closed spin system is obtained after the trace over the lattice variables is taken in Eq. (8):

$$\langle \mathcal{H}_{di} \rangle_f = S_{zz} \mathbf{H}_{\mathbf{di}}^{(s)} \otimes \mathbf{1}^{(f)}, \quad (10)$$

with  $S_{zz} \equiv \langle \mathbf{S}_{\mathbf{zzi}}^{(f)} \rangle_f$ .

Finally, using the Zeeman Hamiltonian

$$\mathcal{H}_Z = -\omega_0 \mathbf{I}_z = -\omega_0 \sum_i \mathbf{I}_{zi}, \quad (11)$$

and the average dipolar Hamiltonian of the spin as a closed system

$$\langle \mathcal{H}_d \rangle_f = \sum_i \langle \mathcal{H}_{di} \rangle_f, \quad (12)$$

we define the Hamiltonians in Eq. (2) as

$$\mathcal{H}_S = \mathcal{H}_Z + \langle \mathcal{H}_d \rangle_f, \quad (13)$$

and

$$\mathcal{H}_{SL} = \mathcal{H}_d - \langle \mathcal{H}_d \rangle_f. \quad (14)$$

In closing the definitions of the Hamiltonians of Eq. (1), it is worth to mention that the environment or lattice Hamiltonian  $\mathcal{H}_L$  is associated with the potential energy of the mechanical interaction between the molecules of the whole sample. This Hamiltonian takes into account the molecules as an ensemble of correlated quantum objects. The details of the mechanical intermolecular interaction are not needed to extract some general conclusions about the influence of the environment on the spin dynamics. In fact, knowing whether  $\mathcal{H}_L$  commutes or not with the interaction Hamiltonian  $\mathcal{H}_{SL}$  is enough for concluding about the reversible or irreversible character of decoherence in some time scale, as was shown in QD-I. However, the influence of  $\mathcal{H}_L$  is indirectly taking into account when we introduced the molecular averaged values of lattice operators, as is seen in Eq. (8), and over the distribution probability function of the eigenvalues of such operators, as we will show in Section II A.

In the following, we will discuss how decoherence induced by the environment emerges under the dynamics of the system described by the Hamiltonian of Eq. (1). We are concerned with expectations values of spin observables, therefore, we need to calculate the reduced spin density matrix. First, we introduce the eigenbasis of the operators  $\mathbf{H}_{\mathbf{di}}^{(s)}$ ,  $\{|\zeta s\rangle \equiv |\zeta_1 s_1\rangle \otimes \cdots \otimes |\zeta_i s_i\rangle \otimes \cdots \otimes |\zeta_N s_N\rangle\}$ , which span the spin Hilbert space of the  $N$  molecules of the sample. The symbols  $\zeta_i$ 's indicate the different eigenvalues and  $s_i$  label their degeneration, thus  $\mathbf{H}_{\mathbf{di}}^{(s)}|\zeta s\rangle = \zeta_i|\zeta s\rangle$ . Then, we calculate the density matrix time evolution under the Hamiltonian of Eq. (1). It is convenient for comparison with NMR experiments to use the rotating-frame representation, namely a frame whose  $z$ -axis is parallel to the external magnetic field, and rotates about it with an angular frequency equal to the Larmor frequency. Thus, in this frame the time evolution of the density matrix is

$$\hat{\rho}(t) = \hat{\mathbf{U}}(t) \hat{\rho}_S(0) \rho_{L(eq)} \hat{\mathbf{U}}^\dagger(t), \quad (15)$$

where  $\hat{\mathbf{O}} \equiv e^{-i\omega_0 \mathbf{I}_z t} \mathbf{O} e^{i\omega_0 \mathbf{I}_z t}$  is the representation of operator  $\mathbf{O}$  in the rotating-frame and

$$\hat{\mathbf{U}}(t) = e^{-i\hat{\mathcal{H}}_S t} e^{-i(\sum_i \mathcal{H}_{SLi} + \mathcal{H}_L)t}, \quad (16)$$

where  $\hat{\mathcal{H}}_S = \sum_i \langle \mathcal{H}_{di} \rangle_f$  is the transformed spin Hamiltonian. The initial state of the spin system  $\hat{\rho}_S(0)$  is obtained, for example, after applying a radiofrequency pulse sequence. Therefore, the matrix elements of the reduced density operator,  $\hat{\sigma}(t)$ , in the basis  $\{|\zeta s\rangle\}$  are

$$\begin{aligned} \langle \zeta s | \hat{\sigma}(t) | \zeta' s' \rangle &= \text{tr}_f \{ \langle \zeta s | \hat{\rho}(t) | \zeta' s' \rangle \} \\ &= e^{-i\sum_i (\zeta_i - \zeta'_i) \bar{S} t} \langle \zeta s | \hat{\rho}_S^{(s)}(0) | \zeta' s' \rangle G_{\{\zeta, \zeta'\}}(t), \end{aligned} \quad (17)$$

where  $\bar{S} \equiv \langle \mathcal{H}_{di}^{(f)} \rangle_f \equiv S_{zz}$  and

$$G_{\{\zeta, \zeta'\}}(t) = \text{tr}_f \left\{ \mathbf{U}^{\dagger(f)}(\zeta', t) \mathbf{U}^{(f)}(\zeta, t) \rho_{L(eq)}^{(f)} \right\}, \quad (18)$$

is the decoherence function associated with the time evolution operator

$$\mathbf{U}^{(f)}(\zeta, t) = e^{-i(\sum_i \zeta_i \mathcal{H}_{SLi}^{(f)} + \mathcal{H}_L^{(f)})t}. \quad (19)$$

In order to explicit the spin dynamics of a representative molecule, say the  $i$ -th one, we use the operator expansion technique due to Zassenhaus to factorize the evolution operator (19) into a product of exponential operators, as follows<sup>11,28</sup>:

$$\mathbf{U}^{(f)}(\zeta, t) = e^{-i\mathcal{H}_{Ri}^{(f)}(\zeta)t} e^{-i\zeta_i \mathcal{H}_{SLi}^{(f)}t} \mathbf{U}_C^{(f)(SLi)}(\zeta, t), \quad (20)$$

where we defined the operator

$$\mathcal{H}_{Ri}^{(f)}(\zeta) \equiv \sum_{j \neq i} \zeta_j \mathcal{H}_{SLj}^{(f)} + \mathcal{H}_L^{(f)}. \quad (21)$$

In turn, the third factor in (20) can be expanded as

$$\mathbf{U}_C^{(f)(SLi)}(\zeta, t) = e^{t^2 \mathbf{C}_2^{(f)(SLi)}(\zeta)} e^{t^3 \mathbf{C}_3^{(f)(SLi)}(\zeta)} \cdots, \quad (22)$$

where  $\mathbf{C}_q^{(f)(SLi)}(\zeta)$  represents some  $(q-1)$ -order nested commutator between Hamiltonians  $\mathcal{H}_{Ri}^{(f)}(\zeta)$  and  $\zeta_i \mathcal{H}_{SLi}^{(f)}$ .

In keeping with the same spirit of separating the molecular spin dynamics, we consider the cases where the initial condition  $\hat{\rho}_S(0)$  can be expressed as

$$\hat{\rho}_S(0) = \frac{1}{\mathcal{N}_{S_1}^{N-1}} \sum_i \hat{\rho}_{Si}^{(s)}(0) \otimes \mathbf{1}^{(f)}, \quad (23)$$

where  $\mathcal{N}_{S_1} \equiv \text{tr}_{s_1} \{ \mathbf{1}^{(s_1)} \}$  is the trace of the identity operator in the Hilbert space of the spins belonging to a molecule,  $\hat{\rho}_{Si}^{(s)}(0) = \mathbf{1}^{(s_1)} \otimes \cdots \otimes \hat{\rho}^{(s_i)}(0) \otimes \cdots \otimes \mathbf{1}^{(s_N)}$ , where  $\hat{\rho}^{(s_i)}(0)$  is the initial condition of the spin variables of the  $i$ -th molecule, which is assumed identical for all molecules. Then, the matrix elements of (23) in the spin space are

$$\begin{aligned} \langle \zeta s | \hat{\rho}_S^{(s)}(0) | \zeta' s' \rangle &= \frac{1}{\mathcal{N}_{S_1}^{N-1}} \sum_i \langle \zeta s | \hat{\rho}_{Si}^{(s)}(0) | \zeta' s' \rangle \\ &= \frac{1}{\mathcal{N}_{S_1}^{N-1}} \sum_i \langle \zeta_i s_i | \hat{\rho}^{(s_i)}(0) | \zeta'_i s'_i \rangle \prod_{j \neq i} \delta_{\zeta'_j s'_j}^{\zeta_j s_j}, \end{aligned} \quad (24)$$

where we defined

$$\prod_{j \neq i} \delta_{\zeta'_j s'_j}^{\zeta_j s_j} \equiv \delta_{\zeta_1 s_1, \zeta'_1 s'_1} \cdots \delta_{\zeta_N s_N, \zeta'_N s'_N},$$

as the product of the  $N - 1$  Krönecker deltas associated with all the molecules different from the  $i$ -th one. Then, by using Eqs. (20) and (24), Eq. (17) can be expressed as

$$\begin{aligned} \langle \zeta s | \hat{\sigma}(t) | \zeta' s' \rangle &= \sum_i e^{-i(\zeta_i - \zeta'_i) \bar{S} t} \langle \zeta_i s_i | \hat{\rho}^{(s_i)}(0) | \zeta'_i s'_i \rangle \\ &\times \prod_{j \neq i} \delta_{\zeta'_j s'_j}^{\zeta_j s_j} G_{\{\zeta, \zeta'\}}(t) / \mathcal{N}_{S_1}^{N-1}, \end{aligned} \quad (25)$$

where  $G_{\{\zeta, \zeta'\}}(t)$  is the decoherence function (18) for the cases where the Krönecker deltas present in Eq. (24) do not cancel. Because of the delta functions, (18) is evaluated when  $\zeta_j = \zeta'_j \forall j / j \neq i$  for the expression shown in Eq. (20), hence  $\mathcal{H}_{Ri}^{(f)}(\zeta) = \mathcal{H}_{Ri}^{(f)}(\zeta')$  and in  $\mathbf{U}_C^{(f)(SLi)}(\zeta, t)$  only  $\zeta_i$  is unaffected by such delta functions (i.e. it can be  $\zeta_i \neq \zeta'_i$ ). This reasoning leads to the following expression for the decoherence function

$$\begin{aligned} G_{\{\zeta, \zeta'\}}(t) &= \text{tr}_f \left\{ \mathbf{U}_{C, \zeta'_i}^{\dagger(f)(SLi)}(\zeta, t) e^{-i(\zeta_i - \zeta'_i) \mathcal{H}_{SLi}^{(f)} t} \right. \\ &\quad \left. \times \mathbf{U}_C^{(f)(SLi)}(\zeta, t) \rho_{L(eq)}^{(f)} \right\}, \end{aligned} \quad (26)$$

where we introduced the operator  $\mathbf{U}_{C, \zeta'_i}^{(f)(SLi)}(\zeta, t)$  which can differ from  $\mathbf{U}_C^{(f)(SLi)}(\zeta, t)$  only by the replacement of  $\zeta_i$  by  $\zeta'_i$ . It is worth to remark that if  $\zeta_i = \zeta'_i$  in (26), then the decoherence function satisfies

$$G_{\{\zeta, \zeta_i\}}(t) = \text{tr}_f \left\{ \rho_{L(eq)}^{(f)} \right\} = 1,$$

which indicates that decoherence does not affect the subspace associated with a given degenerate eigenvalue  $\zeta_i$ . An important consequence of this is that, if in the matrix representation of the spin density operator  $\hat{\rho}^{(s_i)}(0)$  in the eigenbasis of  $\mathcal{H}_{SL}^{(s_i)}$  the eigenstates are ordered, in such way that blocks associated with a given eigenvalue  $\zeta_i$  are formed in the diagonal, these blocks remain invariant under decoherence. This property, which was already reflected in Eq. (18) for  $\zeta = \zeta'$ , is of great importance in the dynamics that brings the spin system into a quasi-equilibrium state.

Finally, a zero-trace spin observable acting on the spin spaces of individual molecules, and whose operator is time independent in the rotating-frame, has the general form:

$$\hat{\mathbf{O}} = \sum_i \hat{\mathbf{O}}_i^{(s)} \otimes \mathbf{1}^{(f)}, \quad (27)$$

with  $\hat{\mathbf{O}}_i^{(s)} = \mathbf{1}^{(s_1)} \otimes \cdots \otimes \hat{\mathbf{O}}^{(s_i)} \otimes \cdots \otimes \mathbf{1}^{(s_N)}$ . By using

Eq. (25), the expectation value of  $\hat{\mathbf{O}}$  can be written as

$$\begin{aligned} \langle \hat{\mathbf{O}} \rangle(t) &= \sum_i \sum_{\zeta_i s_i, \zeta'_i s'_i} \langle \zeta_i s_i | \hat{\rho}^{(s_i)}(0) | \zeta'_i s'_i \rangle \\ &\times \langle \zeta'_i s'_i | \hat{\mathbf{O}}^{(s_i)} | \zeta_i s_i \rangle e^{-i(\zeta_i - \zeta'_i) \bar{S} t} G_{\{\zeta_i, \zeta'_i\}}(t), \end{aligned} \quad (28)$$

with

$$G_{\{\zeta_i, \zeta'_i\}}(t) \equiv \sum_{\zeta_1 s_1, \dots, \zeta_N s_N}^{\zeta_k \neq \zeta_i, s_k \neq s_i} G_{\{\zeta, \zeta'\}}(t) / \mathcal{N}_{S_1}^{N-1}, \quad (29)$$

where the sum in Eq. (29) runs over all the values of  $\zeta_k$  and  $s_k$  with  $k \neq i$ .

The irreversibility of the spin dynamics is introduced through of decoherence associated with an open quantum system characterized as an *essentially adiabatic system*. According to the theory, the eigen-selection process, prominently involved in the decoherence process, leaves invariant the block diagonal space of the density operator drawing it to a quasi-equilibrium representation.

As will be shown below, the experimental measurements exhibit the eigen-selection effects during the coherence evolution under a process of partial reversion of the spin dynamics. Besides, two different time scales associated to different sources of decoherence will be distinguished, one of them during free evolution and the other under time reversion of the coherences. In Section II A the reversion pulse sequences used in the experiments are described. The experiments are designed for the case of evolution of single quantum coherence corresponding to the FID signal. However, the procedure and the results can be extended to any kind of coherence. The measurements and the analysis of the results are presented in Section II B. Finally, in Section II C the different sources of error in the experiments are considered.

## A. Definition of the experiments

In order to highlight the contribution to the coherence signal decay coming from sources other than the Liouvillian dynamics corresponding to an isolated spin system (i.e. quantum interference), we will measure the single coherence signal evolution of the FID, when the spins are subjected to a rf pulse sequence configured to compensate the Liouvillian evolution. An experiment of reversion of the spin dynamics under the high field secular dipolar Hamiltonian can be performed by means of the sequence known as MREV8<sup>29-31</sup>, which is shown in Figure 1 (b). An explanation of the effect on the spin dynamics due to such kind of reversion sequence can be found in the supplementary material (see supplementary material<sup>27</sup>, section “Misadjustments in the dynamics under reversion”, for details on the reversion spin dynamics). This sequence was selected because that the quality

in the reversion process relies on the relationship between the total time of the FID evolution and the setting time between pulses. In this reversion pulse sequence, the smaller the setting times  $\tau_1$  and  $\tau_2$  are, the better the reversion will be. Therefore, to access to long reversion periods while keeping the time parameters as small as possible, we apply a pulse sequence consisting of a chain of blocks of the same reversion unit, as is shown in Figure 1 (c). On the other hand, in other techniques like the ‘magic sandwich’,<sup>22,32–34</sup> the mentioned quality relies on the high intensity of the rf pulses and it could become inadequate for cases of long time evolutions due to the requirement of rf pulses of long duration, as is the case of the nematics PAA<sub>d6</sub> and PAA studied in this work.

For the sake of simplicity in the analytical calculation, we will first use the simple unit of Figure 1 (a) to obtain the analytical decoherence function under reversion of a FID. This procedure will allow us to extract general conclusions which can be later extended to the sequences used in the experiments, such as those shown in Figure 1 (b). To study decoherence under reversion, the spin dynamics can be considered as a composition of a free evolution during  $\tau_1$  followed by a ‘reversion’ evolution due to the two pulses separated by the time  $\tau_2$ , as shown in Figure 1 (a). By applying the free evolution operator (16) over the state  $|\zeta s\rangle$ , it is obtained

$$\hat{U}(t)|\zeta s\rangle = e^{-i\sum_i \zeta_i \bar{S}t} |\zeta s\rangle \otimes U^{(f)}(\zeta, t), \quad (30)$$

where  $U^{(f)}(\zeta, t)$  was defined in Eq. (20). Truncating the expansion of Eq. (22) to the first order gives

$$U^{(f)}(\zeta, t) \cong e^{-i\mathcal{H}_{Ri}^{(f)}(\zeta)t} e^{-i\zeta_i \mathcal{H}_{SLi}^{(f)}t} \times e^{\zeta_i \mathbf{C}_{i,SL}^{(f)}(\zeta)t^2/2} e^{\zeta_i \mathbf{C}_{i,L}^{(f)}t^2/2}, \quad (31)$$

which is valid for the intermediate time scale, under the postulate of the existence of different time scales described in the introduction of Section II. The anti-Hermitian operators

$$\mathbf{C}_{i,SL}^{(f)}(\zeta) \equiv \left[ \sum_{j \neq i} \zeta_j \mathcal{H}_{SLj}^{(f)}, \mathcal{H}_{SLi}^{(f)} \right], \quad (32)$$

$$\mathbf{C}_{i,L}^{(f)} \equiv [\mathcal{H}_L^{(f)}, \mathcal{H}_{SLi}^{(f)}], \quad (33)$$

have pure imaginary eigenvalues.

The evolution operator of the dynamics under reversion in the rotating frame can be written, in general, as (see section III.D.2 of QD-I):

$$\hat{U}_{\text{rt}}(t) = e^{i\hat{\mathcal{H}}_S t/\kappa} e^{i(\sum_i \mathcal{H}_{SLi}/\kappa - \mathcal{H}_L)t}, \quad (34)$$

where  $\kappa$  is a positive constant whose value depends on the particular refocusing technique used. The evolution operator factor  $e^{i\hat{\mathcal{H}}_S t/\kappa}$  for the closed spin system under an MREV8 experimental reversion sequence, with a

particular time setting, is obtained in the supplementary material (see supplementary material<sup>27</sup>, section “Misadjustments in the dynamics under reversion”, for details about the analytical expression of the evolution operator of the MREV8 reversion dynamics). For the cases (a) and (b) of Figure 1,  $\kappa = 2$ . By applying (34) over the state  $|\zeta s\rangle$  and truncating as in Eq. (31), we get

$$\hat{U}_{\text{rt}}(t)|\zeta s\rangle = e^{i\sum_i \zeta_i \bar{S}t/\kappa} |\zeta s\rangle \otimes U^{(f)}(-\zeta/\kappa, t), \quad (35)$$

with

$$U^{(f)}(-\zeta/\kappa, t) \cong e^{-i\mathcal{H}_{Ri}^{(f)}(-\zeta/\kappa)t} e^{i\zeta_i \mathcal{H}_{SLi}^{(f)}t/\kappa} \times e^{\zeta_i \mathbf{C}_{i,SL}^{(f)}(\zeta)t^2/(2\kappa^2)} e^{-\zeta_i \mathbf{C}_{i,L}^{(f)}t^2/(2\kappa)}, \quad (36)$$

which is also valid for the intermediate time scale.  $\mathcal{H}_{Ri}^{(f)}(-\zeta/\kappa)$  is obtained by replacing  $\zeta_j$  by  $-\zeta_j/\kappa$ ,  $\forall j$ , in Eq. (21).

The complete evolution operator of the reversion sequence of Figure 1 (a) will be the composition of Eqs. (16) and (34), that is

$$\hat{U}(t_2, t_1) = \hat{U}_{\text{rt}}(t_2) \hat{U}(t_1), \quad (37)$$

written in the rotating system. For a single sequence we have  $t_1 \equiv \tau_1$  and  $t_2 \equiv \tau_2$ , with  $\tau_1$  and  $\tau_2$  defined in Figure 1 (a). In the case of the chaining block sequence shown in Figure 1 (c), the complete evolution operator has the same form as Eq. (37) except that  $t_1 \equiv n\tau_1$  and  $t_2 \equiv n\tau_2$ , being  $n$  the number of blocks. Again, by applying (37) to the state  $|\zeta s\rangle$ , we obtain

$$\hat{U}(t_2, t_1)|\zeta s\rangle = e^{-i\sum_i \zeta_i \bar{S}(t_1 - t_2/\kappa)} |\zeta s\rangle \otimes U^{(f)}(\zeta, t_2, t_1), \quad (38)$$

where

$$U^{(f)}(\zeta, t_2, t_1) \cong e^{-i\mathcal{H}_{Ri}^{(f)}(-\zeta/\kappa)t_2} e^{-i\mathcal{H}_{Ri}^{(f)}(\zeta)t_1} \times e^{-i\zeta_i \mathcal{H}_{SLi}^{(f)}(t_1 - t_2/\kappa)} e^{\zeta_i \mathbf{C}_{i,SL}^{(f)}(\zeta)(t_1^2 + t_2^2/\kappa^2 - 2t_1 t_2/\kappa)/2} \times e^{\zeta_i \mathbf{C}_{i,L}^{(f)}(t_1^2 - t_2^2/\kappa - 2t_1 t_2/\kappa)/2}. \quad (39)$$

Eq. (39) represents the dynamics under an MREV8-like sequence when the experimental setting has  $\tau_1$  and  $\tau_2$  small enough to neglect the non-secular terms of the dipolar Hamiltonian which arises from applying the  $\pi/2$  pulse pairs<sup>35</sup> (see also supplementary material<sup>27</sup>, section “Misadjustments in the dynamics under reversion”, for details about the influence of such non-secular dipolar terms on the MREV8 reversion dynamics). This constraint is imposed over each block in the sequence of Figure 1 (c) but the total times  $n\tau_1$  and  $n\tau_2$  do not need to be so small.

Finally, the evolution operator that represents the spin dynamics due to the pulse sequence of Figure 1 (c) is

completed by adding in Eq. (37) the time operator corresponding to the FID evolution during the time  $t$ , that is

$$\hat{\mathbf{U}}(t, t_2, t_1) = \hat{\mathbf{U}}(t) \hat{\mathbf{U}}_{\text{rt}}(t_2) \hat{\mathbf{U}}(t_1), \quad (40)$$

with the corresponding effect over the state  $|\zeta s\rangle$

$$\begin{aligned} \hat{\mathbf{U}}(t, t_2, t_1) |\zeta s\rangle &= e^{-i \sum_i \zeta_i \bar{S}(t+t_1-t_2/\kappa)} |\zeta s\rangle \\ &\otimes \mathbf{U}^{(f)}(\zeta, t, t_2, t_1), \end{aligned} \quad (41)$$

where we defined

$$\mathbf{U}^{(f)}(\zeta, t, t_2, t_1) \equiv \mathbf{U}^{(f)}(\zeta, t) \mathbf{U}^{(f)}(\zeta, t_2, t_1), \quad (42)$$

which can be approximated by

$$\begin{aligned} \mathbf{U}^{(f)}(\zeta, t, t_2, t_1) &\cong e^{-i \mathcal{H}_{Ri}^{(f)}(\zeta) t} e^{-i \mathcal{H}_{Ri}^{(f)}(-\zeta/\kappa) t_2} \\ &\times e^{-i \mathcal{H}_{Ri}^{(f)}(\zeta) t_1} e^{-i \zeta_i \mathcal{H}_{SLi}^{(f)}(t+t_1-t_2/\kappa)} \\ &\times e^{\zeta_i \mathbf{C}_{i,SL}^{(f)}(\zeta) (t^2-2tt_2/\kappa+2tt_1+t_1^2+t_2^2/\kappa^2-2t_1t_2/\kappa)/2} \\ &\times e^{\zeta_i \mathbf{C}_{i,L}^{(f)}(t^2+2tt_2+2tt_1+t_1^2-t_2^2/\kappa-2t_1t_2/\kappa)/2}, \end{aligned} \quad (43)$$

for small  $\tau_1$  and  $\tau_2$  as in Eq. (39). Now, using Eq. (43) we can obtain, with the same spirit as in QD-I, the decoherence function for the spin dynamics valid for a first time scale longer than the Liouville characteristic time scale, that is

$$\begin{aligned} G_{\{\zeta, \zeta'_i\}}(t, t_2, t_1) &= \text{tr}_f \left\{ \mathbf{U}_{\zeta'_i}^{\dagger(f)}(\zeta, t, t_2, t_1) \right. \\ &\quad \times \left. \mathbf{U}^{(f)}(\zeta, t, t_2, t_1) \rho_{L(eq)}^{(f)} \right\} \\ &= \text{tr}_f \left\{ e^{-i(\zeta_i - \zeta'_i) \mathcal{H}_{SLi}^{(f)}(t+t_1-t_2/\kappa)} \right. \\ &\quad \times e^{-i(\zeta_i - \zeta'_i) i \mathbf{C}_{i,SL}^{(f)}(\zeta) (t^2-2tt_2/\kappa+2tt_1+t_1^2+t_2^2/\kappa^2-2t_1t_2/\kappa)/2} \\ &\quad \times \left. e^{-i(\zeta_i - \zeta'_i) i \mathbf{C}_{i,L}^{(f)}(t^2+2tt_2+2tt_1+t_1^2-t_2^2/\kappa-2t_1t_2/\kappa)/2} \rho_{L(eq)}^{(f)} \right\}, \end{aligned} \quad (44)$$

where we introduced the operator  $\mathbf{U}_{\zeta'_i}^{(f)}(\zeta, t, t_2, t_1)$  which can differ from  $\mathbf{U}^{(f)}(\zeta, t, t_2, t_1)$  only by the replacement of  $\zeta_i$  by  $\zeta'_i$ . The operators  $i \mathbf{C}_{i,SL}^{(f)}$  and  $i \mathbf{C}_{i,L}^{(f)}$  appearing in Eq. (44), are Hermitian due to the anti-Hermitian character of the commutators, as we have seen in (32) and (33), thus their eigenvalues are pure real numbers. By making  $t_2 = \kappa t_1$  (i.e.  $\tau_2 = \kappa \tau_1$ ), we eliminate the Liouville dynamic during the reversion and Eq. (44) becomes in this case

$$\begin{aligned} G_{\{\zeta, \zeta'_i\}}(t, t_1) &= \text{tr}_f \left\{ e^{-i(\zeta_i - \zeta'_i) \mathcal{H}_{SLi}^{(f)} t} \right. \\ &\quad \times e^{-i(\zeta_i - \zeta'_i) i \mathbf{C}_{i,L}^{(f)} \{ [t + (\kappa+1)t_1]^2 - (\kappa^2 + 3\kappa + 2)t_1^2 \} / 2} \\ &\quad \times \left. e^{-i(\zeta_i - \zeta'_i) i \mathbf{C}_{i,SL}^{(f)}(\zeta) t^2 / 2} \rho_{L(eq)}^{(f)} \right\}, \end{aligned} \quad (45)$$

with  $G_{\{\zeta, \zeta'_i\}}(t, t_1) \equiv G_{\{\zeta, \zeta'_i\}}(t, \kappa t_1, t_1)$ . Notice that Eq. (45) depends just on the reversion time  $t_1$ , due to the election  $t_2 = \kappa t_1$ .

To extract a final expression for the decoherence function, we use that the environment states form a continuous and dense space, so that we can replace in the trace the sum by an integral over the lattice space, obtaining

$$\begin{aligned} G_{\{\zeta, \zeta'_i\}}(t, \tau) &= \int df \int dg \int dh k_{f,g} k_{g,h} \rho_{L(eq)}^{h,f} \\ &\times e^{-i(\zeta_i - \zeta'_i) \Delta S_i(f_i) t} e^{-i(\zeta_i - \zeta'_i) C_i^{SL}(h) t^2 / 2} \\ &\times e^{-i(\zeta_i - \zeta'_i) C_i^L(g) \{ (t+\tau)^2 - [1 + (\kappa+1)^{-1}] \tau^2 \} / 2}, \end{aligned} \quad (46)$$

where  $\tau = (\kappa + 1) t_1$  is the total time under reversion,  $k_{f,g} \equiv \langle f | g \rangle$ ,  $k_{g,h} \equiv \langle g | h \rangle$  and  $\rho_{L(eq)}^{h,f} \equiv \langle h | \rho_{L(eq)}^{(f)} | f \rangle$ . We have used in (46) the eigenbasis  $\{|f\rangle\}$ ,  $\{|g\rangle\}$  and  $\{|h\rangle\}$  of the Hermitian operators  $\mathcal{H}_{SLi}^{(f)}$ ,  $i \mathbf{C}_{i,L}^{(f)}$  and  $i \mathbf{C}_{i,SL}^{(f)}(\zeta)$ , respectively, with  $\mathcal{H}_{SLi}^{(f)} |f\rangle = |f_1\rangle \otimes \dots \otimes \mathcal{H}_{SL}^{(f_i)} |f_i\rangle \otimes \dots \otimes |f_N\rangle = \Delta S_i(f_i) |f\rangle$ ,  $\Delta S_i(f_i) = S_i(f_i) - S_{zz}$ ,  $i \mathbf{C}_{i,L}^{(f)} |g\rangle = C_i^L(g) |g\rangle$  and  $i \mathbf{C}_{i,SL}^{(f)}(\zeta) |h\rangle = C_i^{SL}(h) |h\rangle$ , where  $\Delta S_i(f_i)$ ,  $C_i^L(g)$  and  $C_i^{SL}(h)$  are real numbers. Also, we used the closure relations  $\int dg |g\rangle \langle g| = \mathbf{1}^{(f)}$  and  $\int dh |h\rangle \langle h| = \mathbf{1}^{(f)}$ . Now, defining the eigenbasis of the environment or lattice Hamiltonian  $\mathcal{H}_L$  as  $\{|f^E\rangle\}$ , with the eigenvalues  $E_f(f^E)$ , where  $\mathcal{H}_L^{(f)} |f^E\rangle = E_f(f^E) |f^E\rangle$  and using the closure relation  $\int df^E |f^E\rangle \langle f^E| = \mathbf{1}^{(f)}$ , we can write:

$$\rho_{L(eq)}^{h,f} = \int df^E k_{h,f^E} k_{f^E,f} \rho_{L(eq)}(f^E), \quad (47)$$

where

$$\rho_{L(eq)}(f^E) \equiv \langle f^E | \rho_{L(eq)}^{(f)} | f^E \rangle \equiv e^{-\beta_T E_f(f^E)} / \mathcal{N}_f.$$

The final decoherence expression is obtained changing in Eq. (46) the state integration variables  $df$ ,  $dg$  and  $dh$ , by the eigenvalue integration variables  $d\Delta S_i$ ,  $dC_i^L$  and  $dC_i^{SL}$ , thus we can finally write

$$\begin{aligned} G_{\{\zeta, \zeta'_i\}}(t, \tau) &= \int d\Delta S_i e^{-i(\zeta_i - \zeta'_i) \Delta S_i t} \\ &\times \int dC_i^L e^{-i(\zeta_i - \zeta'_i) C_i^L \{ (t+\tau)^2 - [1 + (\kappa+1)^{-1}] \tau^2 \} / 2} \\ &\times \int dC_i^{SL} e^{-i(\zeta_i - \zeta'_i) C_i^{SL} t^2 / 2} p_i(\Delta S_i, C_i^L, C_i^{SL}), \end{aligned} \quad (48)$$

where it is defined the function

$$p_i(\Delta S_i, C_i^L, C_i^{SL}) = \int dE_f \rho_{L(eq)}(E_f) \left[ \int df^E \times \int dg \int dh k_{f,g} k_{g,h} k_{h,f^E} k_{f^E,f} \right]_{C_i^L, C_i^{SL}}^{E_f, \Delta S_i} \quad (49)$$

and  $[\cdot]_{C_i^L, C_i^{SL}}^{E_f, \Delta S_i}$  indicates that the integrals over  $df^E$ ,  $dg$  and  $dh$  are calculated maintaining constant the eigenvalues  $E_f$ ,  $\Delta S_i$ ,  $C_i^L$  and  $C_i^{SL}$ , respectively. Since  $p_i(\Delta S_i, C_i^L, C_i^{SL})$  satisfies

$$\int d\Delta S_i \int dC_i^L \int dC_i^{SL} p_i(\Delta S_i, C_i^L, C_i^{SL}) = 1,$$

it can be interpreted as a probability distribution function of the eigenvalues given by  $\Delta S_i$ ,  $C_i^L$  and  $C_i^{SL}$ .

We can see from Eq. (48) that the decoherence function is the result of a superposition of complex exponential functions weighted by a distribution of their frequencies. Such kind of superposition can be generically expressed as follows:

$$\mathcal{P}_i(\Delta\zeta_i, t, \tau) = \int dA_i e^{-i\Delta\zeta_i \mathcal{Y}_{A_i}(t, \tau)} p_i(A_i, \Delta\zeta_i, t, \tau), \quad (50)$$

with  $\Delta\zeta_i \equiv \zeta_i - \zeta'_i$  and  $\mathcal{Y}_{A_i}(t, \tau)$  is some polynomial in  $t$  and  $\tau$ , the distribution of frequencies of the complex exponential is determined by  $p_i(A_i, \Delta\zeta_i, t, \tau)$ . The expression (50) is a general form for the different integrals in Eq. (48). Therefore, we can use (50) to extract conclusions about (48).

We are concerned with studying the decoherence function produced by the coupling of the spin system with an environment whose states belong to a continuous and dense Hilbert space, where a distribution of the eigenvalues of each complex exponential in Eq. (48) can be defined. In the physic systems we are concerned with, such distribution is supposed to have a general bell-shape form around the mean value of the eigenvalues, converging to zero fast enough so that integrations in Eq. (48) and Eq. (50) can be extended to  $\pm\infty$ . Presumably, these conditions on the eigenvalue distribution functions are similar to those imposed in the work of reference<sup>19</sup> to derive the equilibration of ‘quasi-isolated quantum systems’ in the strict sense.

We can observe that Eq. (50) is the Fourier transform on the variable  $A_i$  of the function  $p_i(A_i, \Delta\zeta_i, t, \tau)$  valued in  $\Delta\zeta_i \mathcal{Y}_{A_i}(t, \tau)$ , that is

$$\begin{aligned} \mathcal{P}_i(\Delta\zeta_i, t, \tau) &= \mathcal{F}_{A_i} \{p_i(A_i, \Delta\zeta_i, t, \tau)\}_{\Delta\zeta_i \mathcal{Y}_{A_i}(t, \tau)} \\ &= \left[ \int_{-\infty}^{+\infty} dA_i e^{-i\alpha A_i} p_i(A_i, \Delta\zeta_i, t, \tau) \right]_{\alpha=\Delta\zeta_i \mathcal{Y}_{A_i}(t, \tau)}. \end{aligned} \quad (51)$$

Therefore, Eq. (48) is the Fourier transform over all the variables of  $p_i(\Delta S_i, C_i^L, C_i^{SL})$ , which is valued in some polynomial in  $t$  and/or  $\tau$  multiplied by  $\Delta\zeta_i$  for each variable. Due to the general bell-shape form assumed for the distribution functions  $p_i(\Delta S_i, C_i^L, C_i^{SL})$  characterizing the environment of our physical system, the superposition of complex exponentials functions which constitutes (48) and (50) will have a form of a decay function in the time  $t$  and/or  $\tau$ . It is easy to see that the bigger the value of  $\Delta\zeta_i$  is, the faster the decay of such function will be. In the case of  $\Delta\zeta_i = 0$  (i.e.  $\zeta_i = \zeta'_i$ ) we have  $G_{\{\zeta, \zeta'_i\}}(t, \tau) = 1$  and we do not have a decay. All these characteristics are described as the eigen-selectivity or the eigen-selection effect over the dynamic of the observed system, as we have seen in QD-I and at the end of the introduction of Section II.

This behaviour of the decoherence function, produced by the eigen-selectivity, is still obtained from a non-truncated time evolution operator, having a more complex form than (43). In such case the form of the decoherence function will be like (48) but with a more extensive development of integrals due to a bigger amount (maybe infinite) of eigenvalues coming from nested commutators of increasing order, and with a more complex distribution function  $p_i$ . Therefore, a complete form (i.e. without truncating) of the decoherence function (48) can be expressed as

$$\begin{aligned} G_{\{\zeta, \zeta'_i\}}(t, \tau) &= \iiint \prod_{D,n} \left\{ dC_{i\zeta}^{D,n} e^{-i\Delta\zeta_i \mathcal{Y}_{D,n}(t, \tau)} C_{i\zeta}^{D,n} \right\} \\ &\times \int d\Delta S_i e^{-i\Delta\zeta_i \Delta S_i t} p_i \left( \Delta S_i, \left\{ C_{i\zeta}^{D,n} \right\}_{D,n} \right), \end{aligned} \quad (52)$$

with

$$\iiint \prod_{D,n} \left\{ dC_{i\zeta}^{D,n} \right\} \int d\Delta S_i p_i \left( \Delta S_i, \left\{ C_{i\zeta}^{D,n} \right\}_{D,n} \right) = 1,$$

where  $\iiint \prod_{D,n} \{\cdot\}$  represents multiple integrals over the eigenvalues of different class of nested commutators labeled by  $D$  and with a nesting order  $n$ . Such eigenvalues are generically termed  $C_{i\zeta}^{D,n}$ . The polynomials  $\mathcal{Y}_{D,n}(t, \tau)$  are functions of  $t$  and/or  $\tau$  which multiply the corresponding  $C_{i\zeta}^{D,n}$  eigenvalue in the complex exponential functions. The symbol  $\left\{ C_{i\zeta}^{D,n} \right\}_{D,n}$  represents a set of such eigenvalues. It is worth to note that the general expression (52) is valid for any kind of experimental setting, the only difference between experiments can be the forms of the polynomials  $\mathcal{Y}_{D,n}$  with a possibly different time dependence.

To extract a more handleable version for the decoherence function, we will use the hypothesis of the existence of different time scales in the dynamics, as was assumed



previously in the introduction of Section II. The suitability of this assumption to describe the physical systems of interest was experimentally confirmed in other works of the authors<sup>11,13</sup>. Under such hypothesis, the dynamics produced by the exponential operator with  $\mathcal{H}_{SLi}^{(f)}$ , which was called *reversible adiabatic quantum decoherence* in QD-I, is faster than the dynamics produced by the remaining exponential operators with nested commutators, which was called *irreversible adiabatic quantum decoherence* in QD-I. Hence, the decay produced by the complex exponentials with  $\Delta S_i$  is faster than the ones produced by the remainder exponentials with eigenvalues  $C_{i\zeta}^{D,n}$ . The experimental evidences<sup>11,13</sup> show that these two time scales are very well separated. Therefore, in Eq. (52), for a time  $t$  over which the decay function produced by the complex exponential with  $\Delta \zeta_i$  is close to vanish, the values of the exponentials with eigenvalues  $C_{i\zeta}^{D,n}$  do not significantly deviate from their values for  $t = 0$ , thus the decoherence function can be very well approximated replacing the multiple integrals over such eigenvalues by their values in  $t = 0$ , namely, it can be approximated using  $\iiint \prod_{D,n} \{\cdot\}_{t=0}$ . Finally, applying this approximation to the particular case of Eq. (48) gives

$$G_{\{\zeta, \zeta'_i\}}(t, \tau) \simeq \int d\Delta S_i e^{-i(\zeta_i - \zeta'_i)\Delta S_i t} \times \int dC_i^L e^{i(\zeta_i - \zeta'_i)C_i^L \tau^2/[2(\kappa+1)]} p_i(\Delta S_i, C_i^L), \quad (53)$$

where it is defined the function

$$p_i(\Delta S_i, C_i^L) \equiv \int dC_{i\zeta}^{SL} p_i(\Delta S_i, C_i^L, C_{i\zeta}^{SL}) = \int dE_f \rho_{L(eq)}(E_f) \times \left[ \int df^E \int df \int dg k_{f,g} k_{g,f^E} k_{f^E,f} \right]_{C_i^L}^{E_f, \Delta S_i}. \quad (54)$$

From Eq. (53), we see that under such approximation the dependence of the decoherence function on  $C_{i\zeta}^{SL}$  is eliminated in Eq. (48), thus the decoherence function only depends on the values of  $\zeta_i$  and  $\zeta'_i$ . Therefore, we will have from Eq. (29)

$$G_{\{\zeta_i, \zeta'_i\}}(t, \tau) \equiv G_{\{\zeta, \zeta'_i\}}(t, \tau).$$

Two additional hypotheses of general character will be assumed on the decoherence function, as follows:

**HypoG-I: Statistical independence between the eigenvalues  $\Delta S_i$  and  $C_i^L$ ,  $\forall i$ .** This hypothesis is reasonable due to the different nature of the spectral properties of their operators. This is written as  $p_i(\Delta S_i, C_i^L) \cong p_i^{\{\Delta S\}}(\Delta S_i) p_i^{\{C^L\}}(C_i^L)$  and it brings us the possibility of writing Eq. (53) as

$$G_{\{\zeta_i, \zeta'_i\}}(t, \tau) \equiv G_{\{\zeta, \zeta'_i\}}(t) G_{\{\zeta_i, \zeta'_i\}}^{(rt)}(\tau),$$

with

$$G_{\{\zeta_i, \zeta'_i\}}(t) \equiv \int d\Delta S_i e^{-i(\zeta_i - \zeta'_i)\Delta S_i t} p_i^{\{\Delta S\}}(\Delta S_i), \quad (55)$$

and

$$G_{\{\zeta_i, \zeta'_i\}}^{(rt)}(\tau) \equiv \int dC_i^L e^{i(\zeta_i - \zeta'_i)C_i^L \tau^2/[2(\kappa+1)]} p_i^{\{C^L\}}(C_i^L). \quad (56)$$

**HypoG-II: Homogeneous environment for each molecule, i.e. absence of border effects.** This is written as  $p_i(\Delta S_i, C_i^L) \equiv p_j(\Delta S_j, C_j^L)$ ,  $\forall i, j$ , and it brings us the relationship

$$G_{\{\zeta_i, \zeta'_i\}}(t, \tau) \equiv G_{\{\zeta_j, \zeta'_j\}}(t, \tau), \quad \forall i, j.$$

At this point, some comments about the MREV8 pulse sequence used in the experiments are pertinent. This sequence is composed of two sequences WHH-4<sup>36</sup>, which correspond to each half in Figure 1 (b). Due to the symmetric disposition of the pulses in the MREV8 sequence, it can be seen that the dynamics under reversion does not depend on the first-order nested commutator  $\mathbf{C}_2^{(f)(SLi)}(\zeta)$  in Eq. (22), which means that the dynamics under reversion produced by  $\mathbf{C}_{i,L}^{(f)}$  in the decoherence function (45) is completely reverted when  $t_2 = \kappa t_1$ . Therefore, in such reversion experiment, the decoherence function with the evolution operator truncated up to the first-order commutator will be equal to the decoherence function (45) putting  $t_1 = 0$ , and it will be equal to (46) or (48) putting  $\tau = 0$ , so they will be independent of the reversion time. Obtaining the decoherence function under MREV8 using a truncated expression for Eq. (22) up to the second-order commutator  $\mathbf{C}_3^{(f)(SLi)}(\zeta)$  would involve a tough calculation.

However, the approximations and conclusions extracted from the general decoherence function form (52) will still be valid and the result obtained in Eq. (53) will differ in the complex exponential function involving  $C_i^L$ . This function will have a dependence with other additional eigenvalues  $C_{i\zeta}^{D,n}$  and their corresponding polynomials  $\mathcal{Y}_{D,n}(t, \tau)$ . Since that aim is out of the scope of our work, we will conserve the decoherence function (53) for our succeeding analysis. Due to the hypotheses **HypoG-I** and **HypoG-II** will be valid in the general case and the final form of decoherence depends on a proposed distribution function of some eigenvalues (as we will see in the following text), the conclusion will be unchanged if we use the asymmetric single reversion sequence of pulses shown in Figure 1 (a).

We will mention too that the small  $\tau_1$  approximation can be improved by adjusting the time between pulses and the pulse width as small as possible. As was mentioned, the factor  $\kappa$  in the operator Eq. (34) is equal two, thus ideally the sequence MREV8 of Figure 1 (b) will

revert the spin dynamics when the condition  $\tau_2 = 2\tau_1$  is satisfied. The reversion experiment for the FID with MREV8 will be that shown in Figure 1 (c) where each block RS(n) is a sequence like the presented in Figure 1 (b). This configuration allows to set the time between pulses as small as allowed by the experimental apparatus, in order to minimize the effects of non-idealities of the sequence. In this case, the time period of evolution under time reversion is  $\tau = n\tau_c$ , where  $n$  is the number of MREV8-blocks, and the FID is acquired during time  $t$ .

The observed FID corresponds to the expectation value of the observable  $\mathbf{I}_y$ , ensuing the reversion sequence. From the theory presented in QD-I, which was revised in the beginning of Section II, using Eq. (28) with  $\hat{\rho}^{(s_1)}(0) = \frac{\beta_T \omega_0}{N S_1} \mathbf{I}_y^{(s_1)}$  and  $\hat{\mathbf{O}}^{(s_1)} = \mathbf{I}_y^{(s_1)}$ , and the decoherence function (53) under **HypoG-I** and **HypoG-II**, in the ‘on-resonance’ condition, we have:

$$\begin{aligned} \langle \hat{\mathbf{I}}_y(t, \tau) \rangle &= \frac{\beta_T \omega_0 N}{N S_1} \sum_{\zeta_1 s_1, \zeta'_1 s'_1} \left| \langle \zeta_1 s_1 | \mathbf{I}_y^{(s_1)} | \zeta'_1 s'_1 \rangle \right|^2 \\ &\times e^{-i(\zeta_1 - \zeta'_1) \bar{S} t} G_{\zeta_1, \zeta'_1}(t) G_{\zeta_1, \zeta'_1}^{(rt)}(\tau), \end{aligned} \quad (57)$$

where  $\bar{S} \equiv \overline{S_1} \equiv \langle \mathbf{S}_{zz}^{(f)} \rangle_f \equiv S_{zz}$  and the values of  $\tau$  are multiples of  $\tau_c$ .

The result of Eq. (57) is similar to the FID obtained in Section III.E in QD-I, with the addition that the signal is attenuated by a decoherent factor given by  $G_{\zeta_1, \zeta'_1}^{(rt)}(\tau)$ , which depends on eigenvalues  $\zeta_1$  and  $\zeta'_1$  of the dipolar Hamiltonian.

In Eq. (57), the function  $G_{\zeta_1, \zeta'_1}(t)$  corresponds to the main decoherence process under a free evolution of the system. This decoherence was called adiabatic quantum decoherence (AQD) in QD-I, with a time scale shorter than the rest of the decoherence processes and a reversible character of its dynamics. As was analyzed in QD-I, in nematic liquid crystals the AQD is associated with the orientational molecular distribution function (OMDF). That distribution is expressed as a distribution of the values of the order parameter  $S_i$ . The distribution function associated here with such decoherence is  $p_i^{\{\Delta S\}}(\Delta S_i)$ , being  $\Delta S_i = S_i - \bar{S}$  and  $\bar{S} = \int dS_1 S_1 p_1^{\{S\}}(S_1)$ . Using the random variable transformation (RVT) theorem<sup>37</sup>, we have that  $p_i^{\{S\}}(S_i) \equiv p_i^{\{\Delta S\}}(S_i - \bar{S})$  (i.e. the distribution function  $p_i^{\{S\}}$  is the same that the one given by  $p_i^{\{\Delta S\}}$  but with its statistical variable shifted in the mean value  $\bar{S}$ ), thus the AQD function in (57) can be expressed as

$$\begin{aligned} G_{\{\zeta_1, \zeta'_1\}}(t) &= \int_{-\infty}^{\infty} d\Delta S_1 e^{-i(\zeta_1 - \zeta'_1) \Delta S_1 t} p_1^{\{\Delta S\}}(\Delta S_1) \\ &= e^{i(\zeta_1 - \zeta'_1) \bar{S} t} \int_{-\infty}^{\infty} dS_1 e^{-i(\zeta_1 - \zeta'_1) S_1 t} p_1^{\{S\}}(S_1). \end{aligned} \quad (58)$$

From Eq. (58), we can see that  $G_{\{\zeta_1, \zeta'_1\}}(t)$  is the same as the one obtained in Section III.C in QD-I, which exposes the relation between the AQD function and the OMDF given by  $p_1^{\{S\}}(S_1)$ .

In QD-I, we have seen that a gaussian distribution is a suitable approximation for the OMDF in nematic, this is

$$p_1^{\{\Delta S\}}(\Delta S_1) = \frac{1}{\sqrt{2\pi \sigma_{S_1}^2}} e^{-\frac{(\Delta S_1)^2}{2\sigma_{S_1}^2}}, \quad (59)$$

with  $\sigma_{S_1}$  the standard deviation of  $S_1$  which is the same for  $\Delta S_1$ .

Finally, we can see that the distribution (59) yields a gaussian form for the AQD function (58) namely

$$G_{\{\zeta_1, \zeta'_1\}}(t) = e^{-\frac{1}{2}(\zeta_1 - \zeta'_1)^2 \sigma_{S_1}^2 t^2}. \quad (60)$$

In Eq. (57), the function  $G_{\zeta_1, \zeta'_1}^{(rt)}(\tau)$  corresponds to the decoherence function produced by the first-order nested commutator belonging to a set of nested commutators which conform the complete evolution operator. The dynamics produced just by this decoherence function could be eventually reverted, by using a particular pulse setting, but it is impossible to revert simultaneously the dynamics of the whole set of commutators, as was demonstrated in Section III.D.2 of QD-I. Therefore, such decoherence function produced by the complete set of nested commutator is irreversible; it was called *essentially adiabatic quantum decoherence* in QD-I and it has a slower dynamics than the reversible AQD, introducing an intermediate time scale between the AQD or Liouvillian process and the process of thermalization.

We can obtain different decay functions for  $G_{\zeta_1, \zeta'_1}^{(rt)}(\tau)$  depending on the form of  $p_1^{\{C^L\}}(C_1^L)$ . For instance, if we have for such distribution a gaussian form

$$p_1^{\{C^L\}}(C_1^L) = \frac{1}{\sqrt{2\pi \sigma_{C_1^L}^2}} e^{-\frac{(C_1^L)^2}{2\sigma_{C_1^L}^2}}, \quad (61)$$

thus decoherence has the following gaussian behavior

$$G_{\zeta_1, \zeta'_1}^{(rt)}(\tau) = e^{-(\zeta_1 - \zeta'_1)^2 \sigma_{C_1^L}^2 \tau^4 / [8(\kappa+1)^2]}. \quad (62)$$

By other hand, for a Lorentzian distribution

$$p_1^{\{C^L\}}(C_1^L) = \frac{1}{\pi} \frac{\delta C_1^L}{(\delta C_1^L)^2 + (C_1^L)^2}, \quad (63)$$

decoherence has the following exponential decay behavior

$$G_{\zeta_1, \zeta'_1}^{(rt)}(\tau) = e^{-|\zeta_1 - \zeta'_1| \delta C_1^L \tau^2 / [2(\kappa + 1)]}. \quad (64)$$

In the following, we will calculate the Fourier transform on the time  $t$  of Eq. (57) with the aim of analyzing the spectral properties of the former function. First, we know that the Fourier transform of a complex exponential function is a Dirac delta function, thus we obtain

$$\mathcal{F}_t \left\{ e^{-i(\zeta_1 - \zeta'_1) \bar{S} t} \right\}(\omega) = 2\pi \delta[\omega - (\zeta'_1 - \zeta_1) \bar{S}]. \quad (65)$$

Next, we will calculate the Fourier transform of the AQD function, that is

$$\begin{aligned} \mathcal{F}_t \{ G_{\{\zeta_1, \zeta'_1\}}(t) \}(\omega) &= \int_{-\infty}^{\infty} dt e^{-i\omega t} \\ &\times \int_{-\infty}^{\infty} d\Delta S_1 e^{-i(\zeta_1 - \zeta'_1) \Delta S_1 t} p_1^{\{\Delta S\}}(\Delta S_1) \\ &= 2\pi \int_{-\infty}^{\infty} d\Delta S_1 \delta[\omega - (\zeta'_1 - \zeta_1) \Delta S_1] p_1^{\{\Delta S\}}(\Delta S_1), \end{aligned} \quad (66)$$

where we have used that

$$\delta[\omega - (\zeta'_1 - \zeta_1) \Delta S_1] = \frac{1}{2\pi} \int_{-\infty}^{\infty} dt e^{-i[\omega - (\zeta'_1 - \zeta_1) \Delta S_1] t}.$$

Using in Eq. (66) the delta function property

$$\delta[\omega - (\zeta'_1 - \zeta_1) \Delta S_1] = \frac{1}{|\zeta'_1 - \zeta_1|} \delta[\Delta S_1 - \omega / (\zeta'_1 - \zeta_1)],$$

we have the following result for the Fourier transform of the AQD function

$$\mathcal{F}_t \{ G_{\{\zeta_1, \zeta'_1\}}(t) \}(\omega) = \frac{2\pi}{|\zeta'_1 - \zeta_1|} p_1^{\{\Delta S\}} \left( \frac{\omega}{\zeta'_1 - \zeta_1} \right). \quad (67)$$

The last step to calculate the Fourier transform in the time  $t$  of Eq. (57) is to obtain the Fourier transform of the product of a complex exponential function with the AQD function, which can be calculated using the convolution<sup>38</sup> of the Fourier transforms (65) and (67), thus we obtain

$$\begin{aligned} \mathcal{F}_t \left\{ e^{-i(\zeta_1 - \zeta'_1) \bar{S} t} G_{\{\zeta_1, \zeta'_1\}}(t) \right\}(\omega) &= \frac{1}{2\pi} \mathcal{F}_t \left\{ e^{-i(\zeta_1 - \zeta'_1) \bar{S} t} \right\}(\omega) * \mathcal{F}_t \{ G_{\{\zeta_1, \zeta'_1\}}(t) \}(\omega) \\ &= \frac{2\pi}{|\zeta'_1 - \zeta_1|} \int_{-\infty}^{\infty} d\omega' \delta[\omega - \omega' - (\zeta'_1 - \zeta_1) \bar{S}] \\ &\quad \times p_1^{\{\Delta S\}} \left( \frac{\omega'}{\zeta'_1 - \zeta_1} \right) \\ &= \frac{2\pi}{|\zeta'_1 - \zeta_1|} p_1^{\{\Delta S\}} \left( \frac{\omega - (\zeta'_1 - \zeta_1) \bar{S}}{\zeta'_1 - \zeta_1} \right). \end{aligned} \quad (68)$$

where  $A(\omega) * B(\omega)$  is the convolution between the functions  $A$  and  $B$ , and we used in (68) that

$$\delta[\omega - \omega' - (\zeta'_1 - \zeta_1) \bar{S}] = \delta\{\omega' - [\omega - (\zeta'_1 - \zeta_1) \bar{S}]\}.$$

Finally, using (68) in (57), we obtain the Fourier transform of the signal produced by the reversion experiment as

$$\begin{aligned} \mathcal{F}_t \left\{ \left\langle \hat{\mathbf{I}}_{\mathbf{y}}(t, \tau) \right\rangle \right\}(\omega) &= \frac{\beta_T \omega_0 N}{\mathcal{N}_{S_1}} \sum_{\zeta_1 s_1, \zeta'_1 s'_1} \left| \langle \zeta_1 s_1 | \mathbf{I}_{\mathbf{y}}^{(s_1)} | \zeta'_1 s'_1 \rangle \right|^2 \\ &\times \frac{2\pi}{|\zeta'_1 - \zeta_1|} p_1^{\{\Delta S\}} \left( \frac{\omega - (\zeta'_1 - \zeta_1) \bar{S}}{\zeta'_1 - \zeta_1} \right) G_{\zeta_1, \zeta'_1}^{(rt)}(\tau). \end{aligned} \quad (69)$$

At this point, we will analyze the meaning of the result in Eq. (69). First, we note that if  $G_{\{\zeta_1, \zeta'_1\}}(t) = 1$  and  $G_{\zeta_1, \zeta'_1}^{(rt)}(\tau) = 1, \forall(t, \tau)$ , in (57), we will obtain the resulting signal of a FID under a description of the spin system as a closed system. Therefore, the Fourier transform of such signal will be a superposition of Dirac deltas shifted at the spectrum characteristic frequencies  $(\zeta'_1 - \zeta_1) \bar{S}$ , like (65). By other hand, if in (57) and (69) we just assumed  $G_{\zeta_1, \zeta'_1}^{(rt)}(\tau) = 1, \forall \tau$ , we would obtain the resulting signal of a FID under the AQD dynamics, which is the same result obtained in Section III.E of QD-I.

The AQD produces the line-shape of the spectrum. Such spectrum is obtained as a superposition of copies of the OMDF shifted at the frequencies  $(\zeta'_1 - \zeta_1) \bar{S}$  and scaled by the factor  $|\zeta'_1 - \zeta_1|$ , as can be seen in (69). This scaling effect of  $|\zeta'_1 - \zeta_1|$  produces the eigen-selection effect in the time domain, due to which the bigger the value of  $|\zeta'_1 - \zeta_1|$  is, the faster the decay of the decoherence function will be. Such effect is reflected in the spectrum making that for higher frequencies  $(\zeta'_1 - \zeta_1) \bar{S}$  the corresponding copy of the OMDF is less intense and wider.

Now we gained more insight to understand the resulting signal under reversion in Eqs. (57) and (69). We can see that the spectrum (69) resembles the one obtained for the AQD in in QD-I, but in the present case there is a modulation produced by decoherence during the reversion dynamics. Such decoherence under reversion produces a faster decay if the value of  $|\zeta'_1 - \zeta_1|$  is higher, as can be seen from Eqs. (62) and (64). Therefore, if we have different spectra for different values of  $\tau$  we should see that the higher the frequency  $(\zeta'_1 - \zeta_1) \bar{S}$  of the spectrum line is, the faster the decay in  $\tau$  will be, provoking a kind of compression of the spectrum. This feature of the dynamics under reversion will provide us a clear method to detect the effects of the eigen-selectivity due to the coupling of the system with the environment.

As a final comment, from Eq. (51) and Eq. (56), we can observe that the decoherence function under reversion is the Fourier transform in the variable  $C_i^L$  of the distribution function  $p_i^{\{C^L\}}$ , valued in  $-(\zeta_i - \zeta'_i) \tau^2 / [2(\kappa + 1)]$ , this is

$$\begin{aligned}
G_{\{\zeta_i, \zeta'_i\}}^{(rt)}(\tau) &= \left[ \mathcal{F}_{C_i^L} \left\{ p_i^{\{C^L\}}(C_i^L) \right\}(\alpha) \right]_{\alpha = -\frac{(\zeta_i - \zeta'_i)\tau^2}{2(\kappa+1)}} \\
&= \left[ \int_{-\infty}^{\infty} dC_i^L e^{-i\alpha C_i^L} p_i^{\{C^L\}}(C_i^L) \right]_{\alpha = -\frac{(\zeta_i - \zeta'_i)\tau^2}{2(\kappa+1)}}.
\end{aligned} \tag{70}$$

The expressions (67) and (70) show the close relation existing between the decoherence process and the distribution function of the variables associated with the environment.

The numerical calculation of Eq. (57) is shown in Figures 2 and 4 for 5CB and PAA<sub>d6</sub> respectively, where a frequency selective gaussian decay was proposed for decoherence along  $t$  and  $\tau$  time scales. In the case of 5CB, we used the ten-spin model (core protons plus the  $\alpha - CH_2$  proton pair) from reference<sup>39</sup> because of the high effort that would involve the inclusion of more spins, which is beyond of the current computational facilities. For PAA<sub>d6</sub>, the eight-spin model presented in QD-I was used. In Figure 2 (a) it can be seen the detail of the FID signals for different values of  $\tau$  in 5CB, while Figure 2 (b) shows the corresponding amplitude spectra. The frontal view of the spectra in Figure 2 (c) shows that the faster decays correspond to the components of higher frequency. This feature is more evident for the normalized spectra of Figure 2 (d), where it can be appreciated the compression of the spectrum for increasing values of  $\tau$ , in correspondence with the smoothing of the signals as seen in Figure 2 (a).

The details of the variation of the normalized amplitude of the spectrum lines of frequencies 5.65 KHz and 8.50 KHz is shown in Figure 3, where it can be appreciated the higher decay rate of the high frequency component. The calculations presented in Figure 2 show the effects on the dynamics introduced by the eigen-selectivity of the decoherence process. The choice of the 5CB sample for demonstrating the effects of the eigen-selectivity was motivated by the clear separation existing between the spectral peaks of the two groups of spectral lines around 5.65KHz and 8.50KHz found in the numerical calculation, corresponding to the strong dipolar couplings of the molecular core and the  $\alpha$ -pair respectively. On the contrary, the spectrum of PAA<sub>d6</sub> does not exhibit a clear distinction among the frequency lines, since the strong dipolar couplings have similar values. However, a compression of the spectra as a function of the reversal time  $\tau$  similar to that found in 5CB is still visible in this compound, as can be seen in Figures 4 (a) and (b), because of which it is used to show that this effect is part of the evidence of the eigen-selectivity of the decoherence process. Notice that if decoherence did not present eigen-selectivity during the reversion period, all the spectral lines would decay with the same rate and therefore the spectral compression would not occur.

Finally, it is worth to remark that the occurrence of

decoherent factors is a consequence of incorporating the ‘mechanical’ variables into the description of the dynamics within a full-quantum view, and that the eigen-selectivity is a direct consequence of this fact. As will be shown in Section II C, the relevant experimental errors do not entail eigen-selectivity. The experimental measurements corresponding to the experiments proposed are presented in Section II B.

## B. Measurements

In this section we present the experimental results obtained by application of the refocalization experiment of Figure 1 (c) in the FID dynamics, which was discussed in detail in Section II A.

The experiments were carried out in a home-built spectrometer, based on a magnet of a Varian EM360, of 60 MHz for protons, with the probe adapted for application of pulsed radiofrequency. The electronic setup allows the complete control of the phase of the pulses, with a precision of 0.022°, a time step of 40 ns, and a minimum configurable time of 240 ns. The rf power used permits rf  $\pi/2$  pulses of about 6.5  $\mu$ s. The homogeneity of the magnetic field is controlled with shimming coils, with a minimum half width of 470Hz approximately, for the spectral lines (using a model of gaussian line-form for each spectral line). The maximum dead time in the signal acquisition is about 18  $\mu$ s. The temperature can be set between 25°C y 150°C, with a medium accuracy of  $\pm 1^\circ$ C and a stability of  $\pm 0.1^\circ$ C.

We made experiments in samples of the nematic liquid crystals 5CB (4'-pentyl-4-biphenyl-carbonitrile), PAA<sub>d6</sub> (methyl deuterated para-azoxyanisole) y PAA (para-azoxyanisole), and the solid adamantane. The solid sample was included for comparison, since this system contains an unlimited number of interacting spins, in contrast with the finite ‘clusters’ comprising the protons of LC molecules. Degradation of spin coherence could also occur in a solid induced by non-spin degrees of freedom, for instance due to lattice phonons. However, this point is out of scope of the present work.

With the purpose of reference for subsequent discussion, in Figure 5 we show the measured FID's with the corresponding spectra, for all the samples studied. These signals are the result of eight acquisitions, except in PAA<sub>d6</sub>, where the signal was acquired 208 times. PAA<sub>d6</sub> and PAA molecules differ in that in the first the methyl groups are replaced by  $CD_3$  groups. In adamantane, while the molecules as a whole are fixed on the solid network, they undergo rapid motions, due to which the crystalline spin system can be effectively represented by a lattice of spins  $1/2$ <sup>40</sup>.

It should be noted that the experimental spectrum of 5CB in Figure 5 (a2) is different from the spectrum numerically calculated with the ten-spin model used in Section II A. It can be seen that in the measured spectrum the higher amplitude peaks are shifted to higher frequen-

cies, while in the calculated spectrum the situation is the opposite. This is so because the ten-spin calculation does not include the remaining  $CH_2$  proton pairs of the alkyl chain, which contribute to the high frequency peak. However, these discrepancies do not invalidate the usefulness of the ten-spin model for appreciating the effects on the spin dynamics of the many-body quantum character of the spin interactions, like the eigen-selectivity, as was shown in Section II A.

The measurements in  $PAA_{d6}$  and PAA were made at temperatures  $T = 115^\circ\text{C}$  and  $T = 110^\circ\text{C}$ , respectively. In the remaining cases, the experiments were carried out at room temperature, namely  $T = 27^\circ\text{C}$ . The MREV8 sequence shown in Figure 1 (b) was set up to mitigate the effects of the finite width of the pulses. The total time of each sequence is  $\tau_c = 2(2\tau_2 + 2\tau_1 + 4t_w)^{35}$ , then  $\tau_1 = \tau_c/12 - t_w$  y  $\tau_2 = \tau_c/6 - t_w$ . For a pulse of  $\pi/2$  with a width of  $t_w = 6.56\mu\text{s}$  and a minimum setting time of  $\tau_1 = 1.6\mu\text{s}$ , we have  $\tau_c = 12(\tau_1 + t_w) = 97.92\mu\text{s}$  and  $\tau_2 = 9.76\mu\text{s}$ . By comparing the time scale of the FID's shown in Figure 5, it can be anticipated that the evolution under the dipolar Hamiltonian during the pulse duration will not have relevance in the experimental results.

In Figure 6 we present experimental results corresponding to the refocalization experiments discussed in Section II A in 5CB under the sequence shown in Figure 1 (c). From the spectral evolution of the ‘time-reversed’ FID's of Figure 6 (a), given in Figure 6 (b) or in more detail in Figure 6 (c) and Figure 6 (d), it can be seen how the spin dynamics is affected by the eigen-selection process during the time reversion (in the last figure the spectra as a function of  $\tau$  are normalized to facilitate the comparison). This becomes more evident when comparing the amplitude variation of two groups of spectral lines, those around the frequencies 5.55KHz and 10.60KHz, as shown in Figure 8 (a). There it can be seen that the peak at 10.60KHz presents a higher decay rate for all  $\tau$ . It can be appreciated in Figure 6 (c) how the two peaks match their amplitudes at  $\tau \approx 361.4\mu\text{s}$ , reverting subsequently their initial amplitude relation. It is worth to note that in the spectra the frequencies lines close to  $f=0\text{Hz}$  are affected by instrumental artifacts like noise in the baseline of the signals. Therefore, the variations in such line should not be giving any physical meaning.

The results of the same experiment performed in nematics  $PAA_{d6}$  and PAA, and solid adamantane, are shown in Figure 7. In  $PAA_{d6}$ , in agreement with the results of the numerical calculation shown in Section II A, it is observed a narrowing of the spectrum, in consistency with a more pronounced decay of the higher frequencies lines. By other hand, in the PAA spectrum low and high frequency groups of lines are resolved. Figure 8 (b) shows the detail of the normalized decay of two lines at 1.60KHz and 7.35KHz. It should be noticed that the decay rate depends on the line position in the frequency spectrum, and the ‘bell’ form associated with the homogeneous broadening of every line (the lineshape produced by AQD) is equally affected by decoherence or non-ideal

effects like static field inhomogeneity. Due to this, for general cases the time evolution of the different parts of the spectrum will be masked by the superposition of broadened lines, preventing the experimental resolution of the decay rates of different parts of the spectrum. Therefore, it can be expected to obtain a suitable detection of the eigen-selectivity in samples with spectrum having groups of lines with certain degree of resolution, like nematics 5CB and PAA.

The experiment sketched in Figure 1 (b) can be modified by changing the MREV8-train by a single block, where the time parameter  $\tau_1$  is varied independently, and the value of  $\tau_2$  is defined as to obtain the maximum signal, being  $\tau_2 > \tau_1$ . For these values of  $\tau_2$  as a function of  $\tau_1$  the slope of a straight line is fitted, whose ideal value is two. By using this dependence, the reversion experiment can be done by using a single block, in such a way to minimize non-idealities present in the pulse setting of the experiments. In this experiment, the reversion time  $\tau$  is a linear function of  $\tau_1$ . The advantage of this method is that it permits a continuous variation of  $\tau_1$  yielding a smooth profile for the signal amplitude in the reversion experiments. On the other hand, long-time settings in such experiment can introduce contributions from the non-secular dipolar Hamiltonian on the dynamics (see supplementary material<sup>27</sup>, section “Misadjustments in the dynamics under reversion”, for details about the influence of the non-secular dipolar part on the MREV8 reversion dynamics).

The results of the reversion experiment using the continuous MREV8 method in 5CB are shown in Figure 9. In Figure 10 is shown the normalized variation with the reversion time of the amplitude of two peaks at distinct frequencies, corresponding to the measurement of Figure 9. There it can be appreciated the frequency selective decay. Due to the finite pulse widths, the initial measured amplitudes correspond to a time  $\tau$  significantly shifted from zero. For these reversion times the frequency selective decay is noticeably, accordingly the first spectra in Figure 9 already presents a larger decay of the higher frequency. This explains the difference with the spectra shown in Figure 6. Except for this last detail, the obtained results show the same features than the reversion experiments using blocks of the MREV8 sequence. Similar results were obtained for the other compounds studied in this work.

By means of the continuous MREV8 experiment it is possible to obtain a detail of the maximum amplitude of the reversed FID's, as a function of the reversion time  $\tau$ . In Figure 11, the results obtained by averaging data near the maximum of each reversed FID are shown, where the signal to noise ratio is larger. Besides, the plots were normalized with respect to the first FID obtained in each experiment. We added three gaussian profiles with different values of standard deviation ( $\sigma = 350\mu\text{s}$ ,  $580\mu\text{s}$ ,  $800\mu\text{s}$ ), used as a guide to the eye. Since the first FID signal already present a significant attenuation, the gaussian curves have a value greater than one for  $\tau = 0$ . It can be

seen that the decay time is longer than the characteristic decay time of the FID for every compound (see Figure 5). This is consistent with the theoretical approach proposed in QD-I, where it is considered that the spin dynamics during the reversion period is governed by a different mechanism than the one which control the spin dynamics during the FID evolution. This quantum process is characterized by a longer time scale, since it is associated with higher order terms of a perturbative treatment. Besides, we can see that for times shorter than  $780\mu s$  the PAA<sub>d6</sub> (with 8 spins per molecule) presents a similar decay behavior that the PAA (with 14 spins per molecule) and the 5CB (with 19 spins per molecule) presents a similar decay behaviour that the adamantane (a solid array of spins) for all  $\tau$  time. These results reflect that decoherence is not associated with the nature of the spins as a closed system.

It is also observed in Figure 11 that the decay in PAA<sub>d6</sub> is more similar to that of PAA than to the one of 5CB. The fact of observing similar responses to decoherence for these two samples is consistent with decoherence being controlled by the coupling of the spin system to external degrees of freedom. For values of  $\tau$  greater than  $780\mu s$ , decoherence in PAA turns stronger, which could be indicating the occurrence of an additional decoherent mechanism associated with the protons of the methyl groups. However, because of the low signal to noise ratio of PAA<sub>d6</sub> and other sources of error, which will be discussed in Section II C, more experiments are necessary to confirm this assertion.

It is worth to note that, using a single MREV8 pulse sequence with a continuous variation of time settings, for long  $\tau$  values the decay can be affected by the influence of the non-secular dipolar Hamiltonian part in the dynamics under reversion (see supplementary material<sup>27</sup>, section “Misadjustments in the dynamics under reversion”, for details about the influence of such non-secular dipolar terms on the MREV8 reversion dynamics). However, such experiment is able to show the intermediate time scale of decoherence as it is the aim in this work. For a more exactly measurement of the decoherence time other techniques can be used, like the ‘magic sandwich’<sup>13,22,32–34</sup>, when they are adequate due to constraints in the experimental setting like the duration of the rf pulses.

Summarizing, from the results presented in this section, we have the following conclusions:

1. the time scale of the attenuation of the time reversed FID signal in MREV8 experiments occurs in a longer time scale than the one of the FID evolution,
2. the high-frequency spectral components decay faster, showing an eigen-selection process,

in total agreement with the theory presented in QD-I. Besides, such intermediate time scale for decoherence,

between the FID evolution and the thermalization process time scales, is consistent with the hypothesis about the existence of dynamics with different time scales used in the theoretical approach of this work and QD-I.

### C. Non-ideal behaviors and approximations in the experiments

The MREV8 sequence shown in Figure 1 (b) has been optimized by adjusting the time parameters  $\tau_1$  and  $\tau_2$ , to mitigate the effects of the finite width  $t_w$  of the pulses, as was commented in Section II B. The shortest interval  $\tau_1$  between pulses was fixed in  $1.6\mu s$ . It is worth to note that in a time of  $6.56\mu s$ , corresponding with a  $\pi/2$  pulse in our experiment, the free evolution dynamics produced by the dipolar interaction is not significant as can be seen from the FID’s shown in Figure 5.

The non-ideality arising in the control of the reversion parameter  $\kappa$  (see Section II A for details about this reversion parameter) would come from deviations from the exact value  $\kappa=2$  due to misadjustments of the  $\pi/2$  pulses. In a similar fashion, a correct setting of the  $\pi/2$  pulses with  $\kappa=2$  could be affected by an incorrect adjustment of the time  $\tau_2$  (i.e. with  $\tau_2 \neq \kappa\tau_1$ ), causing an imperfect reversion of the spin dynamics. These errors could introduce an additional dynamics of the ‘essentially closed’ system<sup>11</sup>, generated by the molecular dipolar Hamiltonian, producing perturbations of the signals and their spectra as a function of the reversion parameter  $\tau$ .

With the aim of estimating the effects of experimental misadjustments, in the following we will obtain several analytical expressions for different kind of errors in the reversion sequence shown in Figure 1 (c) using MREV8 blocks of pulses. We will consider the spin system as a closed system to study the possibility of obtaining some eigen-selection effect in such case, which could overlap with the effects of the coupling with the environment. We relegate to the supplementary material<sup>27</sup>, section “Misadjustments in the dynamics under reversion”, the complete analytical demonstration, as well as the numerical calculation of the signal expressions which will be used in this section.

We introduce the error  $\epsilon$  in the setting of the time under the reversion dynamics by writting  $\tau_2 = (\kappa + \epsilon)\tau_1$ . It is worth to note that such error takes account of misadjustments in the time  $\tau_2$  as well as deviations from a perfect setting of the  $\pi/2$  pulses (see supplementary material<sup>27</sup>, section “Misadjustments in the dynamics under reversion”, for details about the equivalence between  $\tau_2$  time misadjustments and  $\pi/2$  pulses misadjustments). Therefore, we have  $t_2 = (\kappa + \epsilon)t_1$  and the total reversion time  $\tau = (\kappa + 1 + \epsilon)t_1$ . Using such erroneous setting of the  $t_2$  time, we obtain for the expectation value of  $\hat{\mathbf{I}}_y$  corresponding to the closed spin system, under ‘on-resonance’ condition, the following result

$$\begin{aligned}
\langle \hat{\mathbf{I}}_{\mathbf{y}}(t, \tau)^\epsilon \rangle &= \frac{\beta_T \omega_0 N}{\mathcal{N}_{S_1}} t r_{s_1} \left\{ \mathbf{I}_{\mathbf{y}}^{(s_1)} e^{-i \hat{\mathcal{H}}_{S_1}^{(s_1)} t} \right. \\
&\quad \times e^{i \hat{\mathcal{H}}_{S_1}^{(s_1)} \frac{\epsilon/\kappa}{\kappa+1+\epsilon} \tau} \mathbf{I}_{\mathbf{y}}^{(s_1)} e^{-i \hat{\mathcal{H}}_{S_1}^{(s_1)} \frac{\epsilon/\kappa}{\kappa+1+\epsilon} \tau} e^{i \hat{\mathcal{H}}_{S_1}^{(s_1)} t} \left. \right\} \\
&\simeq \frac{\beta_T \omega_0 N}{\mathcal{N}_{S_1}} \sum_{\zeta_1 s_1, \zeta'_1 s'_1} \left| \langle \zeta_1 s_1 | \mathbf{I}_{\mathbf{y}}^{(s_1)} | \zeta'_1 s'_1 \rangle \right|^2 \\
&\quad \times e^{-i(\zeta_1 - \zeta'_1) \bar{S} \left( t - \frac{\epsilon/\kappa}{\kappa+1} \tau \right)},
\end{aligned} \tag{71}$$

where we used the approximation  $\epsilon/\kappa \ll 1$  which implies  $t_1 \simeq \tau/(\kappa+1)$ . The Fourier transform of (71) is

$$\begin{aligned}
\mathcal{F}_t \left\{ \langle \hat{\mathbf{I}}_{\mathbf{y}}(t, \tau)^\epsilon \rangle \right\}(\omega) &= \frac{2\pi \beta_T \omega_0 N}{\mathcal{N}_{S_1}} \sum_{\zeta_1 s_1, \zeta'_1 s'_1} \left| \langle \zeta_1 s_1 | \mathbf{I}_{\mathbf{y}}^{(s_1)} | \zeta'_1 s'_1 \rangle \right|^2 \\
&\quad \times \delta \left[ \omega - (\zeta'_1 - \zeta_1) \bar{S} \right] e^{i(\zeta_1 - \zeta'_1) \bar{S} \frac{\epsilon/\kappa}{\kappa+1} \tau}.
\end{aligned} \tag{72}$$

The expression in Eq. (72), for the Fourier transform of the FID signal for a closed spin system, does not present a decay with some eigen-selection effect, but it shows an oscillatory behaviour of each spectral line proportional to the product of the eigenvalue difference  $\zeta_1 - \zeta'_1$  with the error factor  $\epsilon/\kappa$ .

Other interesting case to consider, is when the FID signal is considered as produced by the different signals coming from a distributed molecular orientation of the main molecular axis of the LC system<sup>41</sup>. In such case, with the same misadjustment as in Eq. (71), we have for the FID

$$\begin{aligned}
\overline{\langle \hat{\mathbf{I}}_{\mathbf{y}}(t, \tau)^\epsilon \rangle} &= \frac{\beta_T \omega_0 N}{\mathcal{N}_{S_1}} \sum_{\zeta_1 s_1, \zeta'_1 s'_1} \left| \langle \zeta_1 s_1 | \mathbf{I}_{\mathbf{y}}^{(s_1)} | \zeta'_1 s'_1 \rangle \right|^2 \\
&\quad \times \int_{-\infty}^{\infty} dS_1 e^{-i(\zeta_1 - \zeta'_1) S_1 \left( t - \frac{\epsilon/\kappa}{\kappa+1} \tau \right)} p_1^{\{S\}}(S_1) \\
&= \frac{\beta_T \omega_0 N}{\mathcal{N}_{S_1}} \sum_{\zeta_1 s_1, \zeta'_1 s'_1} \left| \langle \zeta_1 s_1 | \mathbf{I}_{\mathbf{y}}^{(s_1)} | \zeta'_1 s'_1 \rangle \right|^2 \\
&\quad \times e^{-i(\zeta_1 - \zeta'_1) \bar{S} \left( t - \frac{\epsilon/\kappa}{\kappa+1} \tau \right)} e^{-\frac{1}{2}(\zeta_1 - \zeta'_1)^2 \sigma_{S_1}^2 \left( t - \frac{\epsilon/\kappa}{\kappa+1} \tau \right)^2},
\end{aligned} \tag{73}$$

where  $p_1^{\{S\}}(S_1)$  is the OMDF (see Section II A). The expression (73) is the classical representation of the AQD seen in Section II A. Since the dynamics produced by the error factor  $\epsilon/\kappa$  under the reversion time  $\tau$  is very slow in comparison with the one produced under the free-evolution time  $t$ , we can write

$$\begin{aligned}
\overline{\langle \hat{\mathbf{I}}_{\mathbf{y}}(t, \tau)^\epsilon \rangle} &\simeq \frac{\beta_T \omega_0 N}{\mathcal{N}_{S_1}} \sum_{\zeta_1 s_1, \zeta'_1 s'_1} \left| \langle \zeta_1 s_1 | \mathbf{I}_{\mathbf{y}}^{(s_1)} | \zeta'_1 s'_1 \rangle \right|^2 \\
&\quad \times e^{-i(\zeta_1 - \zeta'_1) \bar{S} \left( t - \frac{\epsilon/\kappa}{\kappa+1} \tau \right)} e^{-\frac{1}{2}(\zeta_1 - \zeta'_1)^2 \sigma_{S_1}^2 \left[ t^2 + \left( \frac{\epsilon/\kappa}{\kappa+1} \tau \right)^2 \right]}.
\end{aligned} \tag{74}$$

The Fourier transform of (74) is

$$\begin{aligned}
\mathcal{F}_t \left\{ \overline{\langle \hat{\mathbf{I}}_{\mathbf{y}}(t, \tau)^\epsilon \rangle} \right\}(\omega) &\simeq \frac{\beta_T \omega_0 N}{\mathcal{N}_{S_1}} \sum_{\zeta_1 s_1, \zeta'_1 s'_1} \left| \langle \zeta_1 s_1 | \mathbf{I}_{\mathbf{y}}^{(s_1)} | \zeta'_1 s'_1 \rangle \right|^2 \\
&\quad \times \frac{2\pi}{|\zeta'_1 - \zeta_1|} \frac{1}{\sqrt{2\pi \sigma_{S_1}^2}} e^{-\frac{1}{2} \left[ \frac{\omega - (\zeta'_1 - \zeta_1) \bar{S}}{(\zeta'_1 - \zeta_1) \sigma_{S_1}} \right]^2} \\
&\quad \times e^{i(\zeta_1 - \zeta'_1) \bar{S} \frac{\epsilon/\kappa}{\kappa+1} \tau} e^{-\frac{1}{2}(\zeta_1 - \zeta'_1)^2 \sigma_{S_1}^2 \left( \frac{\epsilon/\kappa}{\kappa+1} \tau \right)^2}.
\end{aligned} \tag{75}$$

We can see from Eq. (75) that there is a decay factor with eigen-selection effect for each spectral line, but it is masked by an oscillatory behaviour of each frequency line, instead of the monotonous decay that is experimentally observed (see for instance Figures 6 and 8). Besides, such predicted decay is reversible and it would, in principle, be possible to increase the decay time by correcting the misadjustment represented by the factor  $\epsilon/\kappa$ , since the dynamics is very susceptible to changes of  $\epsilon$ . Such changes of  $\epsilon$  modify the decay rates for each spectral lines, but the oscillatory behaviour of such lines can not be suppressed in this way. Indeed, this effect is not observed in the experimental measurements, where the correction of the misadjustments produces the extinction of the oscillatory behaviour under the reversion dynamics. If we see the signal under the reversion time  $\tau$  obtained for the time  $t = 0$ , we have

$$\begin{aligned}
\overline{\langle \hat{\mathbf{I}}_{\mathbf{y}}(0, \tau)^\epsilon \rangle} &= \frac{\beta_T \omega_0 N}{\mathcal{N}_{S_1}} \sum_{\zeta_1 s_1, \zeta'_1 s'_1} \left| \langle \zeta_1 s_1 | \mathbf{I}_{\mathbf{y}}^{(s_1)} | \zeta'_1 s'_1 \rangle \right|^2 \\
&\quad \times e^{i(\zeta_1 - \zeta'_1) \bar{S} \frac{\epsilon/\kappa}{\kappa+1} \tau} e^{-\frac{1}{2}(\zeta_1 - \zeta'_1)^2 \sigma_{S_1}^2 \left( \frac{\epsilon/\kappa}{\kappa+1} \tau \right)^2}.
\end{aligned} \tag{76}$$

The expression (76) corresponds to an FID signal but with a slower time behaviour in comparison with the free-evolution FID. Such behaviour under reversion depends on the time  $\frac{\epsilon/\kappa}{\kappa+1} \tau$  instead of the time  $t$ . The dynamics represented by Eq. (76) is reversible and the oscillations in the signal are unavoidable. Clearly, this is not a feature of the experiments, as was mentioned.

If the setting of the  $\pi/2$  pulses is very erroneous or if the dynamics under reversion is very influenced by the effect of the non-secular dipolar Hamiltonian (for instance, when the time  $\tau_1$  is not small enough to neglect the

dynamics produced by the non-secular dipolar Hamiltonian), we can obtain a dynamics for the signal under reversion as

$$\begin{aligned}
\langle \hat{\mathbf{I}}_{\mathbf{y}}(t, \tau)^\dagger \rangle &= \frac{\beta_T \omega_0 N}{\mathcal{N}_{S_1}} tr_{s_1} \left\{ \mathbf{I}_{\mathbf{y}}^{(s_1)} e^{-i \hat{\mathcal{H}}_{S_1}^{(s_1)} t} \right. \\
&\quad \times e^{-i \hat{\mathcal{H}}_{S_1}^{(s_1)} \tau} \mathbf{I}_{\mathbf{y}}^{(s_1)} e^{i \hat{\mathcal{H}}_{S_1}^{(s_1)} \tau} e^{i \hat{\mathcal{H}}_{S_1}^{(s_1)} t} \left. \right\} \\
&= \frac{\beta_T \omega_0 N}{\mathcal{N}_{S_1}} \sum_{\zeta_1 s_1, \zeta'_1 s'_1} \langle \zeta_1 s_1 | \mathbf{I}_{\mathbf{y}}^{(s_1)} | \zeta'_1 s'_1 \rangle e^{-i(\zeta_1 - \zeta'_1) \bar{S} t} \\
&\quad \times \sum_{\alpha_1, \alpha'_1} \langle \zeta'_1 s'_1 | \alpha'_1 \rangle \langle \alpha'_1 | \mathbf{I}_{\mathbf{y}}^{(s_1)} | \alpha_1 \rangle \langle \alpha_1 | \zeta_1 s_1 \rangle \\
&\quad \times e^{-i(\alpha_1 - \alpha'_1) \tau},
\end{aligned} \tag{77}$$

where  $\hat{\mathcal{H}}_{S_1}^{(s_1)}$  is the resulting Hamiltonian under reversion, which is different of  $\hat{\mathcal{H}}_{S_1}^{(s_1)}$  (see supplementary material<sup>27</sup>, section “Misadjustments in the dynamics under reversion”, for details of the definition of  $\hat{\mathcal{H}}_{S_1}^{(s_1)}$ ). In Eq. (77) the eigenbase  $\{|\alpha_1\rangle\}$  of the Hamiltonian  $\hat{\mathcal{H}}_{S_1}^{(s_1)}$  is defined, where  $\hat{\mathcal{H}}_{S_1}^{(s_1)} |\alpha_1\rangle = \alpha_1 |\alpha_1\rangle$ . The Fourier transform of (77) is

$$\begin{aligned}
\mathcal{F}_t \left\{ \langle \hat{\mathbf{I}}_{\mathbf{y}}(t, \tau)^\dagger \rangle \right\}(\omega) &= \frac{2\pi \beta_T \omega_0 N}{\mathcal{N}_{S_1}} \\
&\times \sum_{\zeta_1 s_1, \zeta'_1 s'_1} \langle \zeta_1 s_1 | \mathbf{I}_{\mathbf{y}}^{(s_1)} | \zeta'_1 s'_1 \rangle \delta[\omega - (\zeta'_1 - \zeta_1) \bar{S}] \\
&\times \sum_{\alpha_1, \alpha'_1} \langle \zeta'_1 s'_1 | \alpha'_1 \rangle \langle \alpha'_1 | \mathbf{I}_{\mathbf{y}}^{(s_1)} | \alpha_1 \rangle \langle \alpha_1 | \zeta_1 s_1 \rangle \\
&\quad \times e^{-i(\alpha_1 - \alpha'_1) \tau},
\end{aligned} \tag{78}$$

where we can see that the decay corresponding to the spectral lines does not present any eigen-selection effect. These effects of misadjustments in the reversion time, with the spin system considered as a closed system, were numerically simulated and the results are shown in the supplementary material<sup>27</sup>, section “Misadjustments in the dynamics under reversion”, where we obtain numerical conclusions which coincide with the analytical analysis.

Finally, to contrast with the commented analytical results about misadjustments in the experimental setting in the closed spin system, we derived the analytical signal produced by the same reversion experiment affected by an erroneous setting of the reversion time, for the open quantum system conformed by the protons coupled to the environment. Using the time setting  $t_2 = (\kappa + \epsilon) t_1$  in the evolution operator (43), we obtain the decoherence function

$$\begin{aligned}
G_{\{\zeta, \zeta'\}}(t, \tau)^\epsilon &= \int d\Delta S_i e^{-i(\zeta_i - \zeta'_i) \Delta S_i \mathcal{Y}_{\Delta S}(t, \tau)^\epsilon} \\
&\times \int dC_i^L e^{-i(\zeta_i - \zeta'_i) C_i^L \mathcal{Y}_L(t, \tau)^\epsilon} \\
&\times \int dC_{i\zeta}^{SL} e^{-i(\zeta_i - \zeta'_i) C_{i\zeta}^{SL} \mathcal{Y}_{SL}(t, \tau)^\epsilon} p_i(\Delta S_i, C_i^L, C_{i\zeta}^{SL}),
\end{aligned} \tag{79}$$

instead of the Eq. (48), where we have used the same considerations involved in Eq. (48). In Eq. (79), we defined

$$\mathcal{Y}_{\Delta S}(t, \tau)^\epsilon = t - \frac{\epsilon/\kappa}{\kappa + 1 + \epsilon} \tau, \tag{80a}$$

$$\begin{aligned}
\mathcal{Y}_L(t, \tau)^\epsilon &= \frac{1}{2} \left\{ (t + \tau)^2 - [1 + (\kappa + 1 + \epsilon)^{-1}] \tau^2 \right. \\
&\quad \left. - [(\kappa + 1 + \epsilon)^{-1} + (\kappa + 1 + \epsilon)^{-2}] \frac{\epsilon}{\kappa} \tau^2 \right\},
\end{aligned} \tag{80b}$$

$$\mathcal{Y}_{SL}(t, \tau)^\epsilon = \frac{1}{2} \left( t - \frac{\epsilon/\kappa}{\kappa + 1 + \epsilon} \tau \right)^2. \tag{80c}$$

Under the approximation in the dynamics of  $\iiint \prod_{D,n} \{\cdot\}_{t=0}$ , used to obtain the well approximated decoherence function shown in Eq. (53), and with  $\epsilon/\kappa \ll 1$ , we can write (79) as

$$\begin{aligned}
G_{\{\zeta, \zeta'\}}(t, \tau)^\epsilon &\simeq \int d\Delta S_i e^{-i(\zeta_i - \zeta'_i) \Delta S_i (t - \frac{\epsilon/\kappa}{\kappa + 1} \tau)} \\
&\times \int dC_i^L e^{i(\zeta_i - \zeta'_i) C_i^L \frac{\tau^2}{2(\kappa + 1)} [1 + (\frac{\kappa + 2}{\kappa + 1}) \frac{\epsilon}{\kappa}]} \\
&\times \int dC_{i\zeta}^{SL} e^{-i(\zeta_i - \zeta'_i) C_{i\zeta}^{SL} \frac{1}{2} (\frac{\epsilon/\kappa}{\kappa + 1} \tau)^2} p_i(\Delta S_i, C_i^L, C_{i\zeta}^{SL}).
\end{aligned} \tag{81}$$

The decoherence function (81), affected by a misadjustment of the reversion time  $t_2$ , will affect the expectation value of  $\hat{\mathbf{I}}_{\mathbf{y}}$  in the way shown in Eq. (28). We can see from Eq. (81) that the decays produced by the integration of the complex exponential function under the total reversion time  $\tau$  can be compensated excepting for the dynamics under the eigenvalue  $C_i^L$ . Such decays present the eigen-selection effect and the oscillations in the signals under the reversion time  $\tau$ , due to the misadjustment of  $t_2$ , can be cancelled. It can also be seen that the decays associated to the eigenvalues  $\Delta S_i$  and  $C_{i\zeta}^{SL}$  can be reverted but the decay due to  $C_i^L$  will never be reverted. Such non-reverted decay constitutes an enveloped which constrains the signal as a function of the reversion time  $\tau$  giving it a bell-like shape, as we will shown in the following text about the experimental



measurements. By making  $\epsilon = 0$  in Eq. (81) we recover Eq. (53), as expected.

In Figure 12 (a) we show the effect mentioned above for the reversion experiment in 5CB, where in Figure 12 (b) it can be seen the variations of the amplitudes of the pseudo-FID, obtained extracting the mean values of the amplitudes of the FID around  $t = 0$ , introduced by the error of  $\kappa$ . By comparing Figure 12 and Figure 6, it can be noticed that in Figure 6 (a) the amplitudes decay monotonously, indicating that the error  $\kappa$  has been satisfactorily mitigated. This dynamics induced by experimental mismatches cannot produce a definitive signal decay, because of the small number of spin degrees of freedom. The latter is true for any error in the pulse configuration. In practice, this effect can be attenuated by varying the time between the two WHH-4 blocks comprising the MREV8 sequence until the oscillations of the amplitudes as a function of  $\tau$  disappear (see Figure 1 (b)). The results shown in Figures 6 and 7 were obtained with this procedure.

The observed signal attenuation might be associated with several causes besides the essentially adiabatic decoherence<sup>11</sup>, like fluctuations of the spin-spin interactions due to thermal molecular motions<sup>42</sup> or even experimental non-idealities like inhomogeneity of the static and the rf magnetic fields. In the work of reference<sup>13</sup>, the experimental sources of error in the ‘magic-sandwich’ (MS) reversion experiment were carefully checked by studying the effect of the sequence on the spin system in the isotropic phase of liquid crystal 5CB. Combination of the MS sequence and a  $\pi$  pulse to reverse the static field inhomogeneity yielded the same response than the usual Hahn-echo two pulse sequence ( $T_2 = 70ms$ ). This also showed that the time scale of the decay produced by thermal fluctuations is much greater than that of the MS experiment in the nematic phase.

In the present work, we studied analytically and experimentally the influence of the field inhomogeneity in the FID dynamics and the reversion dynamics performing experiments on isotropic 5CB (see supplementary material<sup>27</sup>, section “Effects of the field inhomogeneity”, for details about such experiment). The experimental results allowed us to conclude that the dynamics produced by the field inhomogeneity has a time scale longer than that of decoherence and it does not present a behaviour with eigen-selectivity. Besides, it is mentioned that MREV8 experiments combined with  $\pi$  pulses were carried out by the authors in 5CB in the isotropic phase where it was also obtained an exponential decay with a  $T_2$  very similar to the obtained in 5CB in reference<sup>13</sup>. On the other hand, the homogeneity of the rf field was optimized by using a low coil filling factor and the signals obtained from samples with different sizes do not present any different behaviour between them.

These observations give support to the statement that while ‘bulk’ effects like inhomogeneity of the rf pulse and thermal fluctuations of dipole-dipole interaction could

eventually perturb the free spin dynamics, their influence is irrelevant in the intermediate time scale of the reversion experiments. Therefore, the observed decay cannot be associated with experimental non-idealities, but it should be assigned to the irreversible spin dynamics induced by quantum decoherence, whose fingerprint is the eigen-selectivity.

Summaryzing, even when the observed signals are affected by magnetic field inhomogeneities and intermolecular dipole interactions, the contribution of the quantum molecular mechanical dynamics is more important along the different time scales.

### III. DISCUSSION AND CONCLUSIONS

In this work, we studied the spin dynamics which characterizes the irreversible decoherence of a finite quantum interacting spin system coupled with an infinite quantum environment. We experimentally detected in nematic liquid crystals the salient characteristics of the spin dynamics predicted by a full theory which considers the spins as an open quantum system, namely eigen-selectivity, spectral compression and irreversible decoherence under refocusing of the dipolar spin interactions.

The experiments were interpreted in the context of the theory presented in the work of reference<sup>11</sup>, under the main assumption that irreversible decoherence occurs well before that thermal fluctuations play any significant role, and long after the dephasing by quantum interference and reversible adiabatic decoherence. This hypothesis is supported both by our experiments and the work of reference<sup>13</sup>, where it was shown that irreversible decoherence, which cannot be associated with thermalization (neither adiabatic nor nonadiabatic), occurs in an intermediate time scale. Besides, the accurate description achieved in reference<sup>11</sup> of the time domain FID signal by including quantum interference and reversible adiabatic decoherence, allowed us to show that the time scale characterizing the Liouvillian dynamics and such reversible decoherence (which can be interpreted semiclassically) is much shorter than the time scale of the irreversible quantum decoherence.

The analytical-numerical treatment of Section II A allowed us to compare the theoretical expressions derived from the proposed theory, with the experiments. By introducing decoherence functions with gaussian decay profiles, in the free-evolution and reversion dynamics, the effect of the environment was included. The calculations were performed on a 10-spin model for 5CB<sup>39</sup> and on the 8-spin model of PAA<sub>d6</sub> presented in QD-I<sup>11</sup>. The results of the calculations are shown in Section II A and the measurements are shown in Section II B. By using reversion experiments we confirmed the occurrence of the intermediate time scale and the characteristic behaviour

of the irreversible decoherence, and comparison of the analytical FID signals and their spectra under reversion dynamics with the experimental ones confirmed the validity of the theoretical approach presented in QD-I<sup>11</sup> and in this work, beyond the experimental non-idealities.

We present a detailed analysis of the experimental causes that could affect our measurements, in order to identify their characteristic time scales. In the supplementary material<sup>27</sup>, section “Effects of the field inhomogeneity”, we analyse the effect of the inhomogeneities of the static magnetic field. We conclude that the dynamics produced by this effect has a longer time scale than decoherence, and most importantly, it does not present eigen-selectivity. With the aim of checking for a possible frequency dependent behavior induced by pulse misadjustment that might be confused with genuine eigen-selectivity, in Section IIC we present a theoretical analysis of the effects of these misadjustments on the FID signals, considering the spins as a closed system. The simulations on PAA<sub>d6</sub> presented in the supplementary material, section “Misadjustments in the dynamics under reversion” show that misadjustment cannot be the source of the observed eigen-selectivity of a closed spin system. Besides, this kind of non-idealities were theoretically analyzed for decoherence produced by the full-quantum dynamics in Section IIC, as well. The behaviour of the signals extracted by such analysis agrees with the measurement observed. Therefore, this detailed analysis leads us to conclude that the observed eigen-selectivity is an evidence of the open quantum system dynamics.

Eigen-selectivity, which introduces a distinction in the response of the diagonal and off-diagonal elements of the density matrix, provides an efficient irreversible mechanism for coherence decay, while preserves the ‘population’ terms which can only change in a much longer time scale. This behavior explains the observed buildup of the quasi-equilibrium in liquid crystals. The results of this work, together with the conclusions obtained in references<sup>11,13</sup>, can contribute to elucidate the quantum mechanisms underlying decoherence of open quantum systems of interacting spins, for instance

the role played by quantum correlations between the observed system and the environment in the damping of the spin coherences<sup>24,25</sup>. Certainly, these works<sup>11,13</sup> show that in liquid crystals it is essential to assume the quantum character of the spin-environment coupling to explain the observed irreversible decoherence. These statements might also apply to interacting spins in ordinary solids, where irreversible adiabatic decoherence could provide an explanation for the quasi-equilibrium states characterized by spin temperatures<sup>43</sup>.

Summarizing, the occurrence of eigen-selectivity in the spin dynamics under reversion was verified in several nematic liquid crystals, through the direct experimental observation of inhomogeneous decay and spectral compression of the NMR spectrum under refocusing of the dipolar spin interactions, over an intermediate time scale. We conclude that the eigen-selection effect is the fingerprint of decoherence associated with a quantum open spin system in liquid crystals. Besides, the dynamics of such interacting spins, with few degrees of freedom, can be described in terms of quasi-equilibrium states of each molecule after the irreversible decoherence damps out the coherent part of the spin state. Therefore, the observed system reaches these states through a genuine quantum process involving spins and environment, being this a process of different nature than the fluctuations which govern thermalization and relaxation. These findings allow to understand the buildup of the quasi-equilibrium states as being a consequence of the correlated dynamics of the observed system and the quantum environment. Accordingly, the quasi-equilibrium representation in liquid crystal needs not being perceived heuristically, instead, it should be considered as a definite stage of the spin system, during its evolution towards equilibrium.

#### IV. ACKNOWLEDGEMENT

This work was supported by Secretaría de Ciencia y Técnica, Universidad Nacional de Córdoba. The authors would like to thank Dr. C.E. González for useful discussions. H.H.S. thanks CONICET for financial support.

<sup>1</sup> S. Popescu, A.J. Short, and A. Winter. *Nature Physics*, 2:754, 2006.

<sup>2</sup> A. Polkovnikov, K. Sengupta, A.Silva, and M. Vengalattore. *Rev. Mod. Phys.*, 83:863, 2011.

<sup>3</sup> V.I. Yukalov. *Laser Phys. Lett.* 8(7):485, 2011.

<sup>4</sup> P. Reimann. *New Journal of Physics*, 12:055027, 2010.

<sup>5</sup> M. Rigol, V. Dunjko, and M. Olshanii. *Nature*, 452:854, 2008.

<sup>6</sup> V.M. Privman, and D. Mozyrsky. *J. of Stat. Phys.*, 91:787, 1998.

<sup>7</sup> G.M. Palma, K.A. Suominen, and A.K. Ekert. *Proc. R.*

*Soc. Lond. A*, 456:567, 1996.

<sup>8</sup> J.H. Reina, L. Quiroga, and N.F. Johnson. *Phys. Rev. A*, 65:032326, 2002.

<sup>9</sup> J. D. van Beek, A. Hemmi, M. Ernst, and B. H. Meier. *J. Chem. Phys.*, 135:154507, 2011.

<sup>10</sup> T. Charpentier, D. Sakellariou, J. Virlet, F.S. Dzheparov, and J.F. Jacquinet. *J. Chem. Phys.*, 127:224506, 2007.

<sup>11</sup> H.H. Segnorile, and R.C. Zamar. *J. Chem. Phys.*, 135:244509, 2011.

<sup>12</sup> P. De Gennes, and J. Proust. *The Physics of Liquid Crystals*, 2nd ed. Oxford University Press, Oxford, 1993.

- <sup>13</sup> C.E. González, H.H. Segnorile, and R.C. Zamar. *Phys. Rev. E*, 83:011705, 2011.
- <sup>14</sup> R. Bruschweiler, and R.R. Ernst. *Chemical Physics Letters*, 264:393, 1997.
- <sup>15</sup> J.S. Waugh. *Mol. Phys.*, 95:731, 1998.
- <sup>16</sup> J.S. Waugh. *Appl. Magn. Reson.*, 27:165, 2004.
- <sup>17</sup> J.D. Walls, and Y. Lin. *Solid State Nuclear Magnetic Resonance*, 29:22, 2006.
- <sup>18</sup> M. E. Halse, J.-N. Dumez, and L. Emsley. *J. Chem. Phys.*, 136:224511, 2012.
- <sup>19</sup> V.I. Yukalov. *Phys. Lett. A*, 376:550, 2012.
- <sup>20</sup> L. Buljubasich, G.A. Monti, R.H. Acosta, C.J. Bonin, C.E. González, and R.C. Zamar. *J. Chem. Phys.*, 130:024501, 2009.
- <sup>21</sup> St. Limmer, H. Schmiedel, B. Hillner, A. Lösche, and S. Grande. *J. Physique*, 41:869, 1980.
- <sup>22</sup> W. K. Rhim, A. Pines, and J. S. Waugh. *Phys. Rev.*, B3:684, 1971.
- <sup>23</sup> M. Goldman. *Spin Temperature and Nuclear Magnetic Resonance in Solids*. Clarendon, Oxford, 1970.
- <sup>24</sup> J. Helm, and W.T. Strunz. *Phys. Rev. A*, 80:04210, 2009.
- <sup>25</sup> A. Pernice, J. Helm, and W.T. Strunz. *J. Phys. B: At. Mol. Opt. Phys.*, 45:154005, 2012.
- <sup>26</sup> M. M. Sahrpour, and N. Makri. *J. Chem. Phys.*, 138:114109, 2013.
- <sup>27</sup> See Supplementary Material, for details on: Effects of the field inhomogeneity; and Misadjustments in the dynamics under reversion.
- <sup>28</sup> K. Kumar. *J. Math. Phys.*, 6:1928, 1965.
- <sup>29</sup> P. Mansfield. *J. Phys. C*, 4:1444, 1971.
- <sup>30</sup> W. K. Rhim, D. D. Elleman, and R. W. Vaughan. *J. Chem. Phys.*, 58:1772, 1973.
- <sup>31</sup> W. K. Rhim, D. D. Elleman, and R. W. Vaughan. *J. Chem. Phys.*, 59:3740, 1973.
- <sup>32</sup> W. K. Rhim, A. Pines, and J. S. Waugh. *Phys. Rev. Lett.*, 25:218, 1970.
- <sup>33</sup> W. K. Rhim, and H. Kessemeier. *Phys. Rev.*, B3:3655, 1971.
- <sup>34</sup> H. Kessemeier, and W. K. Rhim. *Phys. Rev.*, B5:761, 1972.
- <sup>35</sup> A. Abragam, and M. Goldman. *NUCLEAR MAGNETISM: Order and Disorder, chapter 2*. Clarendon Press - Oxford, 1982.
- <sup>36</sup> J. S. Waugh, L. M. Huber, and U. Haeberlen. *Phys. Rev. Lett.*, 20:180, 1968.
- <sup>37</sup> D. T. Gillespie. *Am. J. Phys.*, 51(6):520, 1983.
- <sup>38</sup> A. V. Oppenheim, A. S. Willsky, and I. T. Young. *Signals and Systems*. Prentice-Hall signal processing series, 1982.
- <sup>39</sup> H.H. Segnorile, C.J. Bonin, C.E. González, R.H. Acosta, and R.C. Zamar. *Solid State Nuclear Magnetic Resonance*, 36:77, 2009.
- <sup>40</sup> I. Schnell, and H. W. Spiess. *Journal of Magnetic Resonance*, 151:153, 2001.
- <sup>41</sup> H. Schmiedel, S. Grande, and B. Hillner. *Phys. Letters*, 91A:365, 1982.
- <sup>42</sup> A. Abragam. *The principles of NUCLEAR MAGNETISM, chapter X*. Oxford University Press, 1961.
- <sup>43</sup> V.A. Skrebnev, and R.N. Zaripov. *Appl. Magn. Reson.*, 16:1, 1999.

## Figures

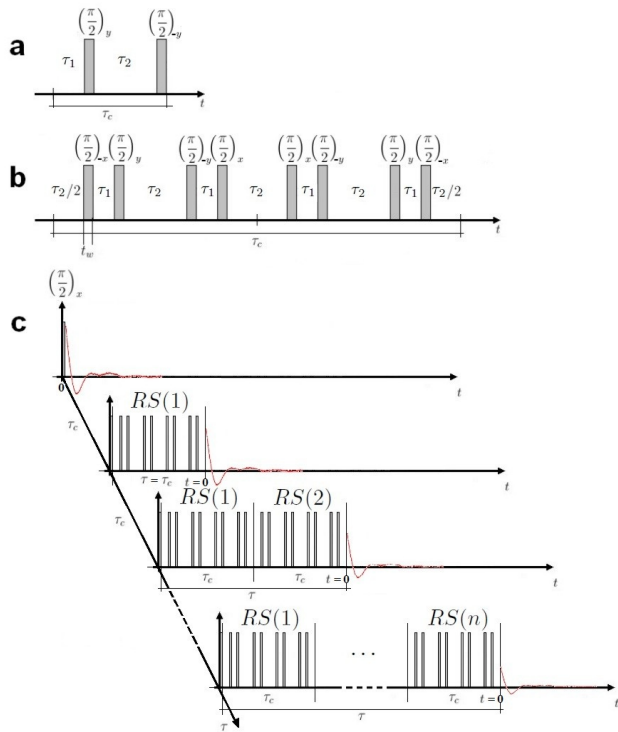


FIG. 1: Experimental pulse sequences. a: Single reversion. b: MREV8. c: Compound reversion sequence, where each reversion block  $RS(i)$  constitutes a single reversion sequence like the MREV8.

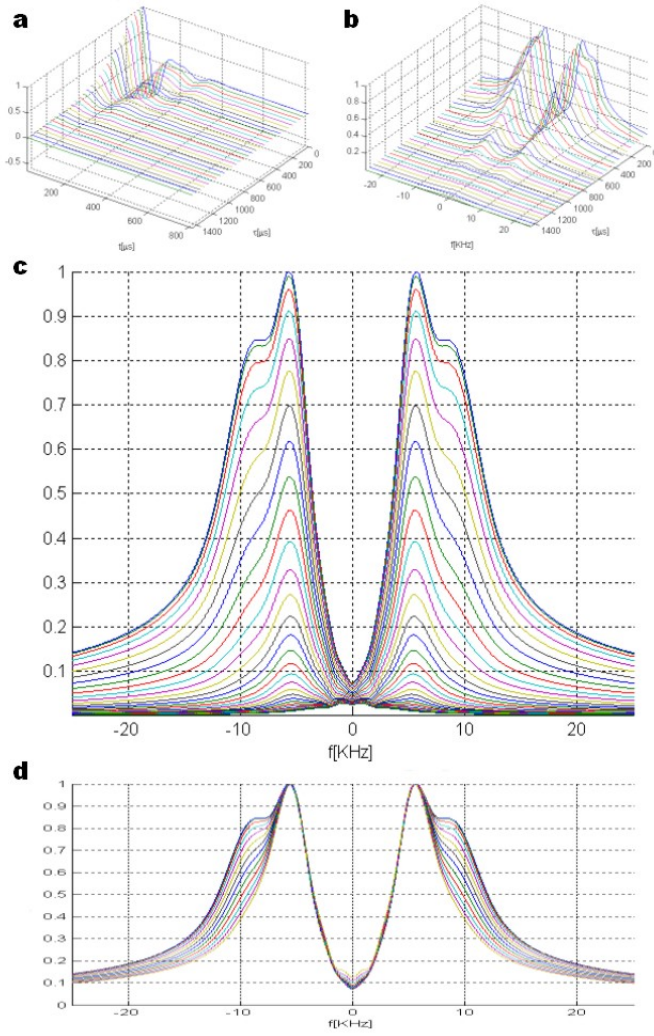


FIG. 2: Calculation of the FID signals under spin reversion dynamics, using MREV8 pulse blocks, for the nematic 5CB molecule in the resonance condition. Decoherence is represented with gaussian profiles in  $t$  and  $\tau$ . Parameters:  $S_{zz} = 0.5403$ ,  $\sigma_t = 0.07$  (standard deviation in  $t$ ),  $\sigma_\tau = 0.04$  (standard deviation in  $\tau$ ). a: FID signals, depending on time  $t$ , as a function of the reversion time  $\tau$ . b: Amplitude spectra for the results in (a). c: Frontal detail of the spectra shown in (b). d: Spectra of (c) normalized to compare the evolution of their frequency components (for clarity only the spectra for the shorter  $\tau$  values are shown). It is observed in (d) the different decay rates of a set of spectral lines close to 5.65KHz and 8.50KHz as well as the spectral compression which are evidences of the eigen-selectivity in the decoherence process.

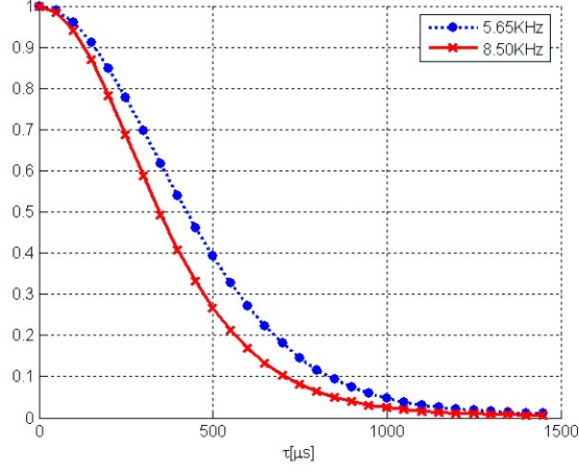


FIG. 3: Calculated evolution of the normalized amplitude as a function of the reversion time  $\tau$  for the spectral lines at 5.65KHz and 8.50KHz of the spectra shown in Figure 2 (b) and (c) for the nematic 5CB.

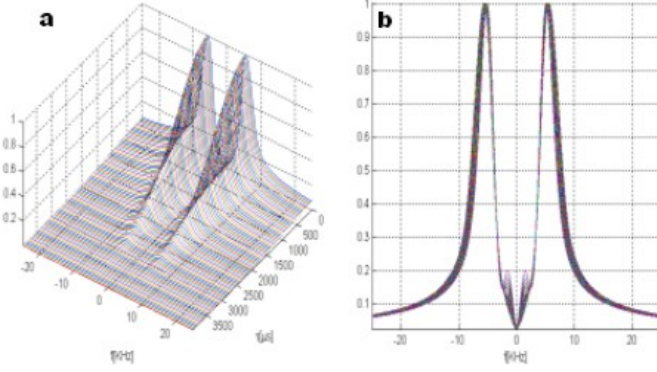


FIG. 4: Calculation of the FID signals under spin reversion dynamics, using MREV8 pulse blocks, for the nematic PAA<sub>d6</sub> molecule in the resonance condition. Decoherence is represented with gaussian profiles in  $t$  and  $\tau$ . Parameters:  $S_{zz} = 0.53$ ,  $\sigma_t = 0.06$  (standard deviation in  $t$ ),  $\sigma_\tau = 0.015$  (standard deviation in  $\tau$ ). a: Amplitude spectra for the calculated FID's. b: Spectra of (a) normalized to compare the evolution of their frequency components (for clarity only the spectra for the shorter  $\tau$  values are shown). It is observed in (b) the spectral compression which is evidence of the eigenselectivity in the decoherence process.

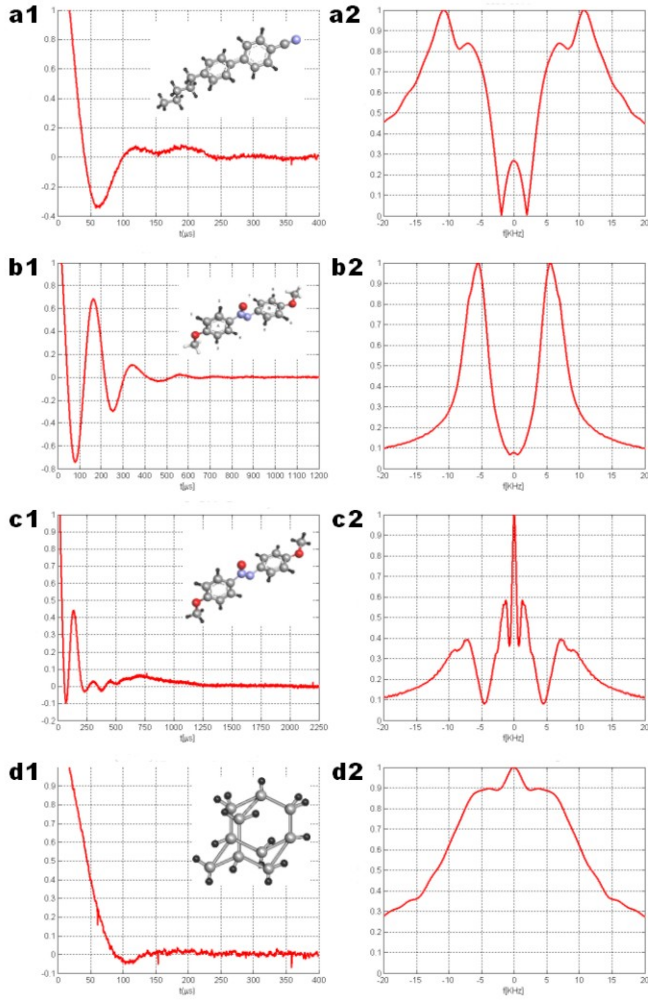


FIG. 5: Molecular sketch (inner detail in the figures), FID evolution (index 1 in the figures) and the FID spectrum (index 2 in the figures) measured for nematic 5CB (a1,a2) at room temperature (namely  $T = 27^\circ\text{C}$ ), PAA<sub>d6</sub> (b1,b2) at  $T = 115^\circ\text{C}$ , PAA (c1,c2) at  $T = 110^\circ\text{C}$ , and solid adamantane (d1,d2).

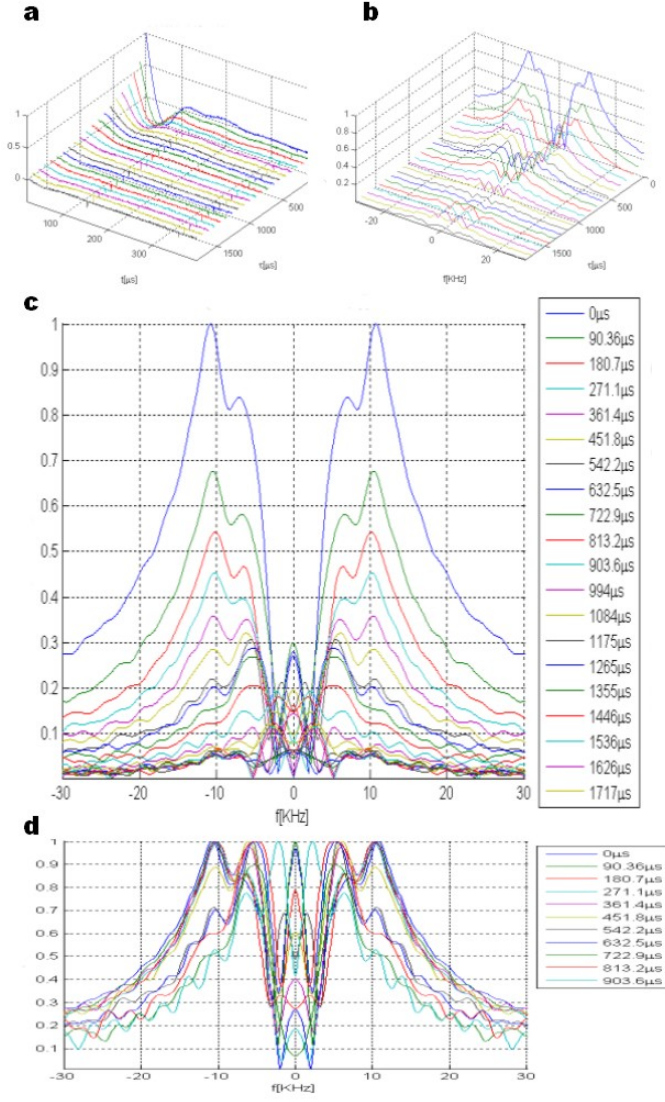


FIG. 6: Experimental results of the FID signals under spin reversion dynamics, using MREV8 pulse blocks, for the nematic 5CB at room temperature (namely  $T = 27^\circ\text{C}$ ) in the resonance condition. a: Measured signals for the FID experiments, depending of the time  $t$ , as a function of the reversion time  $\tau$ . b: Amplitude spectra for the measurements shown in (a). c: Frontal detail of the spectra shown in (b). d: Spectra of (c) normalized to compare the evolution of their frequency components (for clarity only the spectra for the shorter  $\tau$  values are shown). In (c) and (d) is detailed the time  $\tau$  for each spectrum.



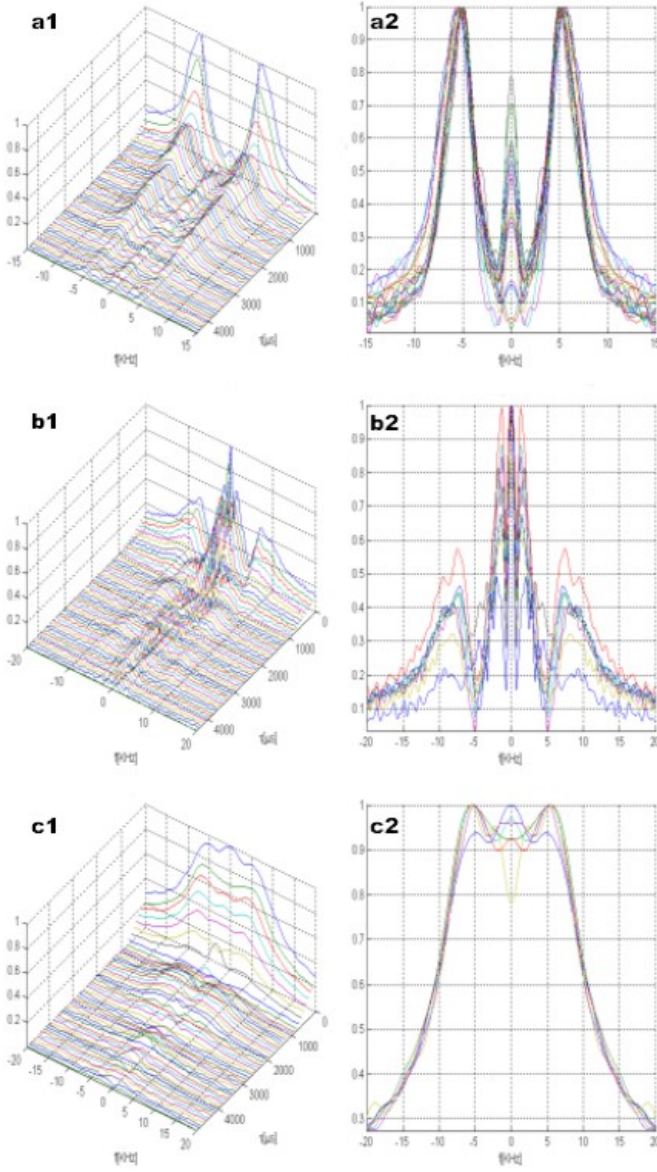


FIG. 7: Experimental results of the FID signals under spin reversion dynamics, using MREV8 pulse blocks, in the resonance condition. The figures with index 1 show the amplitude spectra for the FID measurements and the ones with index 2 show the measured FID spectra, which are normalized to compare the evolution of their frequency components (for clarity only the spectra for the shorter  $\tau$  values are shown). a1,a2: PAA<sub>d6</sub> at T=115°C. b1,b2: PAA at T=110°C. c1,c2: Solid adamantane.

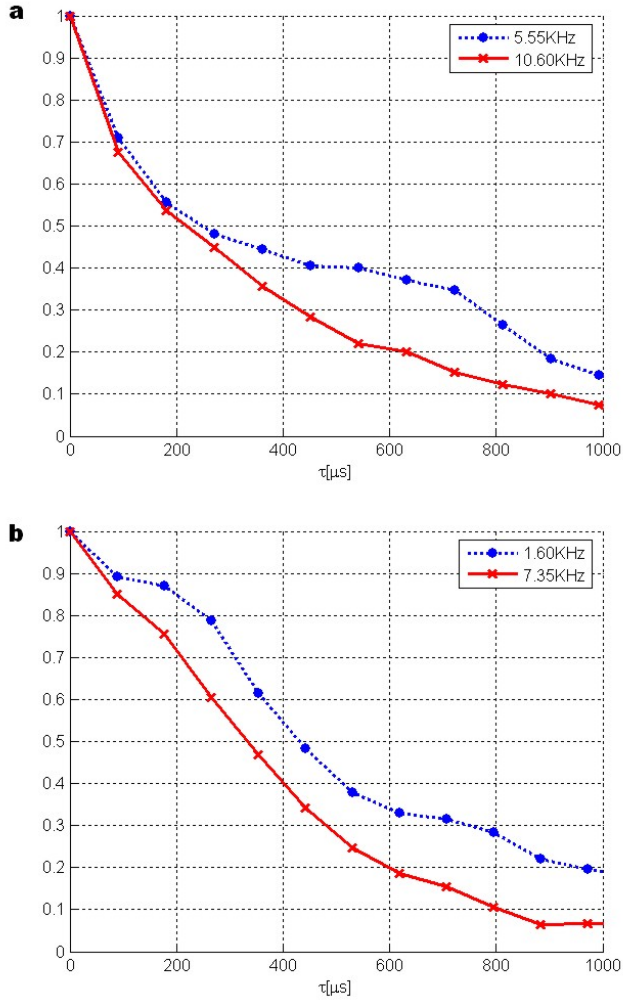


FIG. 8: Measured evolution of the normalized amplitude as a function of the reversion time  $\tau$  for different spectral lines of the FID spectra. a: Spectral lines at 5.55KHz and 10.60KHz for the spectra shown in Figures 6 (b) and (c) for nematic 5CB at room temperature (namely  $T = 27^\circ\text{C}$ ). b: Spectral lines at 1.60KHz and 7.35KHz for the spectra shown in Figure 7 (b1) for the PAA at  $T = 110^\circ\text{C}$ .

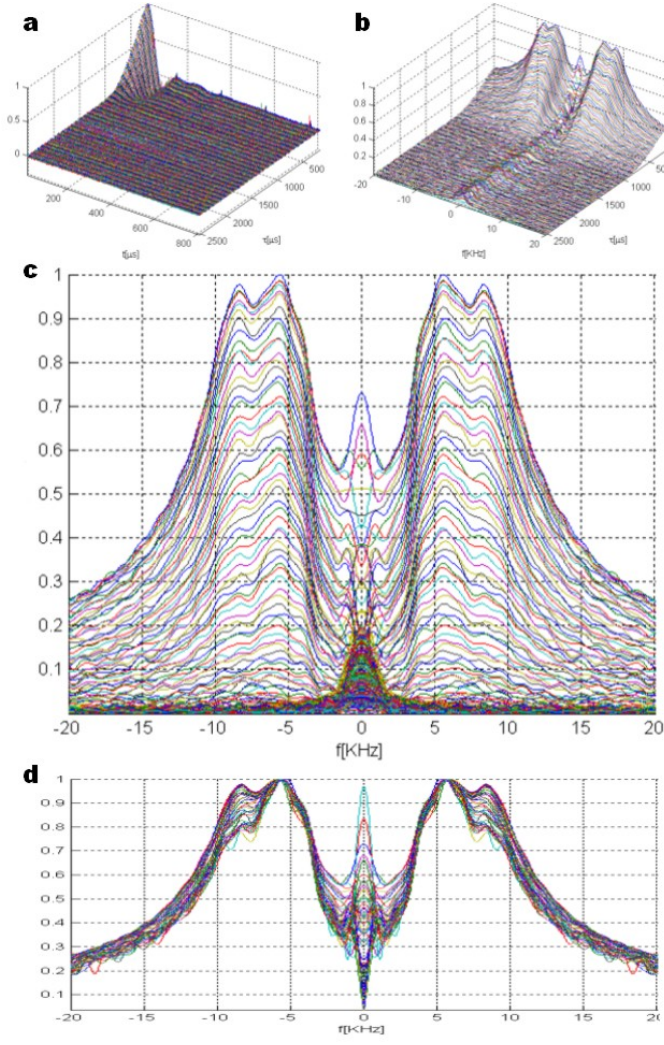


FIG. 9: Experimental results of the FID signals under spin reversion dynamics, using a single MREV8 pulse sequence with a continuous variation of its setting times, for nematic 5CB at room temperature (namely  $T = 27^\circ\text{C}$ ) in the resonance condition. a: Measured signals for the FID experiments, depending of the time  $t$ , as a function of the reversion time  $\tau$ . b: Amplitude spectra for the measurements shown in (a). c: Frontal detail of the spectra shown in (b). d: Spectra of (c) normalized to compare the evolution of their frequency components (for clarity only the spectra for the shorter  $\tau$  values are shown).

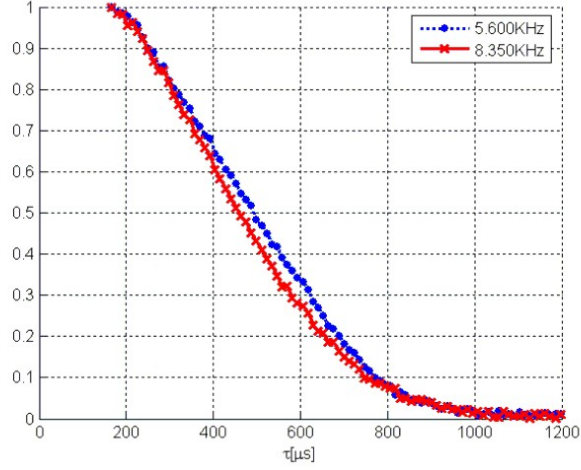


FIG. 10: Measured evolution of the normalized amplitude as a function of the reversion time  $\tau$  for the spectral lines at 5.60 KHz and 8.35 KHz for the spectra shown in Figures 9 (b) and (c) for the nematic 5CB at room temperature (namely  $T = 27^\circ\text{C}$ ). It can be seen the eigen-selectivity where the higher the frequency of the line is, the faster its decay will be. The continuous variation of the setting time allows to see clearly the bell-like form for the decay of the spectral lines.

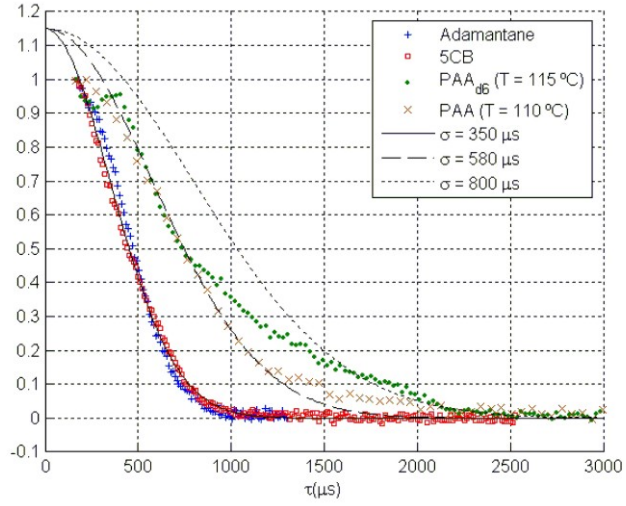


FIG. 11: Experimental results of the normalized evolution of the maximum of the FID signals under spin reversion dynamics, using a single MREV8 pulse sequence with a continuous variation of its setting times, for adamantane and 5CB at room temperature (namely  $T = 27^\circ\text{C}$ ),  $\text{PAA}_{d6}$  at  $T = 115^\circ\text{C}$  and PAA at  $T = 110^\circ\text{C}$ . Three gaussian decays with different standard deviation,  $\sigma$ , are plotted for comparison with the measurements.

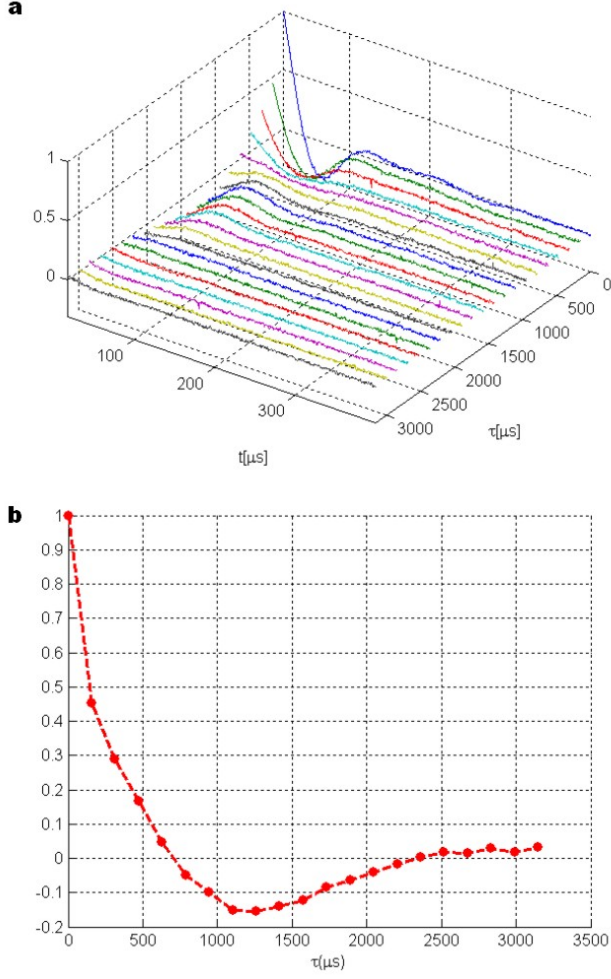


FIG. 12: Experimental results with a misadjustment in the reversion parameter  $\kappa$  of the FID signals under spin reversion dynamics, using MREV8 pulse blocks, in the resonance condition for nematic 5CB at room temperature (namely  $T = 27^\circ\text{C}$ ). a: Measured signals for the FID experiments, depending of the time  $t$ , as a function of the reversion time  $\tau$ . b: Pseudo-FID obtained for the evolutions in  $\tau$  of the FID-signal values in (a) at  $t = 18\mu s$ . Such pseudo-FID presents a signal form similar to the FID signal, but with lower characteristic frequencies.

## Supplementary Material

# Quantum irreversible decoherence behaviour in open quantum systems with few degrees of freedom. Application to $^1\text{H}$ NMR reversion experiments in nematic liquid crystals.

H. H. Segnorile and R. C. Zamar

*Instituto de Física Enrique Gaviola - CONICET, Facultad de Matemática,  
Astronomía y Física, Universidad Nacional de Córdoba*

*M.Allende y H. de la Torre - Ciudad Universitaria, X5016LAE - Córdoba, Argentina*

(Dated: May 7, 2013)

The material below is intended as supplementary material to the article **Quantum irreversible decoherence behaviour in open quantum systems with few degrees of freedom. Application to  $^1\text{H}$  NMR reversion experiments in nematic liquid crystals**. Such manuscript will be referred to as QD-II in the following text.

In Section I we analytically and experimentally will analyse the time scale of the effects produced by the inhomogeneity of the strong magnetic field on the signals obtained from spin observables in liquid crystals (LC). Section II is dedicated to estimate the effects of misadjustments of the characteristic times of the reversion pulse sequence, as well as the influence of the non-secular parts of the dipolar Hamiltonian in such experiments.

## I. EFFECTS OF THE FIELD INHOMOGENEITY

This section is concerned with the analysis of the field inhomogeneity effects on the experimental measurements presented in QD-II. The field inhomogeneity causes the decay of the NMR signals due to a distribution of the  $\hat{\mathbf{z}}$  component of the static magnetic field. Therefore, it is important to know the characteristic behaviour and time scale of that decay in order to compare with the decay produced by decoherence.

To observe the effects of the field inhomogeneity in the nematic phase, we first study the FID signals obtained by applying the Zeeman reversion sequence shown in Figure 1 (a). In a nematic LC, the static magnetic field does not vary significantly inside of each molecule but there is a distribution of the field strength along the whole sample. Such distribution produces a dispersion of the Larmor frequency in the sample. Therefore, the evolution operator due to the field inhomogeneity for a single molecule in the 'on resonance' condition will be

$$\hat{U}^Z(t) = e^{-i\Delta\mathbf{I}_z t}, \quad (1)$$

where  $\Delta = \omega - \omega_0$ . The frequencies  $\omega = \gamma B$  and  $\omega_0 = \gamma B_0$ , with the proton gyromagnetic ratio  $\gamma$ , are produced by the strength  $B$  of the magnetic field inside the molecule and the mean value  $B_0$  of the strength of

the magnetic field of the sample, thus  $\omega_0$  is the frequency of the rotating system and it defines the resonance condition.

The complete dynamics in this condition for the intermediate time scale (see QD-II for details about the existence of different time scales in the dynamics) will be produced by the secular full-quantum dipolar Hamiltonian and the environment or lattice Hamiltonian, studied in QD-II, together with the Zeeman-like Hamiltonian in Eq. (1). Since the Hamiltonian in the evolution operator (1) commutes with the other ones, we can study the dynamics produced by such evolution operator independently of the other evolution operators and readily to include the effects of the inhomogeneity on the complete dynamics.

Keeping the last statement in mind, we can extract the evolution operator due to the field inhomogeneity of the dynamics under the Zeeman reversion experiment shown in Figure 1 (a) for a single molecule and then to conclude how it affects the complete dynamics. Such operator is written as

$$\hat{U}_{RT}^Z(\tau) = \mathbf{R}_x^\dagger e^{-i\Delta\mathbf{I}_z\tau/2} \mathbf{R}_x^\pi e^{-i\Delta\mathbf{I}_z\tau/2} = \mathbf{1}, \quad (2)$$

where is defined the operator  $\mathbf{R}_x^\pi \equiv e^{i\mathbf{I}_x\pi}$  of the pulse in an angle  $\pi$  and direction  $\hat{\mathbf{x}}$  and we used  $\mathbf{R}_x^\dagger \mathbf{I}_z \mathbf{R}_x^\pi = -\mathbf{I}_z$ . Therefore, the expression in Eq. (2) tells us that the field inhomogeneity effect in the whole sample will be removed and the complete dynamics will produce the corresponding signals for the observables, for instance the FID, in the same way as if the inhomogeneity would not exist for an ideal experiment.

We can see the results of such experiments in Figure 2 for the nematic LC's 5CB and PAA<sub>d6</sub>. As is observed there, and comparing with the measured FID's shown in Figure 5 in QD-II, there is no change in the time scale of the FID signals under Zeeman reversion. Therefore, there is not an influence of the field inhomogeneity whose effects can be observed in the FID time scale. It is worth to note that the FID's observed in Figure 2, under a Zeeman reversion dynamics, are different than the free-evolution FID's. Such differences are produced by experimental issue, like the finite width of the  $\pi$  pulses, but they do not change the time scale of the output signals nor the conclusions extracted about that.



Then, we studied the effect of the field inhomogeneity over the dynamics of the pseudo-FID's obtained under the reversion pulse sequence shown in Figure 1 (c) using as  $RS(i)$  blocks an MREV8-like sequence as shown in Figure 1 (b). The aim of such reversion experiment, in our work, is to remove the dynamics produced by the dipolar Hamiltonian. Nevertheless, the environmental decoherence, which is studied in QD-II, and the non-ideal effects or misadjustments in the reversion dynamics, which are studied in Section II in this supplementary material, avoid the complete removal of the dipolar dynamics and a final decay of the signals of the observables is measured. The field inhomogeneity will introduce an extra dynamics produced by a Zeeman-like Hamiltonian (1), and that dynamics will be observed as an extra decay in the measured signals (as we will see), which will be mixed with the other mentioned decays.

To extract the time scale of the decay due to the field inhomogeneity under the mentioned reversion sequence, we performed the experiment described in Figure 1 (c) in a 5CB sample in isotropic phase. In such phase, the dynamics is governed by a Zeeman-like Hamiltonian of the inhomogeneity, which is the same Hamiltonian as in the nematic phase, but in the isotropic phase the dipolar Hamiltonian is averaged out. In the longest time scale, the thermalization, which is studied by relaxation theories, will produce a final decay of the signals, but such time scale is much longer than that of decoherence. Therefore, the fast decays observed in the pseudo-FID's under reversion dynamics in the isotropic phase can be associated mainly to the field inhomogeneity.

In the same way that in the former experiment, where it is obtained the evolution operator (2), we first calculate the evolution operator due to the field inhomogeneity for the sequence shown in Figure 1 (b) for a single molecule. Such evolution operator is written as

$$\hat{U}_{RS}^Z(\tau_1) = e^{-i\Delta\mathbf{I}_z\tau_1} e^{i\Delta\mathbf{I}_y\tau_1} e^{i\Delta\mathbf{I}_x2\tau_1} e^{i\Delta\mathbf{I}_y\tau_1} \times e^{-i\Delta\mathbf{I}_z2\tau_1} e^{-i\Delta\mathbf{I}_y\tau_1} e^{-i\Delta\mathbf{I}_x2\tau_1} e^{-i\Delta\mathbf{I}_y\tau_1} e^{-i\Delta\mathbf{I}_z\tau_1}. \quad (3)$$

It can be observed in Eq. (3) that there are exponential operators with the same exponent and with opposite sign, thus it will produce a cancellation effect of their dynamics. For small enough values of the time  $\tau_1$ , the operator (3) can be approximated as

$$\hat{U}_{RS}^Z(\tau) \simeq e^{-i\Delta\mathbf{I}_z\tau/3}, \quad (4)$$

where  $\tau = 12\tau_1$  for a single MREV8 block. A reversion experiment with  $n$  blocks of the MREV8 pulse sequence will have for the field inhomogeneity a similar evolution operator as in Eq. (4), in the approximation of small times, with  $\tau = 12n\tau_1$ .

Comparing Eq. (4) with Eq. (1), we can see that the dynamics under reversion using MREV8 blocks is a third slower than the free-evolution dynamics, thus the reversion experiment mitigates the decay effect over the

signals due to the field inhomogeneity.

Next, using the evolution operators for a free-evolution dynamics, Eq. (1), and for a reversion dynamics, Eq. (4), we obtain the signals of the whole sample of an isotropic LC affected by a field inhomogeneity as

$$\langle \hat{\mathbf{I}}_y(t, \tau) \rangle^{iso} = \frac{\beta_T \omega_0}{\mathcal{N}_{S_1}} \sum_i \sum_{\zeta_i s_i, \zeta'_i s'_i} \left| \langle \zeta_i s_i | \mathbf{I}_y^{(s_i)} | \zeta'_i s'_i \rangle \right|^2 \times e^{\pm(\zeta_i s_i, \zeta'_i s'_i) i\Delta_i(t+\tau/3)}, \quad (5)$$

where the index  $i$  labels the  $i$ -th molecule (the sum runs over the molecules of the whole sample),  $\{|\zeta_i s_i\rangle\}$  is a base in the Hilbert space of the spins of the  $i$ -th molecule which are eigenstates of the spin part of the interaction dipolar Hamiltonian. Since the dipolar and the Zeeman Hamiltonians commute, such base can be selected as a common eigenbase of the Zeeman Hamiltonian as well. In Eq. (5), the symbol  $\pm(\zeta_i s_i, \zeta'_i s'_i)$  represents the possible values  $+1$  or  $-1$  depending of the difference in the Zeeman eigenvalues of the states  $|\zeta_i s_i\rangle$  and  $|\zeta'_i s'_i\rangle$ , such difference can only have the values  $\pm 1$  due that the non-null matrix elements of the operator  $\mathbf{I}_y^{(s_i)}$  connect eigenstates with such difference of Zeeman eigenvalues. Besides, we defined  $\mathcal{N}_{S_1} \equiv \text{tr}_{s_1} \{\mathbf{1}^{(s_1)}\}$  and  $\beta_T \equiv \frac{1}{k_B T}$ , with  $k_B$  the Boltzmann constant and  $T$  the absolute temperature.

The matrix elements  $\langle \zeta_i s_i | \mathbf{I}_y^{(s_i)} | \zeta'_i s'_i \rangle$  are the same for different molecules. We suppose a dense and continuous distribution of the Larmor frequency shifts  $\Delta$  for the molecules (which is realistic for a typical field inhomogeneity). Due to this, we can replace the sum over the molecules in the sample as an integration over the values of  $\Delta$ . Therefore, Eq. (5) can be written as

$$\langle \hat{\mathbf{I}}_y(t, \tau) \rangle^{iso} = \frac{\beta_T \omega_0 N}{\mathcal{N}_{S_1}} \sum_{\zeta_1 s_1, \zeta'_1 s'_1} \left| \langle \zeta_1 s_1 | \mathbf{I}_y^{(s_1)} | \zeta'_1 s'_1 \rangle \right|^2 \times G_Z(t + \tau/3). \quad (6)$$

In Eq. (6) it is defined

$$G_Z(t) = \int d\Delta e^{i\Delta t} p_Z(\Delta), \quad (7)$$

where  $p_Z(\Delta)$  is the distribution function of  $\Delta$  and  $p_Z(\Delta)d\Delta = n(\Delta)/N$  with  $n(\Delta)$  as the number of molecules with the value of  $\Delta$  and  $N$  as the number of molecules of the whole sample. Given that  $p_Z(\Delta)$  is supposed a symmetric bell-form distribution with a null mean value (which is realistic as well), the integration (7), whose limits of integration can be extended to  $\pm\infty$ , produces the same result if the complex exponential has positive or negative sign, thus it is independent of the values of  $\pm(\zeta_1 s_1, \zeta'_1 s'_1)$  and we only keep the positive sign.

To extract an expression for Eq. (7), we will calculate it using a Lorentzian distribution of  $\Delta$ , only for numerical purpose, this is

$$p_Z(\Delta) = \frac{1}{\pi} \frac{1/t_0}{1/t_0^2 + \Delta^2}. \quad (8)$$

Using Eq. (8) in Eq. (7) we obtain

$$G_Z(t + \tau/3) = e^{-t/t_0} e^{-\tau/\tau_0}. \quad (9)$$

with  $t_0$  as the characteristic decay time and  $\tau_0 = 3t_0$ .

In Figure 3 we showed the measured results for the maximum values of the FID's, i.e. the pseudo-FID obtained by the values for an averaged amplitude close to  $t = 0$ , which are extracted by the reversion experiment in Figure 1 (c) using MREV8-like blocks of pulses as  $RS(i)$  in the isotropic 5CB (at  $T = 37^\circ C$ ). Besides, in Figure 3 the obtained data are fitted with an exponential decay function with characteristic time  $\tau_0 = 4.5ms$ . Comparing with the results of the same experiment in nematic LC's, whose measurements are shown in Figure 11 in QD-II, we can see that for a reversion time of  $\tau \simeq 2.5ms$  the signals in the nematic phase are vanishing but the decay due to inhomogeneity only can produce a reduction around of the 40% in such signals. Therefore, in the reversion experiment in nematic LC's the contribution to the decay of the signals from the field inhomogeneity can be neglected due to it is not an important effect affecting the dynamics. It is worth to note that it is possible to configure a new MREV8-like sequence introducing four  $\pi$  pulses between the  $\pi/2$  pulses in Figure 1 (b) with the aim of removing more efficiently the dynamics due to the field inhomogeneity. Nevertheless, such sequence would double of total time under pulses which adds non-ideal effects over the measurements like those who will be commented in in Section II of this supplementary material. Therefore, to avoid extra non-ideal effects and given that the decay produced by the field inhomogeneity has a longer time scale than the observed decays we used the standard MREV8 sequence.

Finally, using Eq. (6) corresponding to the isotropic phase and the result for the FID signals under the reversion experiments on the nematic LC's, which was obtained in Section II.A in QD-II, it is ready to obtain the corresponding signals for an open quantum spin system in the nematic LC's under such reversion experiments, and affected by the field inhomogeneity, as

$$\begin{aligned} \langle \hat{\mathbf{I}}_y(t, \tau) \rangle &= \frac{\beta_T \omega_0 N}{\mathcal{N}_{S_1}} \sum_{\zeta_1 s_1, \zeta'_1 s'_1} \left| \langle \zeta_1 s_1 | \mathbf{I}_y^{(s_1)} | \zeta'_1 s'_1 \rangle \right|^2 \\ &\times e^{-i(\zeta_1 - \zeta'_1) \bar{S} t} G_{\zeta_1, \zeta'_1}(t) G_{\zeta_1, \zeta'_1}^{(rt)}(\tau) G_Z(t + \tau/3), \end{aligned} \quad (10)$$

where  $\bar{S} \equiv \bar{S}_1 \equiv \langle \mathbf{S}_{zz1}^{(f)} \rangle_f \equiv S_{zz}$ . In Eq. (10)  $G_{\zeta_1, \zeta'_1}$  and  $G_{\zeta_1, \zeta'_1}^{(rt)}$  are the decoherence functions for the free-evolution dynamics and the reversion dynamics, respectively. It is important to note that these decoherence functions depend on the eigenvalues  $\zeta_1$  and  $\zeta'_1$  so imposing eigen-selectivity (see QD-II for details about eigen-selectivity). On the contrary,  $G_Z$  does not depend on such eigenvalues thus it does not involve eigen-selectivity effects.

We conclude in this section that the dynamics produced by the field inhomogeneity has a time scale longer than the decoherence one and it does not involve eigen-selectivity.

## II. MISADJUSTMENTS IN THE DYNAMICS UNDER REVERSION

In this section, we study with numerical simulations the effects of parameter misadjustments or errors in reversion experiments under the dynamics of a closed spin system. The aim of this study is to check for possible eigen-selectivity behaviours due to such misadjustment affecting only the spin dynamics. To do that, we use the eight-spins model of a  $PAA_{d6}$  molecule, which was presented in QD-I<sup>1</sup>.

We simulated the dynamics under the reversion experiment of Figure 1 (c), where each block of reversion  $RS(i)$  is a sequence like the MREV8 one shown in Figure 1 (b). To calculate the effect of the MREV8 sequence on the spin dynamics, first we define the dipolar spin Hamiltonian of a nematic LC molecule as<sup>1</sup>

$$\hat{\mathcal{H}}_{S1} \equiv \pi \sqrt{6} \sum_{j \neq k} D_{jk} \mathbf{T}_{2,0}^{jk}, \quad (11)$$

with the following 2nd order tensor

$$\begin{aligned} \mathbf{T}_{2,0}^{jk} &= \frac{1}{\sqrt{6}} \left( 3 \mathbf{I}_{zj} \mathbf{I}_{zk} - \vec{\mathbf{I}}_j \cdot \vec{\mathbf{I}}_k \right) \\ &= \frac{1}{\sqrt{6}} \left[ 2 \mathbf{I}_{zj} \mathbf{I}_{zk} - \frac{1}{2} (\mathbf{I}_{+j} \mathbf{I}_{-k} + \mathbf{I}_{-j} \mathbf{I}_{+k}) \right], \end{aligned} \quad (12)$$

and the dipolar couplings defined as (in Hz units)

$$D_{jk} \equiv \frac{\mu_0 \gamma^2 \hbar}{8\pi^2} \frac{(1 - 3 \cos^2 \beta_{jk})}{2r_{jk}^3} S_{zz}, \quad (13)$$

under the international system of units (SI), where the indices  $j, k$  run over all the proton sites within the molecule. In Eq. (13),  $\gamma$  is the proton gyromagnetic ratio,  $\mu_0$  is the vacuum permeability,  $r_{jk}$  is the internuclear distance between spins  $j$  and  $k$ ,  $\beta_{jk}$  stand for the polar angle of the vector  $\vec{r}_{jk}$  with respect to the system fixed to the molecule,  $S_{zz}$  is the mean molecular order,



$\vec{\mathbf{I}}_{\mathbf{j}} \equiv \mathbf{I}_{\mathbf{xj}} \hat{\mathbf{x}} + \mathbf{I}_{\mathbf{yj}} \hat{\mathbf{y}} + \mathbf{I}_{\mathbf{zj}} \hat{\mathbf{z}}$  is the vector of the  $i$ -th spin angular momentum and  $\mathbf{I}_{\alpha i}$  is the  $i$ -th spin angular momentum operator, with  $\alpha \equiv \{x, y, z, +, -\}$ . Since all the spin operators in this section act on the spin Hilbert space of one molecule, for instance with the molecular index 1, for simplicity we will not explicit in such operators the upper index ( $s_1$ ) pointing the corresponding molecular spin Hilbert space.

Then, we are calculating a set of operators which result from applying pulses with an angle  $\theta$  and opposite phases on the dipolar Hamiltonian of one molecule,  $\hat{\mathcal{H}}_{S1}$ , such expressions will be useful in the calculation of the dynamics under reversion. The expressions are the following

$$\hat{\mathcal{H}}_{S1}^x(\theta) \equiv \mathbf{R}_{\mathbf{x}}^\theta \hat{\mathcal{H}}_{S1} \mathbf{R}_{\mathbf{x}}^{\dagger\theta} = \frac{3 \cos^2 \theta - 1}{2} \hat{\mathcal{H}}_{S1} - i \sqrt{\frac{3}{2}} \sin \theta \cos \theta \hat{\mathcal{H}}_{S1}^{(1)} - \sqrt{\frac{3}{2}} \frac{\sin^2 \theta}{2} \hat{\mathcal{H}}_{S1}^{(2)}, \quad (14a)$$

$$\hat{\mathcal{H}}_{S1}^{\bar{x}}(\theta) \equiv \mathbf{R}_{\mathbf{x}}^{\dagger\theta} \hat{\mathcal{H}}_{S1} \mathbf{R}_{\mathbf{x}}^\theta = \frac{3 \cos^2 \theta - 1}{2} \hat{\mathcal{H}}_{S1} + i \sqrt{\frac{3}{2}} \sin \theta \cos \theta \hat{\mathcal{H}}_{S1}^{(1)} - \sqrt{\frac{3}{2}} \frac{\sin^2 \theta}{2} \hat{\mathcal{H}}_{S1}^{(2)}, \quad (14b)$$

$$\hat{\mathcal{H}}_{S1}^y(\theta) \equiv \mathbf{R}_{\mathbf{y}}^\theta \hat{\mathcal{H}}_{S1} \mathbf{R}_{\mathbf{y}}^{\dagger\theta} = \frac{3 \cos^2 \theta - 1}{2} \hat{\mathcal{H}}_{S1} - \sqrt{\frac{3}{2}} \sin \theta \cos \theta \hat{\mathcal{H}}_{S1}^{(1)} + \sqrt{\frac{3}{2}} \frac{\sin^2 \theta}{2} \hat{\mathcal{H}}_{S1}^{(2)}, \quad (14c)$$

$$\hat{\mathcal{H}}_{S1}^{\bar{y}}(\theta) \equiv \mathbf{R}_{\mathbf{y}}^{\dagger\theta} \hat{\mathcal{H}}_{S1} \mathbf{R}_{\mathbf{y}}^\theta = \frac{3 \cos^2 \theta - 1}{2} \hat{\mathcal{H}}_{S1} + \sqrt{\frac{3}{2}} \sin \theta \cos \theta \hat{\mathcal{H}}_{S1}^{(1)} + \sqrt{\frac{3}{2}} \frac{\sin^2 \theta}{2} \hat{\mathcal{H}}_{S1}^{(2)}, \quad (14d)$$

where the pulses of an angle  $\theta$  and direction  $\alpha$  are defined as  $\mathbf{R}_{\alpha}^\theta \equiv e^{i \mathbf{I}_{\alpha} \theta}$ , with  $\mathbf{I}_{\alpha} \equiv \sum_i \mathbf{I}_{\alpha i}$ . In Eq. (14) we defined the Hamiltonians

$$\hat{\mathcal{H}}_{S1}^{(1)} \equiv \pi \sqrt{6} \sum_{j \neq k} D_{jk} \left( \mathbf{T}_{2,+1}^{jk} + \mathbf{T}_{2,-1}^{jk} \right), \quad (15a)$$

$$\hat{\mathcal{H}}_{S1}^{(1)} \equiv \pi \sqrt{6} \sum_{j \neq k} D_{jk} \left( \mathbf{T}_{2,+1}^{jk} - \mathbf{T}_{2,-1}^{jk} \right), \quad (15b)$$

$$\hat{\mathcal{H}}_{S1}^{(2)} \equiv \pi \sqrt{6} \sum_{j \neq k} D_{jk} \left( \mathbf{T}_{2,+2}^{jk} + \mathbf{T}_{2,-2}^{jk} \right), \quad (15c)$$

with the following 2nd order tensors

$$\mathbf{T}_{2,+1}^{jk} = -\frac{1}{2} (\mathbf{I}_{\mathbf{zj}} \mathbf{I}_{+\mathbf{k}} + \mathbf{I}_{+\mathbf{j}} \mathbf{I}_{\mathbf{zk}}), \quad (16a)$$

$$\mathbf{T}_{2,-1}^{jk} = \frac{1}{2} (\mathbf{I}_{\mathbf{zj}} \mathbf{I}_{-\mathbf{k}} + \mathbf{I}_{-\mathbf{j}} \mathbf{I}_{\mathbf{zk}}), \quad (16b)$$

$$\mathbf{T}_{2,+2}^{jk} = \frac{1}{2} \mathbf{I}_{+\mathbf{j}} \mathbf{I}_{+\mathbf{k}}, \quad (16c)$$

$$\mathbf{T}_{2,-2}^{jk} = \frac{1}{2} \mathbf{I}_{-\mathbf{j}} \mathbf{I}_{-\mathbf{k}}. \quad (16d)$$

The Hamiltonian  $\hat{\mathcal{H}}_{S1}$  is called the secular part of the dipolar Hamiltonian and the Hamiltonians  $\hat{\mathcal{H}}_{S1}^{(1)}$ ,  $\hat{\mathcal{H}}_{S1}^{(1)}$  and  $\hat{\mathcal{H}}_{S1}^{(2)}$  constitute the non-secular parts of the dipolar Hamiltonian.

Consider the case that the rf pulses in the MREV8 pulse sequence of Figure 1 (b) are of an arbitrary  $\theta$  angle instead of  $\pi/2$  pulses, due to experimental misadjustments. In such a case, and supposing the same angle  $\theta$  for all the pulses, the evolution operator of the sequence in Figure 1 (b) will be

$$\begin{aligned} \hat{\mathbf{U}}_{RS}^\theta(\tau_2, \tau_1) \equiv & \mathbf{R}_{\mathbf{x}}^{\dagger\theta} \hat{\mathbf{U}}_{\mathbf{rt}}^{\mathbf{x},\theta}(\tau_2/2) \hat{\mathbf{U}}(\tau_1) \hat{\mathbf{U}}_{\mathbf{rt}}^{\mathbf{y},\theta}(\tau_2) \hat{\mathbf{U}}(\tau_1) \hat{\mathbf{U}}_{\mathbf{rt}}^{\mathbf{x},\theta}(\tau_2/2) \mathbf{R}_{\mathbf{x}}^\theta \\ & \times \mathbf{R}_{\mathbf{x}}^\theta \hat{\mathbf{U}}_{\mathbf{rt}}^{\bar{\mathbf{x}},\theta}(\tau_2/2) \hat{\mathbf{U}}(\tau_1) \hat{\mathbf{U}}_{\mathbf{rt}}^{\bar{\mathbf{y}},\theta}(\tau_2) \hat{\mathbf{U}}(\tau_1) \hat{\mathbf{U}}_{\mathbf{rt}}^{\bar{\mathbf{x}},\theta}(\tau_2/2) \mathbf{R}_{\mathbf{x}}^{\dagger\theta}, \end{aligned} \quad (17)$$

where

$$\hat{\mathbf{U}}(\tau_1) = e^{-i \hat{\mathcal{H}}_{S1} \tau_1}, \quad (18)$$

$$\hat{\mathbf{U}}_{\mathbf{rt}}^{\alpha,\theta}(\tau_2) = e^{-i \hat{\mathcal{H}}_{S1}^{\alpha}(\theta) \tau_2}, \quad (19)$$

with  $\alpha \equiv \{\mathbf{x}, \mathbf{y}, \bar{\mathbf{x}}, \bar{\mathbf{y}}\}$  and we applied the operator identity  $\mathbf{1} \equiv \mathbf{R}_{\mathbf{x}}^\theta \mathbf{R}_{\mathbf{x}}^{\dagger\theta} \equiv \mathbf{R}_{\mathbf{x}}^{\dagger\theta} \mathbf{R}_{\mathbf{x}}^\theta$  in the ends and in the middle of the sequence.

When the times  $\tau_1$  and  $\tau_2$  are small enough, it is possible to approximate the evolution operator (17) by joining together the exponent of all the operators (18) and (19). In such a case, and when the angle  $\theta$  is close to  $\pi/2$ , the contribution to the dynamics of the non-secular Hamiltonians vanishes due to cancellation of the terms with  $\hat{\mathcal{H}}_{S1}^{(1)}$ ,  $\hat{\mathcal{H}}_{S1}^{(1)}$  and  $\hat{\mathcal{H}}_{S1}^{(2)}$ , and the resulting evolution operator will be

$$\hat{\mathbf{U}}_{RS}^\theta(t_2, t_1) \simeq \mathbf{R}_{\mathbf{x}}^{\dagger\theta} \hat{\mathbf{U}}_{\mathbf{rt}}(t_2) \hat{\mathbf{U}}(t_1) \mathbf{R}_{\mathbf{x}}^\theta, \quad (20)$$

where we defined

$$\hat{\mathbf{U}}(t_1) \equiv e^{-i \hat{\mathcal{H}}_{S1} t_1}, \quad (21)$$

$$\hat{\mathbf{U}}_{\mathbf{rt}}(t_2) \equiv e^{i \hat{\mathcal{H}}_{S1} t_2 / \kappa}, \quad (22)$$

with  $t_1 = 4\tau_1$ ,  $t_2 = 4\tau_2$  and  $\kappa \equiv 2/(1 - 3 \cos^2 \theta)$ . It is worth to note that Eq. (20) has the form of the general evolution operator for reversion experiments analysed in QD-II, except for the pulse operators at the ends

in Eq. (20). Nevertheless, the presence of such pulses does not alter the expectation values of the observables as calculated in QD-II; thus they can be neglected for simplicity in the study of decoherence effects in reversion experiments using the MREV8 sequence. If  $t_2 = \kappa t_1$ , we can see that  $\hat{\mathbf{U}}_{RS}^\theta(t_2, t_1) \simeq \mathbf{1}$ . Therefore, for that time setting, the spin dynamics during  $t_1$  will be perfectly compensated (or will be very close to that) by the dynamics during the evolution time  $t_2$ , and the initial state is recovered after the total time evolution.

The pulse sequence of Figure 1 (c) consists of chains of blocks of MREV8 units. In this case, under the same approximation about the time parameters that yields the operator (20), we will obtain the same evolution operator as in Eq. (20) for the experiment with  $n$  blocks  $RS$  of reversion, but with  $t_1 = 4n\tau_1$  and  $t_2 = 4n\tau_2$ .

In the case of an exact (and ideal) experimental setting of the  $\pi/2$  pulses, the expressions in Eq. (14) simplify to

$$\begin{aligned}\hat{\mathcal{H}}_{S1}^x &\equiv \hat{\mathcal{H}}_{S1}^x(\pi/2) = \hat{\mathcal{H}}_{S1}^{\bar{x}}(\pi/2) \\ &\equiv -\frac{1}{\kappa} \hat{\mathcal{H}}_{S1} - \frac{1}{2} \sqrt{\frac{3}{2}} \hat{\mathcal{H}}_{S1}^{(2)},\end{aligned}\quad (23a)$$

$$\begin{aligned}\hat{\mathcal{H}}_{S1}^y &\equiv \hat{\mathcal{H}}_{S1}^y(\pi/2) = \hat{\mathcal{H}}_{S1}^{\bar{y}}(\pi/2) \\ &\equiv -\frac{1}{\kappa} \hat{\mathcal{H}}_{S1} + \frac{1}{2} \sqrt{\frac{3}{2}} \hat{\mathcal{H}}_{S1}^{(2)},\end{aligned}\quad (23b)$$

and  $\kappa = 2$ .

To observe the effects over the dynamics under reversion due to the non-secular Hamiltonians and/or experimental misadjustments, we performed numerical simulations of the experiment of Figure 1 (c), using the Hamiltonians (23) for a proton system model of a PAA<sub>d6</sub> molecule<sup>1</sup>, and including a parameter misadjustment of the reversion sequence, using  $\tau_2 = (\kappa + \epsilon) \tau_1$  (in this case  $\kappa = 2$ ). In the case of small error in the setting of the  $\pi/2$  pulses, the value of  $\kappa$  will be slightly different of 2. Besides, in Eq. (14) the factors ‘ $\sin \theta \cos \theta$ ’ will be little different of zero and thus there will be a small contribution to the reversion dynamics coming from the non-secular Hamiltonians  $\hat{\mathcal{H}}_{S1}^{(1)}$  and  $\hat{\mathcal{H}}_{S1}^{(1)}$ . However, if the time  $\tau_1$  is small enough (as well as  $\tau_2$ ) the contribution to the dynamics coming from the non-secular parts will be negligible and the resultant effect will be a setting of  $\kappa$  different of 2. In such cases, if we set  $\tau_2 = 2\tau_1$ , the error in the pulse angle will be equivalent to a misadjustment of  $\tau_2$  for a correct setting of the reversion sequence, due to  $\kappa \neq 2$ ; in this way we would be setting  $\tau_2 = (\kappa + \epsilon) \tau_1$  (with  $\kappa + \epsilon = 2$ ).

Since there are only two Hamiltonians in (23) with different contributions of the non-secular Hamiltonian  $\hat{\mathcal{H}}_{S1}^{(2)}$ , the sequence of operators given by Eq. (17) will actually be conformed by two equal sets of reversion evolution operators, i.e. there will be a duplication of such operators.

Therefore, for the sake of simplicity we used in the simulation of the reversion sequence, for each block  $RS$ , the following evolution operator

$$\hat{\mathbf{U}}_{RS}^{\kappa, \epsilon}(\tau_1) \equiv \hat{\mathbf{U}}_{\text{rt}}^y[(\kappa + \epsilon) \tau_1] \hat{\mathbf{U}}(\tau_1) \hat{\mathbf{U}}_{\text{rt}}^x[(\kappa + \epsilon) \tau_1] \hat{\mathbf{U}}(\tau_1), \quad (24)$$

where

$$\hat{\mathbf{U}}(\tau_1) = e^{-i \hat{\mathcal{H}}_{S1} \tau_1}, \quad (25)$$

$$\hat{\mathbf{U}}_{\text{rt}}^x[(\kappa + \epsilon) \tau_1] = e^{-i \hat{\mathcal{H}}_{S1}^x (\kappa + \epsilon) \tau_1}, \quad (26)$$

$$\hat{\mathbf{U}}_{\text{rt}}^y[(\kappa + \epsilon) \tau_1] = e^{-i \hat{\mathcal{H}}_{S1}^y (\kappa + \epsilon) \tau_1}, \quad (27)$$

with  $\kappa = 2$ .

The reversion evolution operator of the total  $n$  blocks has the following expression

$$\hat{\mathbf{U}}_{RS(n)}^{\kappa, \epsilon}(\tau_1) \equiv \hat{\mathbf{U}}_{RS}^{\kappa, \epsilon}(\tau_1) \times \cdots \times \hat{\mathbf{U}}_{RS}^{\kappa, \epsilon}(\tau_1) \equiv \prod \hat{\mathbf{U}}_{RS}^{\kappa, \epsilon}(\tau_1), \quad (28)$$

where the evolution operator is multiplied by itself  $n$  times.

The evolution time of each reversion block  $RS$  is

$$\tau_c = (\kappa + 1 + \epsilon) 2\tau_1, \quad (29)$$

and the total evolution time has the discrete values of  $\tau = n\tau_c$  ( $n = 0, 1, 2, \dots$ ). Thus, we can alternatively define the evolution operator (28) as

$$\hat{\mathbf{U}}_{RS}^{\kappa, \epsilon, \tau_1}(\tau) \equiv \hat{\mathbf{U}}_{RS(n)}^{\kappa, \epsilon}(\tau_1), \quad (30)$$

where  $n = \tau / [(\kappa + 1 + \epsilon) 2\tau_1]$ .

The signals which we obtained from the simulations of the reversion experiments were the normalized expectation values of  $\mathbf{I}_y$  and they were calculated as

$$\begin{aligned}\langle \hat{\mathbf{I}}_y(t, \tau)_{\tau_1}^{\kappa, \epsilon} \rangle &= \frac{1}{\text{tr}_{s_1} \{ \mathbf{I}_y^2 \}} \text{tr}_{s_1} \left\{ \mathbf{I}_y e^{-i \hat{\mathcal{H}}_{S1} t} \right. \\ &\quad \times \hat{\mathbf{U}}_{RS}^{\kappa, \epsilon, \tau_1}(\tau) \mathbf{I}_y \hat{\mathbf{U}}_{RS}^{\dagger \kappa, \epsilon, \tau_1}(\tau) e^{i \hat{\mathcal{H}}_{S1} t} \left. \right\}.\end{aligned}\quad (31)$$

We performed numerical simulations of Eq. (31) for different values of  $\tau_1$  and  $\epsilon$  with  $\kappa = 2$ . The results are shown in Figures 4-9. Figure 4 shows the behavior of Eq. (31) with the free-evolution time  $t$  and the reversion time  $\tau$ . Figure 5 shows the dependence with  $\tau$  of Eq. (31) for  $t = 0$ , which is useful to appreciate the reversion dynamics. Figure 6 shows the  $\tau$  dependent Fourier transforms of Eq. (31) in the time  $t$ ; in this picture we can test the eigen-selection effects on the spectral lines of the signals. For such test, several cuts of the spectra for different normalized frequency lines as function of  $\tau$  are shown in Figure 7.

Figure 8 contains the spectra of Figure 6 with the spectrum normalized for each value of  $\tau$ . In Figure 9 several cuts of the spectra of Figure 8 for different normalized frequency lines are shown. With these normalized spectra it is possible to compare the decay rate in the time  $\tau$  for different spectral line.

The evolution operator (30) can be approximated for small enough values of  $\tau_1$  times as:

$$\begin{aligned}\hat{U}_{RS}^{\kappa,\epsilon,\tau_1}(\tau) &\simeq e^{-i[2\hat{H}_{S1}+(\kappa+\epsilon)(\hat{H}_{S1}^x+\hat{H}_{S1}^y)]n\tau_1} \\ &= e^{-i[\hat{H}_{S1}-(1+\epsilon/\kappa)\hat{H}_{S1}]2n\tau_1} = e^{i\hat{H}_{S1}\frac{\epsilon/\kappa}{\kappa+1+\epsilon}\tau},\end{aligned}\quad (32)$$

where we used  $\hat{H}_{S1}^x + \hat{H}_{S1}^y = -2\hat{H}_{S1}/\kappa$ , with  $\kappa = 2$ , and  $2n\tau_1 = \tau/(\kappa + 1 + \epsilon)$ . Therefore, under this time approximation, using Eq. (32) in Eq. (31), we obtain

$$\begin{aligned}\langle \hat{\mathbf{I}}_y(t, \tau)^{\kappa,\epsilon}_{\tau_1} \rangle &\simeq \frac{1}{tr_{s_1}\{\hat{\mathbf{I}}_y^2\}} tr_{s_1} \left\{ \hat{\mathbf{I}}_y e^{-i\hat{H}_{S1}t} \right. \\ &\quad \times e^{i\hat{H}_{S1}\frac{\epsilon/\kappa}{\kappa+1+\epsilon}\tau} \hat{\mathbf{I}}_y e^{-i\hat{H}_{S1}\frac{\epsilon/\kappa}{\kappa+1+\epsilon}\tau} e^{i\hat{H}_{S1}t} \left. \right\}.\end{aligned}\quad (33)$$

We can note that Eq. (33) is the normalized expression of  $\langle \hat{\mathbf{I}}_y(t, \tau)^\epsilon \rangle$  shown in Section II.C in QD-II. The results showing the effects of the dynamics under the approximation that yields (33) are those corresponding to the settings  $\{\tau_1 = 5\mu s, \epsilon/\kappa = 0.1\}$  and  $\{\tau_1 = 5\mu s, \epsilon/\kappa = 0.3\}$  in the Figures 4-9, where the effects of the non-secular Hamiltonians in the dynamics have been mitigated by adopting a small value of  $\tau_1$ . We can see, using the trace property  $tr\{AB\} = tr\{BA\}$ , that for  $t = 0$  the signal obtained in Eq. (33) as a function of the reversion time  $\tau$  is the same as a single FID signal, but with a factor of time scaling of  $\frac{\epsilon/\kappa}{\kappa+1+\epsilon}$ . Such kind of signals are shown in Figure 5 for the mentioned setting, where it is observed that the behavior of the signals presents oscillations, which are typical of the FID's signals, where the smaller the ratio  $\epsilon/\kappa$  is, the lower the frequency of the oscillation will be.

For general cases of values of  $\tau_1$  and  $\epsilon/\kappa$ , we can write the evolution operator (24) as

$$\hat{U}_{RS}^{\kappa,\epsilon}(\tau_1) \equiv e^{-i\hat{H}_{S1}^{\dagger\kappa,\epsilon}(\tau_1)\tau_c}, \quad (34)$$

with  $\tau_c$  given in (29). We define the eigenbasis  $\{|\alpha_1\rangle\}$  common to the evolution operator  $\hat{U}_{RS}^{\kappa,\epsilon}(\tau_1)$  and the Hamiltonian  $\hat{H}_{S1}^{\dagger\kappa,\epsilon}(\tau_1)$ , and we define the eigenvalues  $A_1^{\kappa,\epsilon}(\tau_1) = \langle \alpha_1 | \hat{U}_{RS}^{\kappa,\epsilon}(\tau_1) | \alpha_1 \rangle$  and  $\alpha_1^{\kappa,\epsilon}(\tau_1) = \langle \alpha_1 | \hat{H}_{S1}^{\dagger\kappa,\epsilon}(\tau_1) | \alpha_1 \rangle$ . Therefore the Hamiltonian  $\hat{H}_{S1}^{\dagger\kappa,\epsilon}(\tau_1)$  can be obtained writing its matrix representation in such eigenbase, where  $\alpha_1^{\kappa,\epsilon}(\tau_1) = i \ln A_1^{\kappa,\epsilon}(\tau_1)/\tau_c$ . Using Eq. (34) in Eq. (28), the evolution operator (30) for the  $n$  blocks of reversion will be

$$\hat{U}_{RS}^{\kappa,\epsilon,\tau_1}(\tau) \equiv e^{-i\hat{H}_{S1}^{\dagger\kappa,\epsilon}(\tau_1)\tau}, \quad (35)$$

with  $\tau = n\tau_c$ , and the expectation value (31) for general cases can be written as

$$\begin{aligned}\langle \hat{\mathbf{I}}_y(t, \tau)^{\kappa,\epsilon}_{\tau_1} \rangle &= \frac{1}{tr_{s_1}\{\hat{\mathbf{I}}_y^2\}} tr_{s_1} \left\{ \hat{\mathbf{I}}_y e^{-i\hat{H}_{S1}t} \right. \\ &\quad \times e^{-i\hat{H}_{S1}^{\dagger\kappa,\epsilon}(\tau_1)\tau} \hat{\mathbf{I}}_y e^{i\hat{H}_{S1}^{\dagger\kappa,\epsilon}(\tau_1)\tau} e^{i\hat{H}_{S1}t} \left. \right\}.\end{aligned}\quad (36)$$

The signals in Eq. (36) are the normalized form of the expectation values  $\langle \hat{\mathbf{I}}_y(t, \tau)^\dagger \rangle$  which were obtained in Section II.C in QD-II, while in Eq. (36) the dependence of  $\hat{H}_{S1}^{\dagger}$  with the parameters  $\kappa$ ,  $\epsilon$  and  $\tau_1$  has been explicitly written.

It can be seen by comparing Eq. (32) and Eq. (35) that under the approximation of small values of  $\tau_1$

$$\hat{H}_{S1}^{\dagger\kappa,\epsilon}(\tau_1) \simeq -\hat{H}_{S1} \frac{\epsilon/\kappa}{\kappa+1+\epsilon}, \quad (37)$$

and the expression of Eq. (36) is approximated by Eq. (33).

In other calculated cases, if we set  $\epsilon = 0$  for different values of  $\tau_1$ , the signals (36) so obtained will show the effects on the reversion dynamics due exclusively to the non-secular Hamiltonians. The results which expose these cases correspond with the settings  $\{\tau_1 = 10\mu s, \epsilon/\kappa = 0\}$  and  $\{\tau_1 = 50\mu s, \epsilon/\kappa = 0\}$  in the Figures 4-9. In the extreme misadjustment setting with  $\tau_1 = 50\mu s$  we can observe from Figure 5 a fast bell-shape decay of the signal, but such experimental setting can be improved drastically in the practice. On the other hand, such decay does not present an eigen-selection effect as can be observed from the comparison between the evolution in  $\tau$  of different spectral lines shown in Figure 6 and Figure 7 or the normalized spectra in Figure 8. Besides, in Figure 9 there is not a monotonous and eigen-selective decay for each spectral line with different frequency.

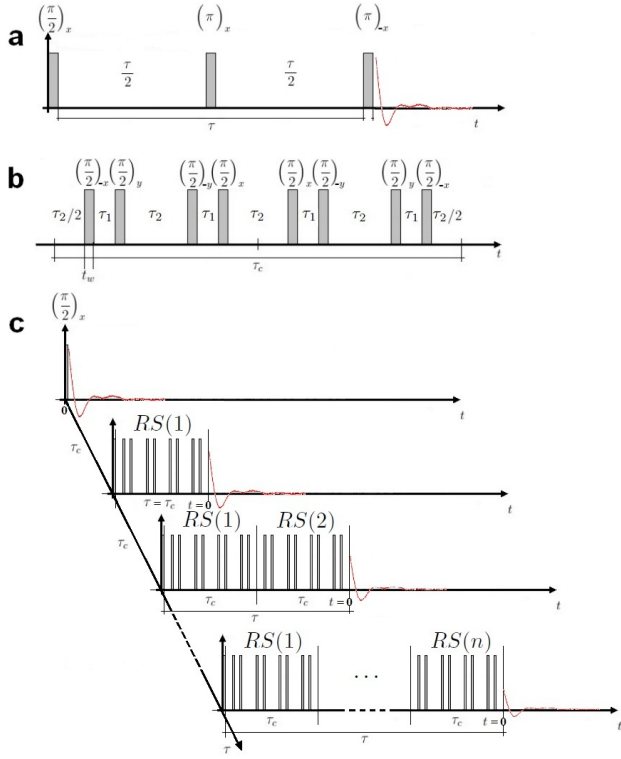
Other results shown are for the settings  $\{\tau_1 = 20\mu s, \epsilon/\kappa = 0.1\}$ , which constitutes an intermediate case between the ones with small values of  $\tau_1$  and  $\epsilon \neq 0$  (expressed by Eq. (33)) and with large values of  $\tau_1$  and  $\epsilon = 0$ , and  $\{\tau_1 = 5\mu s, \epsilon/\kappa = 0\}$ . The latter case would be close to the the best possible practical condition and it is used as contrast with the other setting cases.

The conclusion, extracted from the results of the simulations, is that for the closed spin system there are no eigen-selection effects present in the signals produced by experimental misadjustments or contribution to the dynamics coming from the non-secular Hamiltonians, as can be observed from the spectra evolution and the spectral lines evolution in the results shown in Figures 6 - 9. This conclusion reproduces the one extracted from the theoretical analysis in Section II.C in QD-II.

<sup>1</sup> H.H. Segnorile and R.C. Zamar, J. Chem. Phys. 135, 244509 (2011)

FIG. 1: Experimental pulse sequences. a: Zeeman reversion. b: MREV8. c: Compound reversion sequence, where each reversion block  $RS(i)$  constitutes a single reversion sequence like the MREV8.

Figures



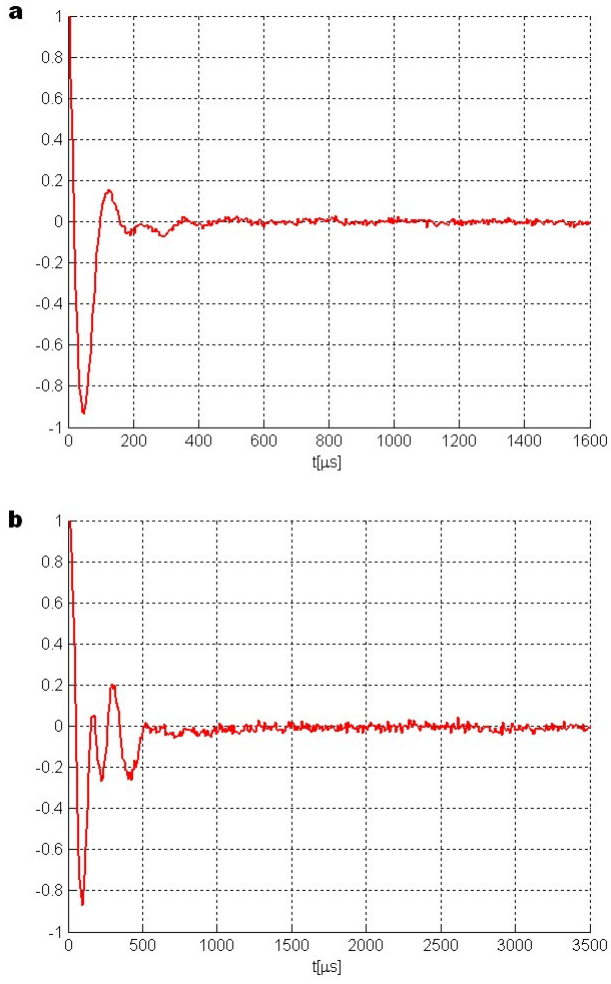


FIG. 2: Zeeman reversion experiment in nematic phase under resonance condition. a: 5CB ( $T = 27^\circ\text{C}$ ). b: PAA<sub>d6</sub> ( $T = 115^\circ\text{C}$ ).

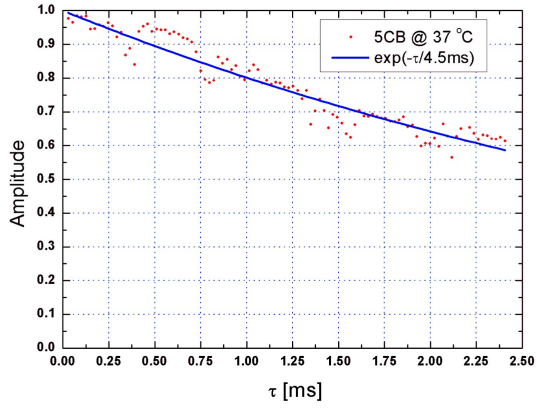


FIG. 3: Measured values of the maximum amplitude of the FID under a single MREV8 reversion, with continuous variation of the setting times, for the 5CB at  $T = 37^\circ\text{C}$  in isotropic phase under resonance condition (dots). The solid line is a fitting of the measured values with an exponential decay function with a characteristic decay time of 4.5ms.

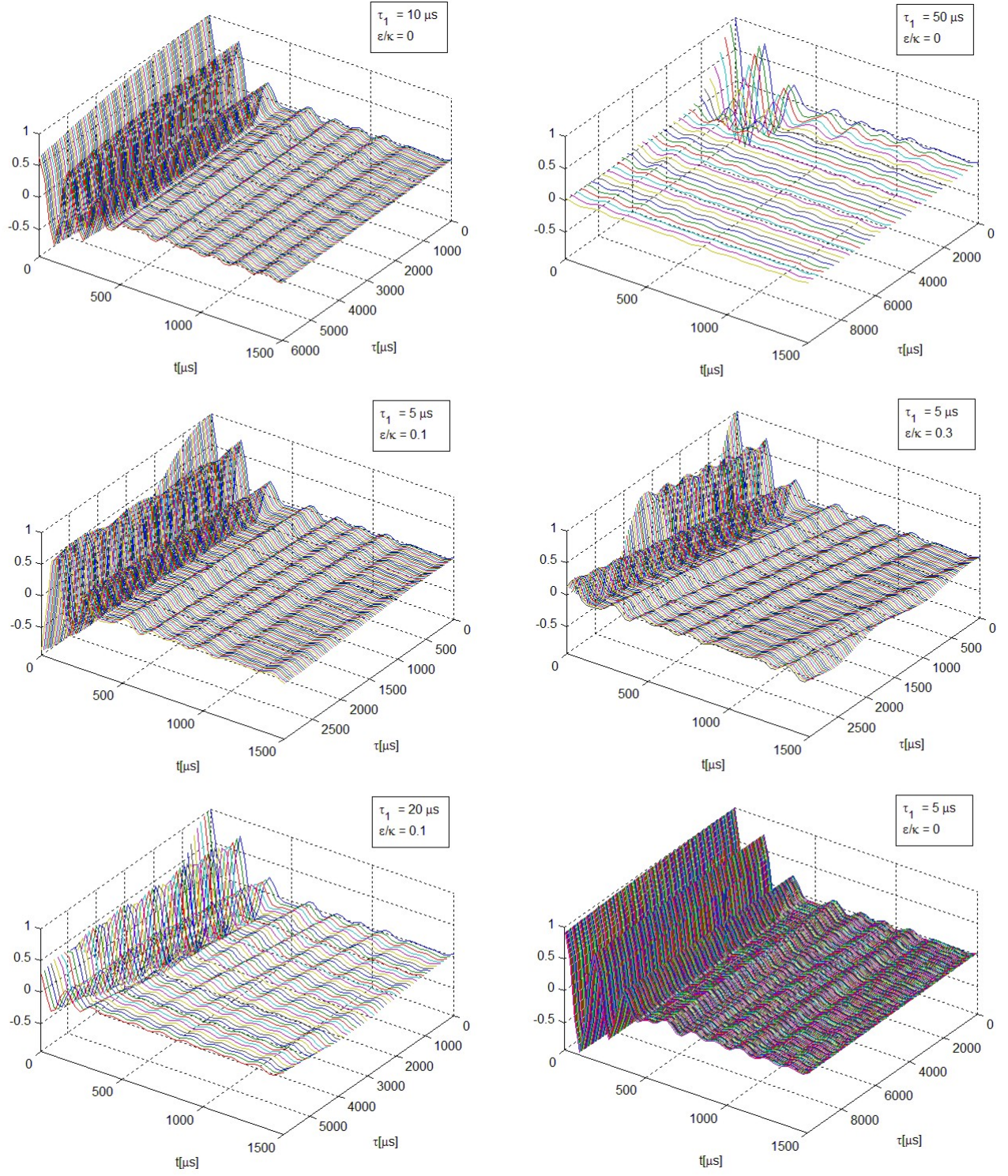


FIG. 4: Simulated results for the FID's as a function of the free-evolution time  $t$  and the reversion time  $\tau$ , produced by reversion experiments with blocks of MREV8 sequence in a nematic PAA<sub>d6</sub> molecule under resonance condition. The results corresponding to different setting of the characteristic reversion time  $\tau_1$  and the error time factor  $\epsilon/\kappa$  are shown.



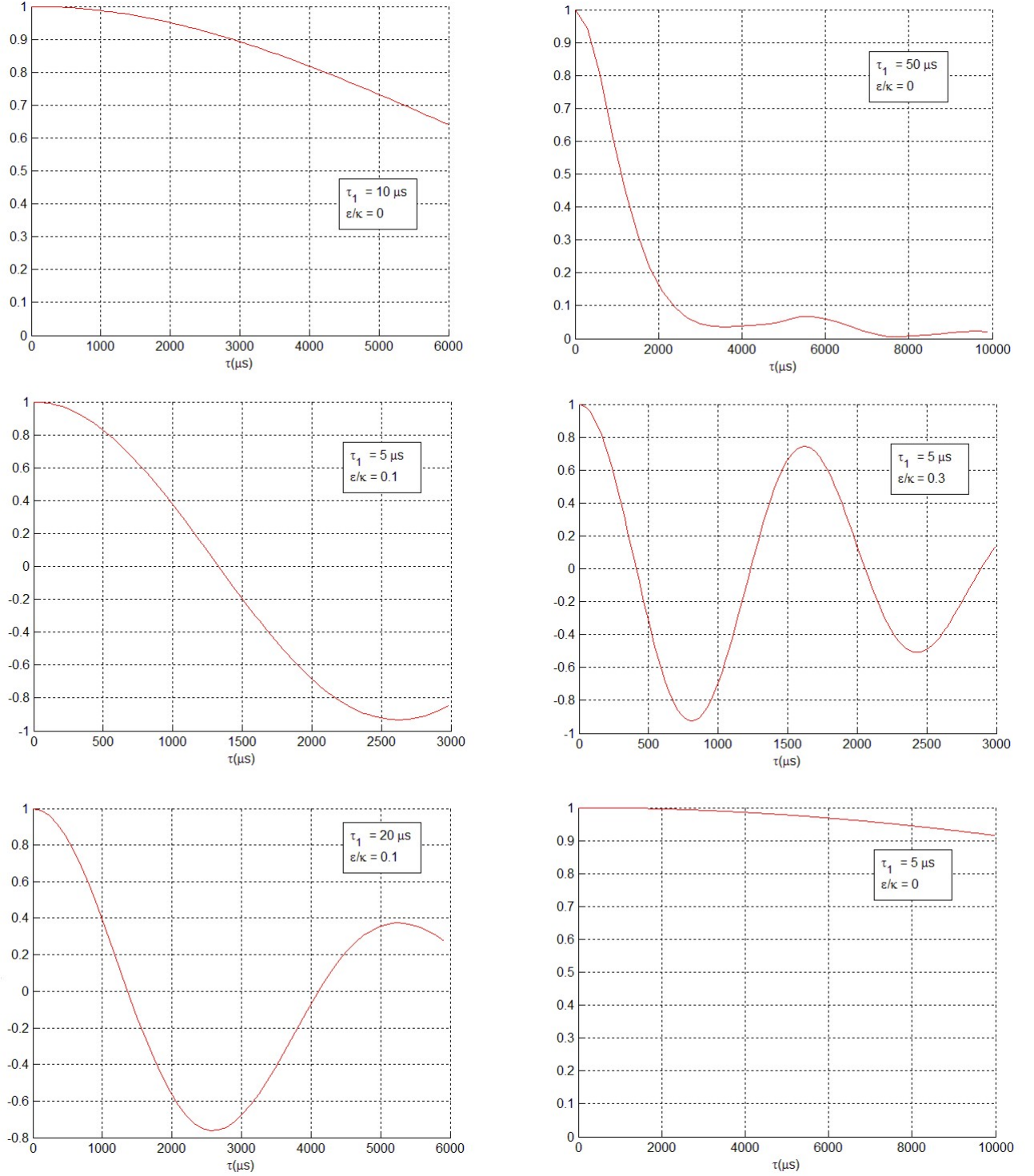


FIG. 5: Simulated results for the amplitude of the FID's for  $t = 0$  as a function of the reversion time  $\tau$ , produced by reversion experiments with blocks of MREV8 sequence in a nematic PAA<sub>d6</sub> molecule under resonance condition. The results corresponding to different setting of the characteristic reversion time  $\tau_1$  and the error time factor  $\epsilon/\kappa$  are shown.



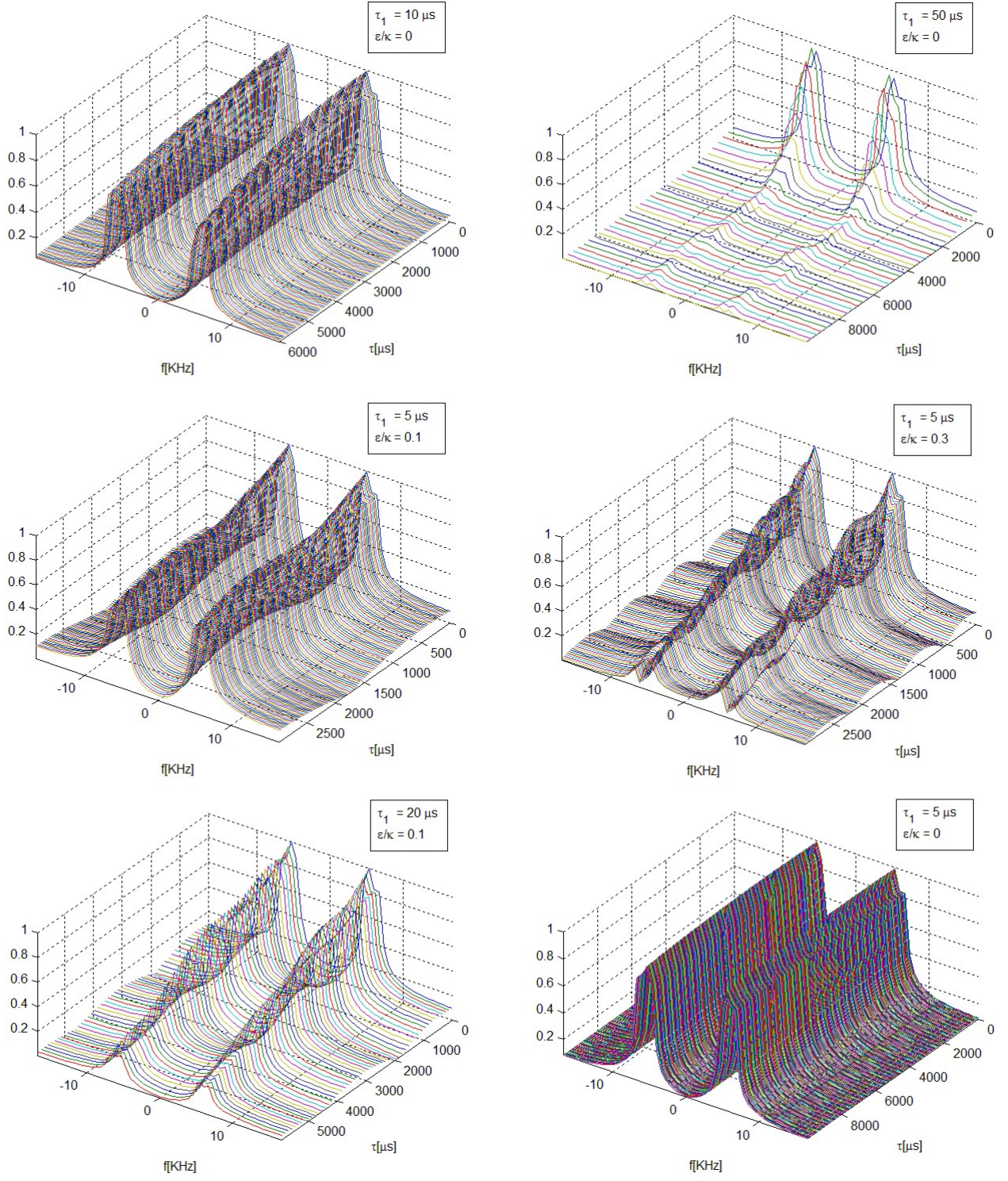


FIG. 6: Simulated results for the Fourier transform in the free-evolution time  $t$  of the FID's as a function of the reversion time  $\tau$ , produced by reversion experiments with blocks of MREV8 sequence in a nematic PAA<sub>d6</sub> molecule under resonance condition. The results corresponding to different setting of the characteristic reversion time  $\tau_1$  and the error time factor  $\epsilon/\kappa$  are shown.

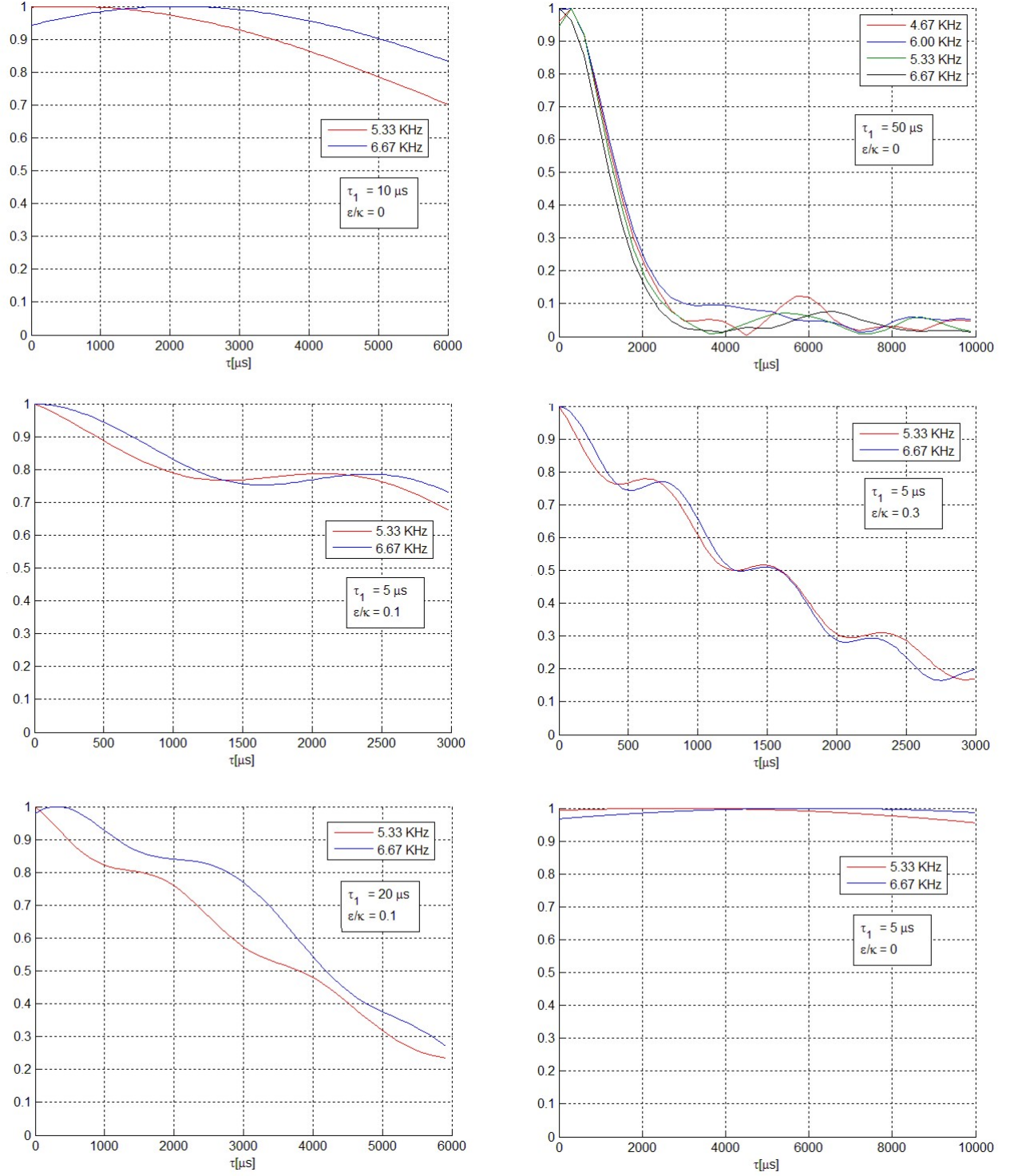


FIG. 7: Simulated results for the evolution of different normalized spectral lines of the Fourier transform in the free-evolution time  $t$  of the FID's as a function of the reversion time  $\tau$ , produced by reversion experiments with blocks of MREV8 sequence in a nematic PAA<sub>d6</sub> molecule under resonance condition. The results corresponding to different setting of the characteristic reversion time  $\tau_1$  and the error time factor  $\epsilon/\kappa$  are shown.



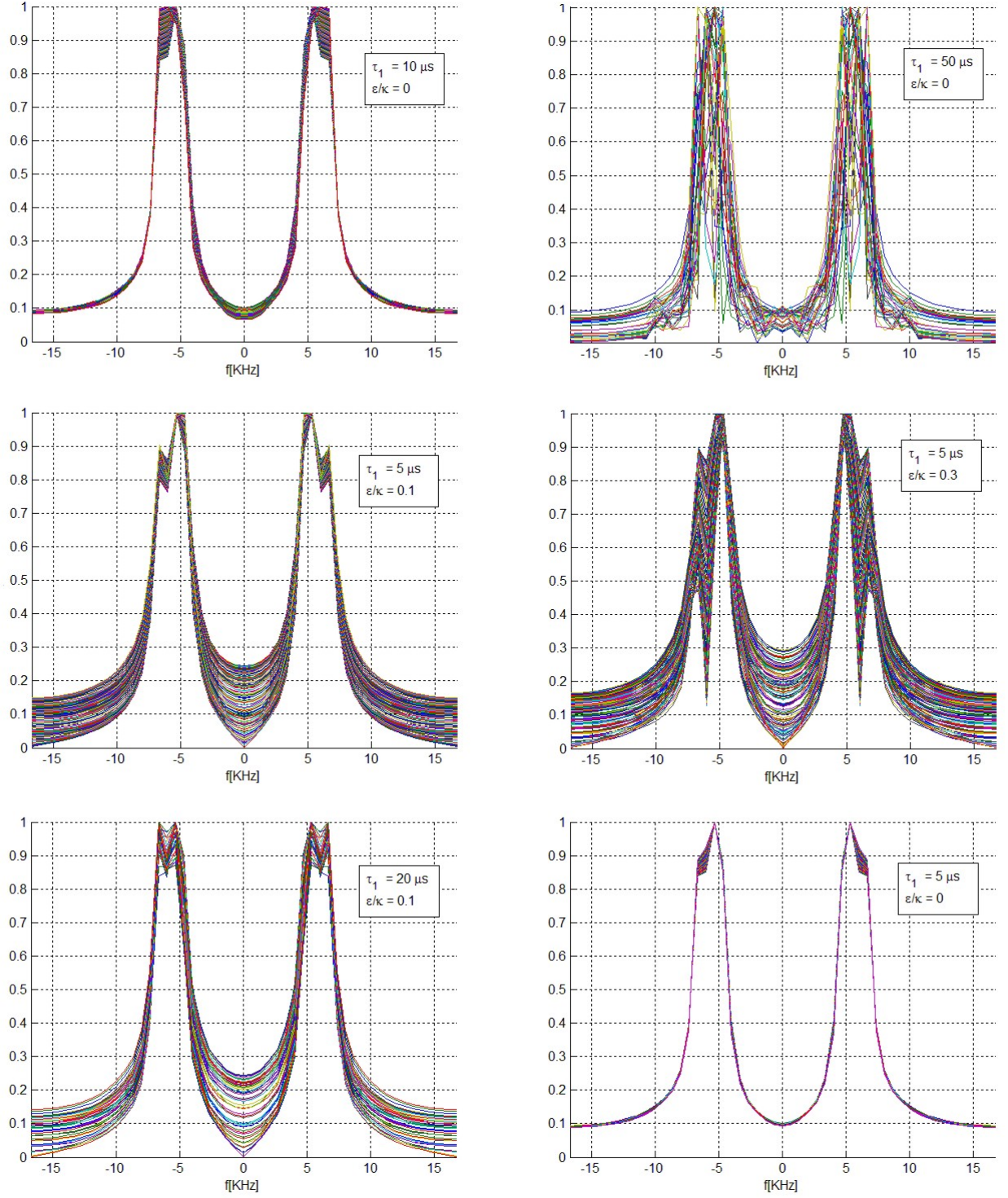


FIG. 8: Simulated results for the normalized Fourier transform in the free-evolution time  $t$  of the FID's as a function of the reversion time  $\tau$ , produced by reversion experiments with blocks of MREV8 sequence in a nematic PAA<sub>d6</sub> molecule under resonance condition. The spectra were normalized for each  $\tau$  value. The results corresponding to different setting of the characteristic reversion time  $\tau_1$  and the error time factor  $\epsilon/\kappa$  are shown.

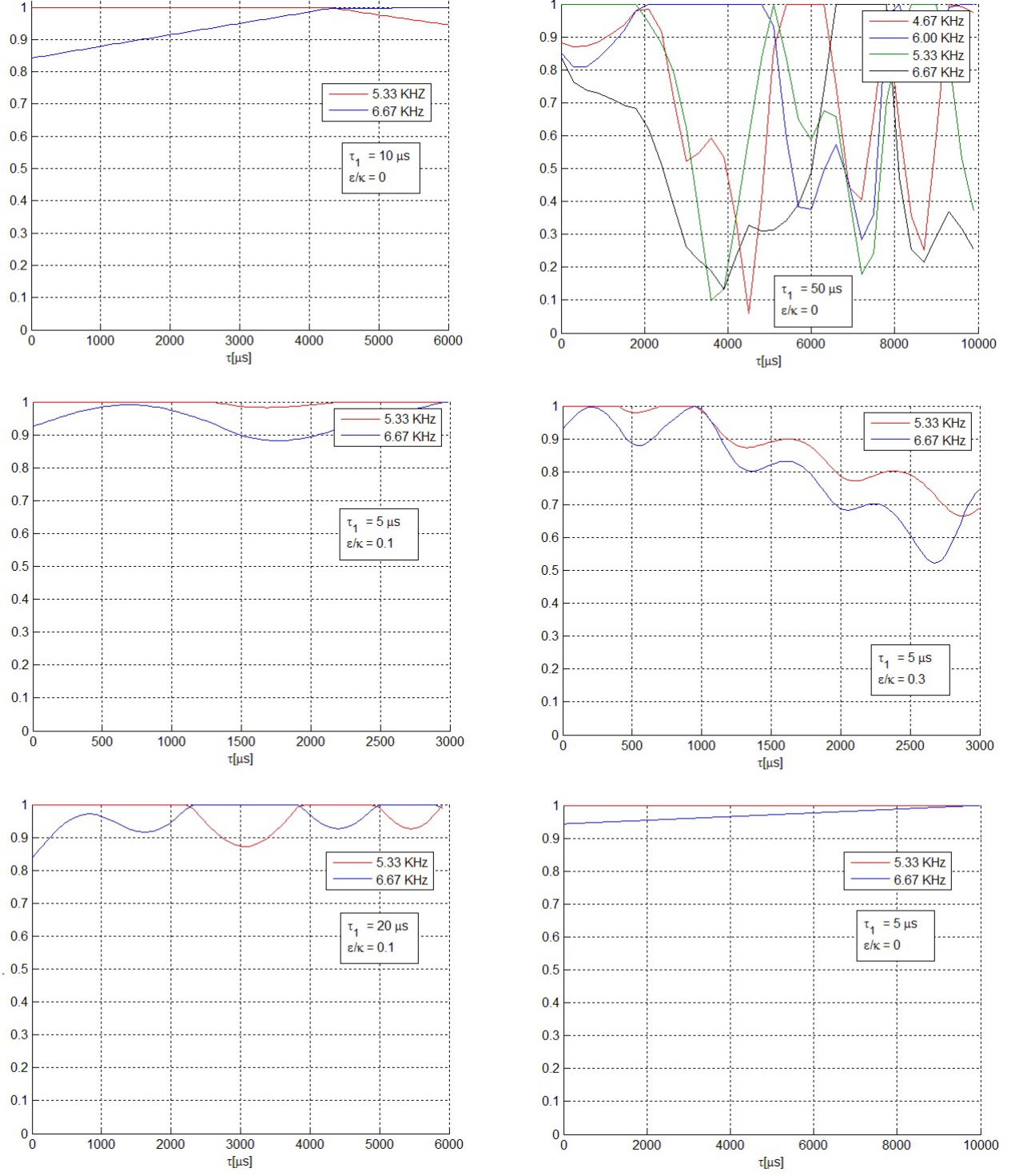


FIG. 9: Simulated results for the evolution of different normalized spectral lines of the Fourier transform in the free-evolution time  $t$  of the FID's as a function of the reversion time  $\tau$ , produced by reversion experiments with blocks of MREV8 sequence in a nematic PAA<sub>d6</sub> molecule under resonance condition. Where the spectra have been normalized for each  $\tau$  value. The results corresponding to different setting of the characteristic reversion time  $\tau_1$  and the error time factor  $\epsilon/\kappa$  are shown.